Journal of Ophthalmology

Novel Diagnostic and Therapeutic Methods in Ocular Surface and Corneal Diseases

Guest Editors: Anna K. Nowinska, László Módis, Robert Koprowski, and Jesús Merayo-Lloves

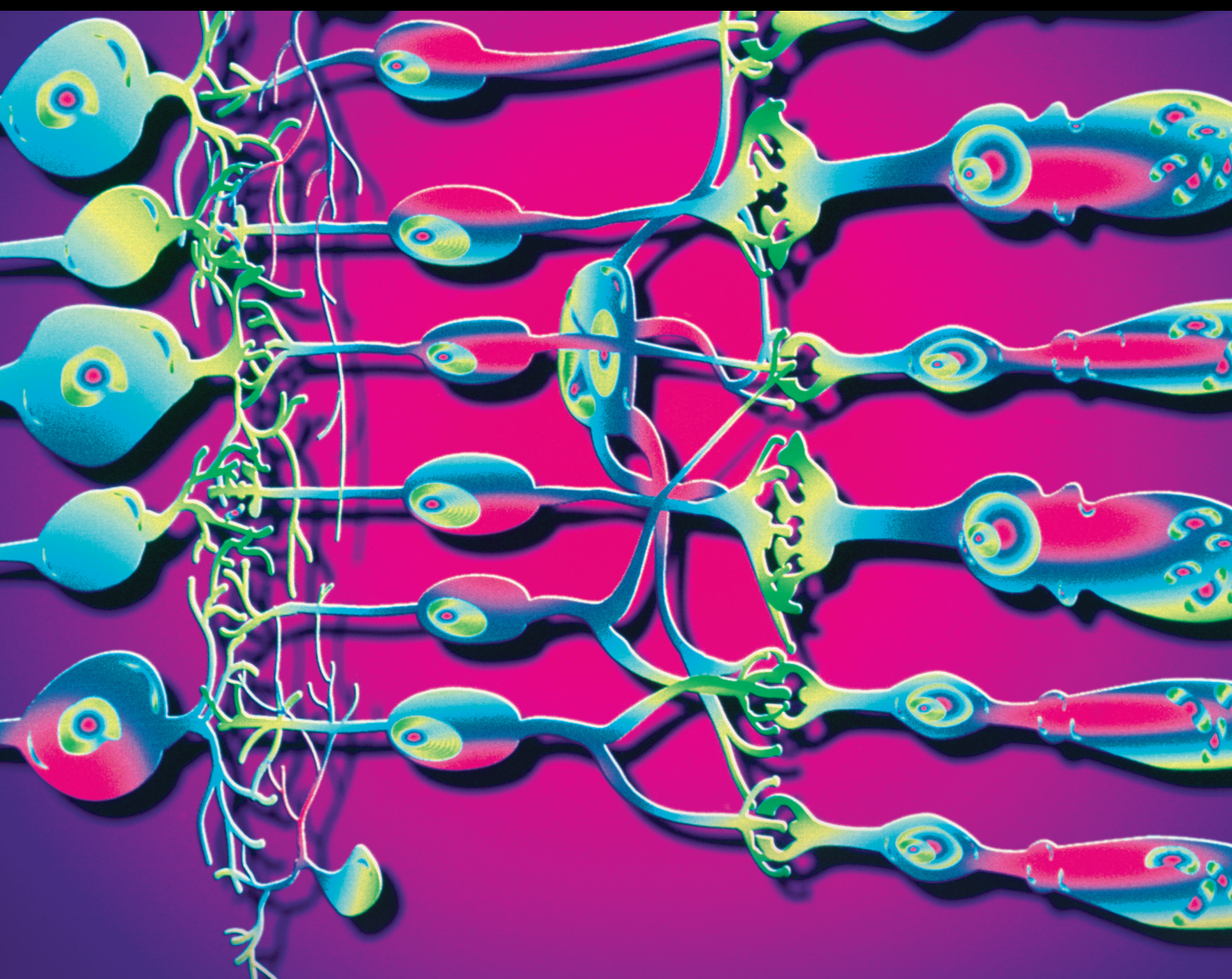

Novel Diagnostic and Therapeutic Methods in Ocular Surface and Corneal Diseases

Journal of Ophthalmology

Novel Diagnostic and Therapeutic Methods in Ocular Surface and Corneal Diseases

Guest Editors: Anna K. Nowinska, László Módis, Robert Koprowski, and Jesús Merayo-Lloves

Editorial Board

Contents

Hindawi
Journal of Ophthalmology
Volume 2017, Article ID 6137821, 2 pages
https://doi.org/10.1155/2017/6137821

Editorial

Novel Diagnostic and Therapeutic Methods in Ocular Surface and Corneal Diseases

Anna K. Nowinska,[1] László Módis,[2] Robert Koprowski,[3] and Jesús Merayo-Lloves[4]

[1]*Clinical Department of Ophthalmology, School of Medicine with the Division of Dentistry in Zabrze, Medical University of Silesia, Katowice, Poland*
[2]*Department of Ophthalmology, University of Debrecen, Debrecen, Hungary*
[3]*Department of Biomedical Computer Systems, Faculty of Computer Science and Materials Science, Institute of Computer Science, University of Silesia, Sosnowiec, Poland*
[4]*Instituto Oftalmológico Fernández-Vega, Oviedo, Spain*

Correspondence should be addressed to Anna K. Nowinska; anna.nowinska@sum.edu.pl

Received 14 March 2017; Accepted 14 March 2017; Published 16 April 2017

Noninfectious, chronic ocular surface and corneal diseases involve disorders in which structural changes are caused by various pathomechanisms including, but not limited to, inflammation, degeneration, autoimmunization, or dystrophy.

In the last 10 years, there has been a huge progress in our understanding of corneal disorders due to the availability of new in vivo imaging techniques, such as confocal microscopy, optical coherence tomography, corneal topography, or aberrometry. Recent advances in treatment methods include new cellular and medical, topical therapy with new biotechnology agents and novel treatment methods of keratoconus as well as further improvement of keratoplasty procedures.

Authors contributed a range of papers including 2 original research on novel anterior eye segment diagnostic methods and 5 original research on innovative ocular surface therapies.

A brief description of these 7 works is detailed below.

Novel diagnostic methods are the following.

The paper authored by R. Koprowski and L. Tian proves that blood pulsation has a statistically significant effect on the results of intraocular pressure measurement performed by Corvis Scheimpflug tonometer. The range of changes in the intraocular pressure measurement is high and can vary up to ±2.31 mmHg. For this reason, authors propose that, in modern ophthalmic devices, the measurement should be synchronized with the heartbeat phases.

The study "Keraring Intrastromal Segment Depth Measured by Spectral-Domain Optical Coherence Tomography in Eyes with Keratoconus" addresses a clinical problem of keratoconus surgery and intrastromal corneal ring segment (ICRS) implantation. The agreement between measured and intended distance of ICRS from the anterior and posterior corneal surfaces was evaluated. The authors proposed a method to analyze the implantation depth of the ICRS in the corneal stroma by measuring the distance of the inner corner from the posterior corneal surface which showed the best agreement with the intended distance.

Novel therapeutic methods are the following.

K. Krysik et al. reported their results on surgical treatment of corneal perforations. The authors analyzed a study group of 247 eyes with corneal perforation with a 6-year observation period. The three surgical procedures, dependent on size and location of perforation, were performed: full-sized penetrating keratoplasty, corneoscleral patch graft, and anterior lamellar keratoplasty. Although a complex treatment approach, the complication rates observed by authors were very high: graft melting was reported in 45 eyes (18.2%), glaucoma was diagnosed in 69 eyes (28%), and reinfections were reported in a total of 34 eyes (13.7%). Based on their observation, the authors claim

Hindawi
Journal of Ophthalmology
Volume 2017, Article ID 1582532, 6 pages
https://doi.org/10.1155/2017/1582532

Research Article

Differences in Surgical Management of Corneal Perforations, Measured over Six Years

Katarzyna Krysik,[1] Dariusz Dobrowolski,[1,2] Anita Lyssek-Boron,[1] Judyta Jankowska-Szmul,[2] and Edward A. Wylegala[2]

[1]*Department of Ophthalmology with Pediatric Unit, St. Barbara Hospital, Trauma Center, Medykow Square 1, 41200 Sosnowiec, Poland*
[2]*Clinical Departament of Ophthalmology, School of Medicine with the Division of Dentistry in Zabrze, Medical University of Silesia in Katowice, District Railway Hospital, Panewnicka 65 St., 40760 Katowice, Poland*

Correspondence should be addressed to Dariusz Dobrowolski; dardobmd@wp.pl

Received 2 October 2016; Revised 1 January 2017; Accepted 2 February 2017; Published 23 February 2017

Academic Editor: Achim Langenbucher

Purpose. To report the surgical approach, anatomical and functional results, and complications in the group of patients with corneal perforation. *Materials and Methods*. 247 eyes with corneal perforation were operated on between January 2010 and July 2016. The three surgical procedures, dependent on size and location of perforation, were performed: full-sized penetrating keratoplasty, corneoscleral patch graft, and anterior lamellar keratoplasty. The eyes underwent the minimum 6-month follow-up visit. *Results*. Between January 2010 and July 2016, 247 surgeries were performed: 116 penetrating keratoplasties, 117 corneoscleral patch grafts, and 14 anterior lamellar keratoplasties. More than one procedure was necessary in 32 eyes. Final improvement of the visual acuity, within a gain of 2 or more lines with the Snellen test, was achieved in 56 operated eyes. To achieve better final visual acuity, 75 eyes required successive surgical treatment. Complications of the surgery comprised persistent epithelial defect, glaucoma or ocular hypertension, corneal oedema, graft melting, loose corneal sutures, reinfection, anterior synechiae and fibrinoid membranes, and endophthalmitis. In 26 eyes, the treatment failure was reported. *Conclusions*. There is no one general-purpose surgical technique to treat corneal perforations. The complex nature of this pathology remains the individual, careful but also very distinct and multifactorial approach.

1. Introduction

Corneal perforation is a common condition, and it can lead to profound vision loss and severe ocular morbidity. It can be caused by infection, bacterial and noninfectious ocular surface disorders, immune disorders, and trauma. Other conditions such as xerosis, exposure, neurotrophic disorders, corneal degeneration, and ectasia and surgical and toxic/keratolytic treatment can lead to corneal perforation. Primary or secondary epithelial defects facilitate the development of corneal inflammation with subsequent perforation [1, 2].

A diagnosis of corneal perforation does not always require immediate surgical treatment. The primary goal in repairing the corneal perforation is to achieve a watertight globe with structural integrity in order to prevent severe complications such as globe tissue prolapse, endophthalmitis, and glaucoma [1, 3]. Frequently, the surgical procedure first provides temporary treatment, and the final treatment to restore visual function involves a multistage surgical approach. The therapeutic procedure and its timing depend on various conditions, such as cause, location, size of perforation, corneal infiltration and melting, and state of internal globe tissues [1, 4–7].

The nonsurgical approach includes limitation of inflammation, the treatment of coexistent infection, the use of anticollagenase and antiglaucomatous treatment, and the optimization of epithelial healing (bandage soft contact lenses, autologous serum eye drops, and punctal occlusion) [1, 8]. Surgical treatment includes tissue adhesives, amniotic

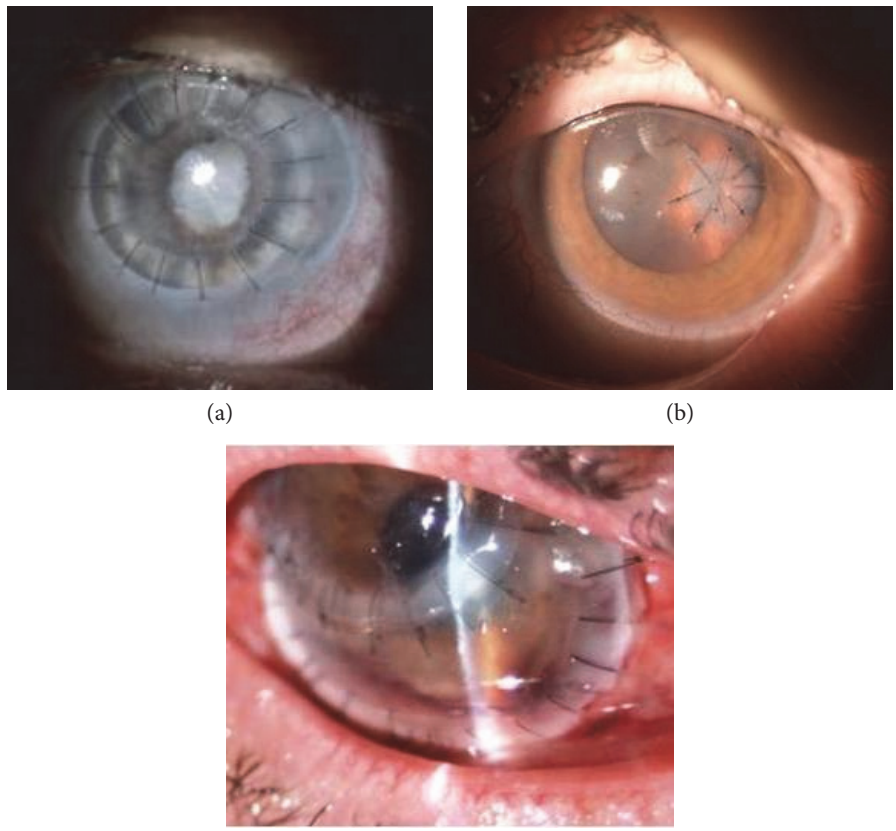

(a) (b) (c)

Figure 1: Surgical procedures applied in corneal perforations: (a) full-sized penetrating keratoplasty in fungal keratitis, (b) corneoscleral patch graft in RA patient, and (c) anterior lamellar keratoplasty in necrotizing peripheral keratitis.

membrane transplants, conjunctival flaps, pericardial membranes, tarsorrhaphy, and therapeutic ptosis with botulinum toxin [1, 6, 9–12].

The surgical procedure of tectonic keratoplasty is used to restore globe integrity. This procedure includes full-thickness penetrating keratoplasty, anterior lamellar keratoplasty (ALK), and corneal patch grafts. Penetrating keratoplasty (PK) is limited to large perforations with extensive necrosis [2–5, 13, 14]. In peripheral corneal perforations and descemetoceles and when the perforation is relatively small (i.e., it does not require full-sized penetrating keratoplasty but is too large for tissue adhesive) [1, 15, 16], tectonic corneoscleral patch grafting is performed as a temporary or definitive treatment. Lamellar keratoplasty is performed in the case of leaking descemetocele, to reinforce the thinned and necrotic stroma, and in corneal perforations. The advantage of this method is lower risk of corneal rejection [17, 18].

The aim of this study is to report on a sample of patients who underwent surgical treatment for corneal perforation. We report on the surgical techniques, anatomical and functional results, and complications of treatment in this group of patients.

2. Materials and Methods

This study was a retrospective review of the surgical treatment of 247 eyes with corneal perforation, which were operated between January 1, 2010, and July 31, 2016, at the Ophthalmology Department of Saint Barbara Hospital, Trauma Center, Sosnowiec, Poland. The analysed data from the medical records included demographics, medical history, corrected-distance preoperative and postoperative Snellen visual acuity, details, outcome and complications of surgery, and ocular integrity. All patients with diagnosed corneal perforation who underwent complete ocular examination were treated using one of three surgical techniques: full-sized penetrating keratoplasty (Figure 1(a)), corneal or corneoscleral patch grafts of varying sizes and shapes (Figure 1(b)), and anterior lamellar keratoplasty (Figure 1(c)). The main purpose of the treatment was to achieve the structural integrity of the globe. The choice of surgical procedure depended on the size and location of the perforation, the state of the internal ocular tissues, and intraocular infection. Surgeries were done as quickly as possible after diagnosis of disease origin was established and sufficient topical and general treatment was administered.

Size was classified according to three groups: small (0.1–2.5 mm diameter), medium (2.5–5.0 mm diameter), and large (over 5.0 mm diameter). Location was categorised as central (involving visual axis, ≤5.0 mm diameter of the central cornea), paracentral (zone over 5.0 mm up to 8.0 mm), or peripheral (≥8.0 mm, also including the limbus). If the perforation was small or medium and the visual axis was free of pathology, corneoscleral patch grafting was

usually performed. For large perforations with intensive corneal melting or thinning, necrosis, and internal bulbar tissue injury, penetrating keratoplasty was the preferred surgical approach. Fresh corneas were applied for each trephination. The graft diameter was 2.5–12.0 mm, with an oversize of 0.5–1.0 mm, and the donor-recipient junction was sewn by 10-0 nylon interrupted sutures. Anterior lamellar therapeutic keratoplasties were performed for leaking descemetoceles, and they depended on the depth and severity of the corneal pathology. All surgical procedures were performed under local or general anaesthesia. The donor corneas originated from our own or cooperative tissue banks. For PK, we used a Hanna vacuum trephine system (Moria Inc., Antony, France); for ALK, a manual or automated technique was employed, using a femtosecond laser (FL-assisted lamellar keratoplasties) or microkeratome dissection (Hanna trephine). The freehand technique was applied for corneoscleral patch grafts. Additional treatment was given according to the aetiology. All patients were hospitalised for the first 3–7 days after operation and were followed up every two weeks for a period of two months, monthly for a minimum of six months, and at differing intervals thereafter.

Table 1: Surgical techniques and indications for surgery in corneal perforation.

Characteristics	Total *n* (%) (*n* = 247)	Female *n* (%) (*n* = 125)	Male *n* (%) (*n* = 122)
Penetrating keratoplasty (PK)	116 (47.0)	60 (52)	56 (48)
Indication for surgery			
Infection	60 (24.3)	36 (28.8)	24 (19.7)
Inflammation	33 (13.4)	17 (13.6)	16 (13.1)
Ocular trauma	23 (9.3)	7 (5.6)	16 (13.1)
Patch graft (PK)	117 (47.3)	56 (48)	61 (52)
Indication for surgery			
Infection	47 (19.0)	22 (17.6)	25 (20.5)
Inflammation	54 (21.9)	27 (21.6)	27 (22.1)
Ocular trauma	16 (6.5)	7 (5.6)	9 (7.4)
ALK	14 (5.7)	9 (64)	5 (36)
Indication for surgery			
Infection	4 (1.6)	3 (2.4)	1 (0.82)
Inflammation	7 (2.8)	5 (4.0)	2 (1.64)
Ocular trauma	3 (1.2)	1 (0.8)	2 (1.64)

3. Results

Between January 1, 2010, and July 31, 2016, 247 surgeries for corneal perforations were performed. This involved 125 procedures in the group of 81 females, where the mean age was 65.22 ± 15.4 (range 9–90 years), and 122 procedures in the group of males, where the mean age was 57.56 ± 17.07 (range 20–88 years). To restore ocular integrity, more than one procedure in each eye was required for 21 females (26%) and for 11 males (11%). Two patients presented bilateral perforation. A 69-year-old female with rheumatoid arthritis was operated four times, twice in both eyes with penetrating keratoplasty. Because of the size and location of the corneal perforation, penetrating keratoplasty was the method of choice. A 38-year-old male with primary immunodeficiency also presented bilateral perforation. For his right eye, two corneoscleral patch grafts and one penetrating keratoplasty were performed, and one penetrating keratoplasty and one anterior lamellar keratoplasty were performed for his left eye.

There were 125 surgical tectonic procedures in the female group with corneal perforation. This comprised 60 penetrating keratoplasties (48%), 56 corneoscleral patch grafts (45%), and 9 anterior lamellar keratoplasties (7%), including 3 FL-assisted procedures. In the male group of patients, 122 tectonic procedures were performed, comprising 56 penetrating keratoplasties (46%), 61 corneoscleral patch grafts (50%), and 5 anterior lamellar keratoplasties, including 2 FL-assisted procedures. The penetrating approach was chosen for cases with large, full-thickness stromal involvement (infections, melting). For cases with local lesions, we preferred patch grafts. Such eyes included peripheral perforations (29%) and central or paracental disorders (18.1%). Surgical host's bed preparation with removal of necrotic tissue was done in each case. Lamellar surgery was done; despite leakage for exposed Descemets' membrane, we were able to continue surgery with lamellar separation of the affected tissue.

Three main causes of corneal perforation were reported. The most common cause was infection (45%), mainly bacterial (76%); inflammatory conditions (38%), mainly autoimmune causes; and ocular trauma (17%), mainly alkali burns (86%). The indications and details of the surgical tectonic treatment of the corneal perforations are presented in Tables 1 and 2.

Initial treatment after surgery included broad-spectrum antibiotic/antimycotic (fluoroquinolones (moxiflixacin or levofloxacin), aminoglycosides (gentamycin), fluconazole, voriconazole, and amphotericin B); steroid (dexamethasone 5 times a day); lubricants (including autologous serum); and general antibiotics, steroids, immunosuppressive agents (azathioprine, mofetil mycophenolate). In majority of cases, the individual approach was confirmed by microbiologists and rheumatologists to establish balance between antimicrobial agents and immunosuppressive drugs. Modifications were applied according to progress of the disease. Topical antimicrobial therapy was routinely applied for 21 days, extended if needed. Steroid doses were lowered (each month 1 drop less) to stop before the 6th month of therapy. Instable epithelia needed persistent intensive lubrication up to each hour of administration.

Final improvement of visual acuity, within a gain of two or more lines with the Snellen test, was achieved in 56 operated eyes (22.7%), that is, for 29 females (52%) and 27 males (48%). VA improvement was observed in 8 of 14 in the lamellar keratoplasty group, 32 of 116 in the penetrating keratoplasty group, and 16 of 117 in the corneoscleral patch graft group. Initial VA ranged no light perception to 20/30 before treatment, and final VA ranged no light perception to 20/25.

Table 2: Subgroups of indications for each surgical treatment.

Indications	Subgroup	PK *n* (%)	PG *n* (%)	ALK *n* (%)
Infections	Bacterial	45 (38.7)	41 (35.9)	2 (14.2)
	Fungal	12 (10.3)	6 (5.1)	2 (14.2)
	Viral	3 (2.5)	0	0
Inflammatory disorders	Rheumatoid	26 (22.4)	33 (28.2)	2 (14.2)
	Neurotrophic	5 (4.3)	10 (8.5)	3 (21.4)
	Mooren's ulcer	0	8 (6.8)	2 (14.2)
	Lyell's syndrome	1 (0.8)	2 (1.7)	0
	OCP	1 (0.8)	1 (9.8)	0
Traumatic	Alkali burn	12 (10.3)	7 (5.9)	3 (21.4)
	Melting	10 (8.6)	7 (5.9)	0
	Acidic burn	1 (0.8)	2 (1.7)	0

Table 3: Successive surgical treatment after primary tectonic keratoplasty.

Surgical technique	Total *n* (%) (*n* = 75)	Female *n* (%) (*n* = 31)	Male *n* (%) (*n* = 44)
PK	15 (20.0)	9 (29.0)	6 (13.6)
PK with cataract surgery and PC IOL implantation	11 (14.7)	4 (12.9)	7 (15.9)
Cataract surgery with PC IOL implantation	19 (25.3)	8 (25.8)	11 (25.0)
Secondary in-the-bag PC IOL implantation	5 (6.7)	4 (12.9)	1 (2.3)
Secondary in-the-sulcus PC IOL implantation	4 (5.3)	0	4 (9.1)
Transscleral fixation of IOL	8 (10.7)	2 (6.5)	6 (13.6)
Iridoplasty	6 (8.0)	2 (6.5)	4 (9.1)
Pars plana vitrectomy (PPV)	3 (4.0)	1 (3.2)	2 (4.6)
PPV with cataract surgery and PC IOL implantation	4 (5.3)	1 (3.2)	3 (6.8)

Seventy-five eyes (30.4%) of 31 females and 44 males treated initially for corneal perforation required successive surgical treatment to achieve useful visual acuity. Table 3 presents the successive procedures performed to improve visual acuity.

There were various complications of the surgical treatment. The most common complication was persistent epithelial defect, reported in 121 eyes (49%). Many of them occurred in PK patients with a diameter of the graft greater than 5 mm (37.1%). There were patients with all types of infections (14.5%), autoimmune diseases (7.6%), and burns (7.6%). The main reason for persistent epithelium was decreased corneal sensitivity. The same reason with insufficient tearing was observed in the patch graft group suffering from autoimmune diseases. Both caused epithelium loss in patch graft performed for bacterial and viral ulcer (6.4%) or in disorders combined with rheumatoid diseases (8.0%). Treatment of erosions was based on application of 20% solution of autologous serum combined with an antibiotic agent and dexamethasone 3 times a day. In 17 eyes, additionally, an amniotic membrane was applied for 2 weeks to support reepithelialisation. Further evolution of persistent erosion to stromal melting caused a need of re-PK or PK in the PG/ALK group.

Graft melting was reported in 45 eyes (18.2%). This complication was common in PK and PG groups. 10 PKs for bacterial and one for fungal infection developed necrosis in the periphery of the graft. The treatment focused on intensive antimicrobial treatment. In failed cases, 8 re-PKs were done with a large oversize to cover infected stroma. Patch graft performed for perforations due to local infections developed melting in 16 cases; 12 patients with rheumatoid arthritis and 4 with neurotrophic ulcer also presented signs of graft necrosis with involvement of surrounding host's stroma in 12 eyes. This enlargement of necrosis caused a need of penetrating keratoplasty in 12 eyes. Corneal suture loosening was reported in 43 eyes (17.4%). This factor was considered an initial factor in melts at the periphery of small grafts if combined with autoimmune origin of the primary disease.

Glaucoma or ocular hypertension was reported in 69 eyes (28%). Majority of them were treated with 1 or 2 topical agents (timolol 0.5%, brimonidine) or referred to trabeculectomy in 16 cases.

Corneal oedema was reported in 56 eyes (22.7%): 12 cases of PK and 44 patch grafts. Persistent oedema in PK patients in 6 cases caused a need to exchange the lenticule. 18.6% of eyes developed stromal vasculature. Risk of that complication rises with the diameter of the graft and the distance to the limbus. Keratoplasties with a diameter over 8 mm developed neovascularisation in a graft-host interface in 14 cases for overall 32 such interventions. Patch grafts in autoimmune

disorders (rheumatoid arthritis, Mooren's ulcer) presented vascular ingrowths in graft bed in over 50% of cases, commonly present in periphery.

Reinfections, as mentioned before, were reported in total 34 eyes (13.7%), anterior synechiae and fibrin retrocorneal membranes, reported in 17 eyes (6.8%), and endophthalmitis, reported in 7 eyes (3%). In 26 eyes (10.5%) with corneal perforation, despite repeated surgical treatment and intensive pharmacological treatment, treatment failure was reported. There was loss of light perception in 11 eyes (4.4%), persistent hypotony in 4 eyes (1.6%), and retinal detachment in 5 eyes (2.0%); in 4 eyes (1.6%), evisceration was necessary.

4. Discussion

Our study aimed to achieve and maintain anatomical and functional integrity of the ocular surface. This was possible using corneal donor tissues originating from ocular tissue banks. We used three types of tectonic corneal grafts: penetrating keratoplasty, anterior lamellar keratoplasty, and corneoscleral patch graft. The grafts varied in size, shape, and position, depending on the aetiology, extensity, location, and infiltration of the corneal tissue. In addition, the state of the internal bulbar tissues determined the time and method of the surgical approach. We operated on various corneal perforations that were the result of infection (mainly bacterial), inflammatory disease (mainly collagen vascular diseases), and trauma.

Surgical techniques such as lamellar keratoplasties, patch grafting, and keratolimbal allografting have become more popular in recent times [2, 19, 20]. In our department, corneoscleral patch grafts have been used in peripheral or less frequently central corneal perforations only since 2006. Since 2010, our department has also performed FL-assisted anterior lamellar keratoplasties for corneal perforations.

In the current study, we reported that the therapeutic approach to corneal perforation is challenging and unpredictable. The tectonic keratoplasties used in our study are often more favourable in cases of stomal involvement by necrosis than local or general medication, using adhesive tissues or other forms of treatment. Frequently, there is only one possible approach to restore ocular surface integrity. Removal of infected tissue decreases the risk of endophthalmoitis (the rate of that complication is really low—3%). In autoimmune diseases, therapeutic graft restores stromal integrity and delivers the basement membrane of the epithelium. However, it does not exclude support of epithelial healing, which in cases with necrosis is very slow.

A very important aspect of surgical treatment for corneal perforation is the availability of tissue necessary for the procedure. When there is no donor cornea, the amniotic membrane should be accesible or we need to use a conjunctival flap to restore ocular surface integrity temporarily or definitely [6, 9].

In our sample of patients with corneal perforation who were treated with lamellar keratoplasty, the advantage of this surgical technique conferred lower risk of subsequent allograft rejection and graft failure. This is the result of the preservation of recipient endothelium [5, 18, 21]. On the other hand, there is a risk of stromal or epithelial graft failure, with subsequent visual loss, in this type of corneal graft [21]. Our patients who underwent surgical treatment with ALK more frequently demonstrated an improvement in visual acuity than did patients after other treatment methods (57% versus 27.6% after penetrating keratoplasty and 13.7% after corneoscleral patch graft) [18]. The size, location, and aetiology of the corneal perforation also contribute to visual acuity [4, 6].

Penetrating keratoplasty also remains more popular than anterior lamellar keratoplasty because of the lower risk of donor tissue injuries, such as Descemet membrane perforation [18, 20].

In cases of corneal perforation originating from infectious keratitis, we strongly advise antibacterial, antifungal, or antiviral general and topical intensive medication as the first treatment before surgical treatment. This is not always possible, and the sequence of procedures and timing of the surgery also depend on the control and severity of the infection and globe integrity [1, 4].

The functional result of the surgical treatment of the corneal perforation is often secondary to anatomical disorders. Visual outcomes are not so important in the first surgical approach; a stable, watertight ocular surface is the first goal of treatment of corneal perforation. Grafts in eyes with perforations have usually active primary ocular disease. It is better and more predictive in results when the ocular surface is quiet. Active infection, inflammation, or other conditions present before remained immediately after surgery.

To achieve the best final results of treatment, we had to perform different and often multistage surgical procedures, spread over time [4]. Repeat penetrating keratoplasty was the most frequent treatment in our study group, because of corneal scars and allograft rejection, especially in eyes with active keratitis. In 14.7% of reoperated eyes, repeat penetrating keratoplasty was performed simultaneously with cataract extraction and PC IOL implantation. Cataract surgery alone or secondary intraocular lens implantation in aphakic eyes was also beneficial for restoring better visual acuity. With more complicated cases after tectonic keratoplasty, such as in 7 eyes (9.3%) with previous intrabulbar inflammation with inflammatory membranes and vitreoretinal tractions or retinal detachment, pars plana vitrectomy was necessary to improve visual outcome.

In summary, our results of the surgical treatment of corneal perforations show that there is no one-size-fits-all surgical approach to corneal perforation. Because of the complex nature of the tectonic indications for surgery and their modalities, it is very difficult to present final and unequivocal forms of treatment. The choice of surgical technique and the results of surgical treatment depend on numerous factors. The further development of surgical and lamellar surgical techniques applied in corneal perforations is also necessary.

Competing Interests

The authors declare that there is no conflict of interest regarding the publication of this paper.

References

[1] V. Jhanji, A. L. Young, J. S. Mehta, N. Sharma, T. Agarwal, and R. B. Vajpayee, "Management of corneal perforation," *Survey of Ophthalmology*, vol. 56, no. 6, pp. 522–538, 2011.

[2] H. Yokogawa, A. Kobayashi, N. Yamazaki, T. Masaki, and K. Sugiyama, "Surgical therapies for corneal perforations: 10 year of cases in a tertiary referral hospital," *Clinical Ophthalmology*, vol. 8, pp. 2165–2170, 2014.

[3] D. Loya-Garcia, J. C. Serna-Ojeda, L. Pedro-Aguilar, A. Jimenez-Corona, A. Olivo-Payne, and E. O. Graue-Hernandez, "Non-traumatic corneal perforations: aetiology, treatment and outcomes," *The British Journal of Ophthalmology, Electronic Publication*, 2016.

[4] M. Ang, J. S. Mehta, C. C. A. Sng, H. M. Htoon, and D. T. Tan, "Indications, outcomes, and risk factors for failure in tectonic keratoplasty," *Ophthalmology*, vol. 119, no. 7, pp. 1311–1319, 2012.

[5] A. Anshu, A. Parthasarathy, J. S. Mehta, H. M. Htoon, and D. T. Tan, "Outcomes of therapeutic deep lamellar keratoplasty and penetrating keratoplasty for advanced infectious keratitis," *Ophthalmology*, vol. 116, no. 4, pp. 615–623, 2009.

[6] M. Bouazza, A. A. Bensemlali, M. Elbelhadji et al., "Non-traumatic corneal perforations: therapeutic modalities," *Journal Français d'Ophtalmologie*, vol. 38, no. 5, pp. 395–402, 2015.

[7] Y. F. Yao, Y. M. Zhang, P. Zhou, B. Zhang, W. Y. Qiu, and S. C. Tseng, "Therapeutic penetrating keratoplasty in severe fungal keratitis using cryopreserved donor corneas," *The British Journal of Ophthalmology*, vol. 87, no. 5, pp. 543–547, 2003.

[8] A. Poon, G. Gerd, J. K. G. Dart, G. E. Fraenkel, and J. T. Daniels, "Autologous serum eyedrops for dry eyes and epithelial defects: clinical and in vitro toxicity studies," *The British Journal of Ophthalmology*, vol. 85, no. 10, pp. 1188–1197, 2001.

[9] M. Berguiga, E. Mameletzi, M. Nicolas, D. Rivier, and F. Majo, "Long-term follow-up of multilayer amniotic membrane transplantation for non-traumatic corneal perforations or deep ulcers with descemetocele," *Klinische Monatsblätter für Augenheilkunde*, vol. 230, no. 4, pp. 413–418, 2013.

[10] J. I. Weiss, P. Williams, R. L. Lindstrom, and D. J. Doughman, "The use of tissue adhesive in corneal perforations," *Ophthalmology*, vol. 90, no. 6, pp. 610–615, 1983.

[11] P. Prabhasawat, N. Tesavibul, and W. Komolsuradej, "Single and multilayer amniotic membrane transplantation for persistent corneal epithelial defect with and without stromal thinning and perforation," *The British Journal of Ophthalmology*, vol. 85, no. 12, pp. 1455–1463, 2001.

[12] A. Azuara-Blanco, C. T. Pillai, and H. S. Dua, "Amniotic membrane transplantation," *The British Journal of Ophthalmology*, vol. 83, pp. 399–402, 1999.

[13] M. Vanathi, N. Sharma, J. S. Titiyal, R. Tandon, and R. B. Vajpayee, "Tectonic grafts for corneal thinning and perforations," *Cornea*, vol. 21, no. 8, pp. 792–797, 2002.

[14] H. Kazuomi, I. Sho, M. Osamu, and Y. Akitoshi, "Therapeutic keratoplasty for corneal perforation: clinical results and complications," *Cornea*, vol. 27, no. 2, pp. 156–160, 2008.

[15] C. Vasseneix, D. Toubeau, G. Brasseur, and M. Muraine, "Surgical management of nontraumatic corneal perforations: an 8-year retrospective study," *Journal Français d'Ophtalmologie*, vol. 29, no. 7, pp. 751–762, 2006.

[16] M. Fernandes and D. Vira, "Patch graft for corneal perforation following trivial trauma in bilateral Terrien's marginal degeneration," *Middle East African Journal of Ophthalmology*, vol. 22, no. 2, pp. 255–257, 2015.

[17] J. H. Jang and S. D. Chang, "Tectonic deep anterior lamellar keratoplasty in impending corneal perforation using cryopreserved cornea," *Korean Journal of Ophthalmology*, vol. 25, no. 2, pp. 132–135, 2011.

[18] M. Ang, J. S. Mehta, A. Arundhati, and D. T. H. Than, "Anterior lamellar keratoplasty over penetrating keratoplasty for optical, therapeutic, and tectonic indications: a case series," *American Journal of Ophthalmology*, vol. 147, no. 4, pp. 697–702, 2009.

[19] J. C. Park and N. E. Habib, "Tectonic lamellar keratoplasty: simplified management of corneal perforations with an automated microkeratome," *Canadian Journal of Ophthalmology*, vol. 50, no. 1, pp. 80–84, 2015.

[20] P. C. Maier, F. Birnbaum, and T. Reinhard, "Therapeutic applications of the femtosecond laser in corneal surgery," *Klinische Monatsblätter für Augenheilkunde*, vol. 227, no. 6, pp. 453–459, 2010.

[21] S. L. Watson, S. J. Tuft, and J. K. G. Dart, "Patterns of rejection after deep lamellar keratoplasty," *Ophthalmology*, vol. 113, no. 4, pp. 556–560, 2006.

that the therapeutic approach to corneal perforation is challenging and unpredictable. The further development of surgical and lamellar surgical techniques applied in corneal perforations is also necessary.

In the paper titled "A Novel Technique for Conjunctivoplasty in a Rabbit Model: Platelet-Rich Fibrin (RRF) Membrane Grafting" by M. E. Can et al., the effect of platelet-rich fibrin membrane (PRFM) on wound healing in experimental conjunctival tissue damage was investigated. PRF membrane was proved to have the beneficial effects on conjunctival healing. Besides its chemical effects, it provides mechanical support as a scaffold for the migrating cells that are important for the ocular surface regeneration. Authors promising results on PRF membrane application could encourage surgeons to applicate autologous PRF membrane as a growth factor-enriched endogenous scaffold for ocular surface reconstruction.

The authors of the paper "Biocompatibility and Biomechanical Effect of Single Wall Carbon Nanotubes Implanted in the Corneal Stroma: A Proof of Concept Investigation" conducted an experimental investigation where New Zealand rabbits were treated with a composition of carbon nanotubes (CNTs) suspended in balanced saline solution which was applied in the corneal tissue. Biocompatibility of CNTs has been previously reported in other fields of biology and medicine, for example, tissue engineering, regenerative medicine, drug delivery systems, and reinforcement of biological tissues. In the present study, it was found that carbon nanomaterials do not induce any inflammatory or foreign body reaction in the corneal stroma. The corneal biomechanical evaluation, as performed in this investigation, showed that there is a trend to obtain more rigidity of the corneal tissue after carbon nanostructure implantation, although these changes were not statistically significant. This method of treatment seems to be very promising in the variety of ectatic corneal disorders, but further research is necessary in order to comprehend and improve the biomechanical assessment of the present investigation and also to understand the potential use of these materials and this novel technology for the development of new applications of nanomedicine in visual sciences.

The purpose of the retrospective study "Active Pedicle Epithelial Flap Transposition Combined with Amniotic Membrane Transplantation for Treatment of Nonhealing Corneal Ulcers" was to evaluate the efficacy of active pedicle epithelial flap transposition combined with amniotic membrane transplantation in treating persistent corneal ulcer with epithelial nonhealing. The authors stated that the active epithelial flap inhibited inflammatory cell infiltration in the inflamed tissue and reduced the quantity of proteinases and cytokines released into the inflammatory cornea. Covering the ulcer with the active epithelial flap provided a relatively healthy substrate and microenvironment. This facilitated epithelial migration, reinforced basal epithelial adhesion, and promoted ocular surface healing. The proposed method has limitations, because this combined surgery is not suitable for corneal ulcers with a diameter exceeding 5 mm which are hard to make a peripheral epithelial flap to cover it. Despite its limitations, it seems a promising treatment method of the management of nonhealing corneal ulcers, which is one of the most difficult challenges faced by ophthalmologists.

Authors of the paper "Evaluation of Monocular Treatment for Meibomian Gland Dysfunction with an Automated Thermodynamic System in Elderly Chinese Patients: A Contralateral Eye Study" present a prospective, examiner-masked, contralateral eye clinical trial on the safety and efficacy of monocular treatment for elderly Chinese patients with meibomian gland dysfunction (MGD) with an automated thermodynamic system (LipiFLow). All patients had a significant reduction in dry eye symptoms accompanied by an increase of invasive tear breakup time (ITBUT) and meibomian glands yielding liquid secretion (MGYLS) and a reduction in corneal staining compared with the baseline parameters. LipiFlow was proved to be an effective treatment option for MGD.

Acknowledgments

We would like to extend our gratitude to all the authors who submitted their work for consideration in our special issue and to the reviewers for their critical feedback. We hope that this collection of works provides a new insight into diagnostic and treatment methods of corneal disorders.

Anna K. Nowinska
László Módis
Robert Koprowski
Jesús Merayo-Lloves

Hindawi
Journal of Ophthalmology
Volume 2017, Article ID 4313784, 9 pages
https://doi.org/10.1155/2017/4313784

Clinical Study

Keraring Intrastromal Segment Depth Measured by Spectral-Domain Optical Coherence Tomography in Eyes with Keratoconus

Ugo de Sanctis,[1] Carlo Lavia,[1] Marco Nassisi,[1] and Savino D'Amelio[2]

[1]*Department of Surgical Sciences, Eye Clinic, University of Turin, Turin, Italy*
[2]*Department of Eye Diseases, Ophthalmic Hospital of Turin, Turin, Italy*

Correspondence should be addressed to Ugo de Sanctis; ugo.desanctis@unito.it

Received 20 September 2016; Revised 13 December 2016; Accepted 29 December 2016; Published 2 February 2017

Academic Editor: Anna Nowinska

Purpose. To evaluate agreement between measured and intended distance of Keraring (Mediphacos, Belo Horizonte, Brazil) intracorneal ring segments from the anterior and posterior corneal surfaces. *Methods*. Twenty-six Keraring ICRS implanted in 24 keratoconic eyes were examined. The distance from the Keraring apex to the anterior corneal surface and the distance from the inner and the outer corners to the posterior corneal surface were measured 3 months postoperatively using spectral-domain optical coherence tomography. Agreement between measured distance and intended distance was assessed by calculating the absolute differences and 95% limits of agreement (95% LoA). *Results*. The mean absolute difference was significantly lower ($p < 0.001$) for the measurements taken at the inner corner (23.54 ± 15.90 μm) than that for those taken at the apex (108.92 ± 62.72 μm) and the outer corner (108.35 ± 56.99 μm). The measurements taken at the inner corner were within ±25 and ±50 μm of the intended distance in 15/26 (57.7%) and 24/26 (92.3%) cases, respectively, and showed the narrowest 95% LoA with the intended distance (−57.61 to 55.15 μm). *Conclusions*. The distance of the inner corner from the posterior corneal surface showed the best agreement with the intended distance. This measurement is suitable for determining whether the actual Keraring depth matches the intended depth.

1. Introduction

Intrastromal corneal ring segments (ICRS) are used for the surgical treatment of corneal ectasia [1–3]. These space-occupying elements are implanted into a tunnel created in the deep stroma at the midperiphery of the cornea. Segment implantation generates an arc-shortening effect that flattens the central cornea and reduces curvature asymmetry [4–6]. The depth of ICRS placement is planned according to individual corneal thickness and is crucial for achieving efficacy and safety of the procedure. Incorrect depth results in unpredictable changes in corneal curvature and increases the risk of complications such as corneal perforation, superficial erosion, and ring extrusion [7, 8].

The depth of ICRS in the corneal stroma can be assessed with different methods, including slit lamp biomicroscopy, rotating Scheimpflug camera, and optical coherence tomography (OCT). Slit lamp biomicroscopy is based on examiner impression and does not allow precise and quantitative estimation of the implant depth [8]. OCT examination permits imaging of the cornea at a higher resolution than the rotating Scheimpflug camera and measurement of the ICRS distance from the anterior and the posterior corneal surface.

A widely used implant is the Keraring (Mediphacos, Belo Horizonte, Brazil) ICRS, which is made of polymethyl methacrylate (PMMA) and has a triangular cross-section [2, 3]. It is inserted with the apex facing the anterior corneal surface and the base facing the posterior corneal surface. Several authors used the OCT to measure the distance from Keraring to the anterior corneal surface [9–11]. To the best of our knowledge, this is the first study to investigate the implant distance also with reference to the posterior corneal surface. We then evaluated the agreement between the measured and the intended distance to determine which measurement might be suitable to verify that segment depth matches intended depth.

2. Patients and Methods

This prospective observational case series comprised 24 eyes of 21 consecutive patients (mean age 35.2 ± 8.4 years, range 22–54) with keratoconus that underwent Keraring ICRS implantation at the Eye Clinic of Turin University between July 2014 and September 2015. The study was approved by the Institutional Review Board of the Ophthalmic Hospital of Turin and followed the tenets of the Declaration of Helsinki. The patients signed a consent form and they were aware of the nature of the study.

The patients were recruited at the Cornea Service according to the following criteria: age > 18 years, dissatisfaction with spectacle-corrected vision, and intolerance to contact lens use. Patients with corneal thickness < 400 μm, central corneal scarring, presence of other corneal diseases, and previous ocular surgery were excluded.

Preoperative data, surgical details, and postoperative results were recorded on a standardized form and entered in a computerized database. Preoperative data included patient age, Snellen uncorrected and corrected distance visual acuity (UDVA and CDVA), mean keratometry (Km) measured on a ring of 15° around the corneal apex (Pentacam HR, Oculus, Germany), and corneal thinnest point in the hypothetical tunnel area as measured by means of the OCT pachymetry map (RTVue 100, Optovue, USA). Surgical details included Keraring characteristics (model, arc length, and thickness), incision depth for tunnel creation, and intraoperative complications. Postoperative data included Snellen UDVA and CDVA, Km, and any complications.

2.1. Surgery. The surgical procedure was carried out under sterile conditions and topical anesthesia by a single surgeon (U.d.S.). The intrastromal tunnel was created via manual technique in 19 eyes and femtosecond laser technology (IntraLase 150 kHz, Advanced Medical Optics, Santa Ana, CA, USA) in 5 eyes. Preoperatively the corneal vertex was marked with a methylene blue-tinted Sinskey hook. In the manual technique, the tunnel was outlined on the corneal surface with a circular marker. A 1-mm entry incision was made with a calibrated, diamond square-bladed knife on the steepest axis. The incision depth was set at 80% of the thinnest point measured in the tunnel area. The corneal tunnel was then created with curved corneal dissectors. For the femtosecond laser procedures, the energy was set at 1.5 mJ to create a 1.4-mm entry incision on the steepest axis and the stromal tunnel. The incision and the tunnel depth were set at 70% of the thinnest point measured in the tunnel area. The Keraring ICRS were implanted with the manufacturer's forceps. The segment arc length and thickness were selected according to the manufacturer nomograms (other cited materials: Keraring Calculation Guidelines 2009; http://smmedical.cl/wp-content/uploads/2013/10/Agrupado.pdf). At completion of surgery, a bandage contact lens was placed on the cornea. Tobramycin 0.3% and dexamethasone 0.1% eye drops were prescribed 3 times a day for 1 month. Postoperative visits were scheduled at 1, 7, 30, and 90 days after surgery.

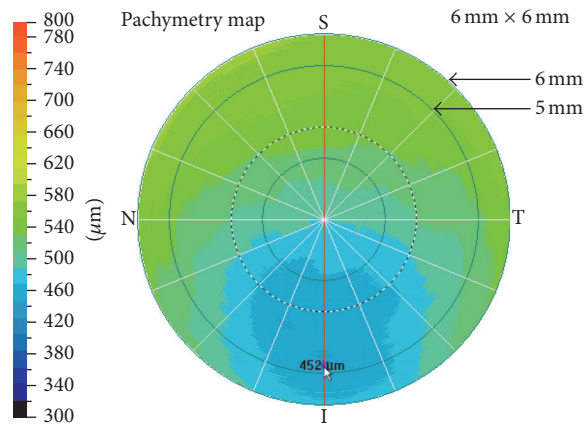

Figure 1: The pachymetry map in RTVue 100 is divided into a central circular area (0–2 mm), sixteen pericentral sectors (2–5 mm), and sixteen transitional sectors (5-6 mm). To find the thinnest point in the hypothetical tunnel area, the mouse cursor was slowly dragged along the transitional sectors between the 5-mm and the 6-mm ring. The lowest value found in that area was recorded as the thinnest point (452 μm in this case).

2.2. Spectral-Domain OCT Corneal Examination. One investigator (M.N.) scanned each cornea with RTVue100 (software version 2.6). This spectral-domain OCT uses a superluminescent diode (λ 830 nm) as light source. The effective acquisition speed is 26.000 A-scans/s. The depth and the transverse resolution are 5 μm and 15 μm, respectively. The instrument was equipped with the low magnification lens of the Corneal Adaptor Module that provides a scan length of 6 mm and a scan depth of 1.96-mm.

The Corneal Adaptor Module allows corneal examination with different scan patterns. The pachymetry map pattern was used to measure the thinnest point in the hypothetical tunnel area a few days before surgery. The high definition (HD) line pattern was used for measuring the Keraring depth inside the corneal stroma at 3 months after implantation. Using these scan patterns, the instrument software transforms the OCT optical images into physical images of the cornea by means of a dewarp calculation that takes into account corneal curvature and the index of refraction of the media [12, 13]. Only good quality scans showing a signal strength index (>30) were accepted as valid.

The pachymetry map pattern includes 8 meridional cross-section scans (6 mm in length, 1024 A-scans each) at 22.5-degree intervals automatically captured in 0.32 seconds. The computer algorithm generates a corneal thickness profile from each meridional scan and computes a color-coded pachymetry map by interpolation. The pachymetry map was centered on the corneal vertex and displayed on the instrument monitor. The examiner then slowly dragged the mouse cursor along the hypothetical tunnel area to find the thinnest point and calculate the incision depth (Figure 1).

The HD line pattern includes one meridional cross-section scan of the cornea (6 mm in length, 4096 A-scans) acquired automatically in 0.16 seconds. The scan was aligned so that it passed through the corneal vertex and Keraring center (Figure 2).

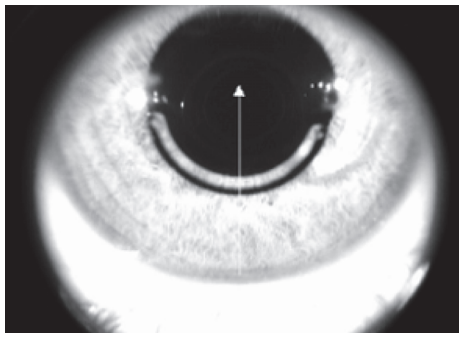

Figure 2: Enface OCT image of the Keraring showing the HD line scan aligned on the segment center and corneal vertex.

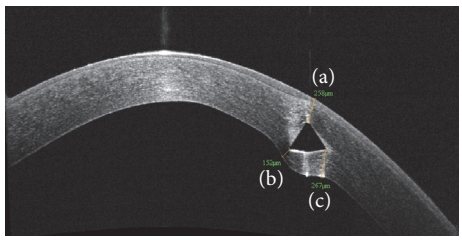

Figure 3: The segments traced to measure the distance from the apex to the anterior corneal surface (a) and the distance from the inner (b) and the outer (c) basal corners to the posterior corneal surface.

The HD line was displayed on the instrument monitor and the "distance" tool of the instrument software was selected. The mouse cursor was positioned at the Keraring apex, and a segment was traced to the anterior corneal surface. Using the mouse cursor, the distal point of segment was slowly dragged along the anterior corneal surface to identify the shortest segment. The length of this segment was recorded as the distance from the apex to the anterior corneal surface. The same procedure was done at the inner corner and the outer corner to measure the distance between them and the posterior corneal surface (Figure 3).

These measurements were taken by a second investigator (C.L.) in a separate session. The two sets of measurements were compared to assess interexaminer reproducibility. The first set of measurements was used to assess the difference with respect to the intended distance. The intended distance from the apex to the anterior corneal surface was the depth of the incision made to create the tunnel. The intended distance from the inner and the outer corners to the posterior corneal surface was the difference between the preoperative corneal thickness and the depth of the incision made to create the tunnel. For this calculation, the corneal thickness was measured on the preoperative pachymetry map. On this map, using the enface OCT image of the segment as a reference (Figure 2), the corneal thickness was measured at the point where the distance from the Keraring inner and outer corner to the posterior corneal surface was calculated.

2.3. Statistical Analysis. Statistical analysis was performed using STATA software package version 8.0 (StataCorp LP, College Station, TX, USA). The significance of differences between preoperative and postoperative data was assessed using Student's paired t-test for continuous variables and the Wilcoxon test for noncontinuous variables. The 95% limits of agreement (LoA) were calculated to estimate the agreement between examiners in measuring Keraring distance from the anterior and the posterior corneal surface and the agreement between the measured and the intended distance. The 95% LoA was calculated as described by Bland and Altman (95% LoA = mean difference ± 1.96 × SD) [14]. The absolute difference was calculated to assess the absolute value of the difference between the measured and the intended distance. A χ^2 or Fisher's exact test was used to determine the differences in the proportion of eyes in which the measured distance fell within ±25 μm and ±50 μm of the intended distance. Differences were considered statistically significant when p value was less than 0.05.

3. Results

Overall, 26 Keraring ICRS were implanted: one per eye in 22 cases and 2 per eye in 2 cases. Surgery was uneventful and no major postoperative complications, such as corneal infections or ICRS extrusion, were observed.

The Keraring characteristics, UDVA, CDVA, and Km, of each case are shown in Table 1.

The Keraring SI-5 model (inner diameter 4.40 mm, base width 0.60 mm) was used in 21 cases and the SI-6 model (inner diameter 5.40, base width 0.80 mm) in 5 cases. The mean UDVA and CDVA were significantly improved ($p < 0.001$) after surgery. On average, UDVA improved by 0.19 ± 0.17 and CDVA by 0.22 ± 0.15. The postoperative mean Km was significantly reduced ($p < 0.001$) as compared with the preoperative value.

The distance from Keraring to the anterior and the posterior corneal surface measured by the two examiners was not statistically different ($p < 0.05$). Individual differences between examiners are presented graphically through Bland-Altman plots (Figure 4).

The 95% LoA between examiners were −9.95 to 9.49 for the distance from the apex to the anterior corneal surface, −8.36 to 7.67 μm for the distance from the inner corner to the posterior corneal surface, and −11.19 to 10.50 μm for the distance from the outer corner to the posterior corneal surface.

The measured distance, intended distance, and absolute difference between the measured and the intended distance in each case are reported in Table 2.

The distance from the inner corner to the posterior corneal surface was not statistically different from the intended distance ($p = 0.83$). The distance from the apex to the anterior corneal surface was significantly less ($p < 0.001$) and the distance from the outer corner to the posterior corneal surface was significantly greater ($p < 0.001$) than the intended distance.

The mean absolute difference with respect to the intended distance was significantly lower ($p < 0.001$) for the distance from the inner corner to the posterior corneal surface as compared with those obtained for the other measurements.

Table 1: Keraring characteristics, uncorrected distance visual acuity (UDVA), corrected distance visual acuity (CDVA), and mean keratometry (Km) of each patient.

Case	Eye	Keraring		UDVA		CDVA		Km (D)	
		Model	Arc length (°)/ thickness (μm)	Pre	Post	Pre	Post	Pre	Post
1	RE	SI-5	160/300	0.04	0.10	0.50	0.80	50.15	48.68
2	LE	SI-5	120/200	0.10	0.10	0.60	0.70	50.82	49.77
		SI-5	120/200						
3*	LE	SI-5	160/250	0.10	0.10	0.40	0.70	49.31	45.12
4*	LE	SI-6	150/150	0.10	0.20	0.70	1.00	43.89	43.48
5*	RE	SI-5	160/300	0.30	0.80	0.50	1.00	45.27	43.41
6	LE	SI-5	160/250	0.10	0.20	0.60	1.00	42.98	41.19
7	RE	SI-5	160/250	0.30	0.60	0.70	0.90	51.49	49.00
8	RE	SI-5	160/250	0.08	0.60	0.60	0.90	45.39	43.68
	LE	SI-6	150/250	0.10	0.30	0.50	0.90	47.19	44.07
9	RE	SI-5	160/300	0.04	0.40	0.60	0.80	48.06	45.62
10	RE	SI-5	160/250	0.10	0.40	0.80	1.00	48.44	47.90
	LE	SI-5	160/200	0.20	0.40	0.90	1.00	49.45	46.15
11	RE	SI-5	160/300	0.10	0.10	0.70	0.80	50.10	49.31
12	RE	SI-6	150/200	0.40	0.80	0.90	0.90	46.48	45.74
	LE	SI-6	150/250	0.40	0.40	0.80	1.00	45.41	41.00
13	RE	SI-5	120/250	0.10	0.20	0.60	0.80	51.70	50.30
14	LE	SI-5	160/300	0.08	0.30	0.40	0.50	46.40	44.40
	LE	SI-5	90/150						
15	LE	SI-5	160/250	0.20	0.30	0.60	0.80	45.95	44.20
16*	LE	SI-5	160/250	0.10	0.60	0.50	0.80	50.30	50.00
17*	RE	SI-5	160/250	0.06	0.20	0.30	0.80	46.75	45.60
18	LE	SI-5	210/200	0.06	0.30	0.40	0.70	49.04	46.83
19	RE	SI-5	160/250	0.10	0.40	0.40	0.80	49.40	45.96
20*	RE	SI-6	150/300	0.10	0.40	0.80	0.80	46.12	45.17
21	RE	SI-5	160/300	0.10	0.10	0.50	0.70	45.64	41.19
MEAN				0.14	0.35	0.60	0.84	47.74	45.74
SD				0.10	0.21	0.17	0.13	2.44	2.79
Range				0.04–0.4	0.1–0.80	0.3–0.9	0.5–1	42.98–51.7	41–50.3

RE: right eye. LE: left eye. *Eyes with intrastromal tunnel created using femtosecond laser. SD: Standard Deviation. D: diopters.

The measurements taken at the inner corner were within ±25 μm and ±50 μm of the intended distance in 15/26 (57.7%) and 24/26 (92.3%) cases, respectively. For the measurements taken at the apex and the outer corner, the proportions were significantly ($p < 0.001$) lower (3/26 (11.5%) and 5/26 (19.2%) cases, resp.).

The 95% LoA between the measured and the intended distance was −231.85 to 14.01 μm for the distance from the apex to the anterior corneal surface, −57.61 to 55.15 μm for the distance from the inner corner to the posterior corneal surface, and −3.35 to 220.04 μm for the distance from the outer corner to the posterior corneal surface (Figures 5–7).

The pachymetry map and the Keraring OCT images of 5 representative patients are shown in Figure 8.

4. Discussion

In the postoperative assessment of patients implanted with ICRS, it is essential to determine whether the segment is actually lying at the intended depth. Any error in implantation depth may reduce procedure efficacy and increase the risk of complications. Actual depth may differ from intended depth due to inaccurate measurement of corneal thickness preoperatively or to creation of the stromal tunnel at the

Table 2: Keraring measured and intended distance from the anterior and the posterior corneal surfaces.

Case	Eye	Intended distance (μm)		Distance apex/ anterior surface (μm)		Distance inner corner/ posterior surface (μm)		Distance outer corner/ posterior surface (μm)	
		Anterior surface	Posterior surface	Measured	Absolute difference	Measured	Absolute difference	Measured	Absolute difference
1	RE	391	136	205	186	98	38	225	89
2	LE	333	176	287	46	120	56	207	31
		335	199	313	22	146	53	210	11
3*	LE	350	162	258	92	152	10	267	105
4*	LE	370	147	306	64	119	28	328	181
5*	RE	399	122	201	198	154	32	260	138
6	LE	377	125	216	161	157	32	266	141
7	RE	405	180	250	155	169	11	285	105
8	RE	400	100	302	98	98	2	198	98
	LE	358	118	343	15	101	17	239	121
9	RE	366	142	171	195	181	39	318	176
10	RE	344	118	167	177	143	25	285	167
	LE	357	121	215	142	154	33	260	139
11	RE	399	145	328	71	130	15	217	72
12	RE	400	152	303	117	173	21	314	162
	LE	401	160	198	203	176	16	359	199
13	RE	323	164	270	53	119	45	197	33
14	LE	356	125	255	101	126	1	251	126
	LE	354	190	321	33	190	0	245	55
15	LE	362	90	296	66	87	3	166	76
16*	LE	360	156	349	11	145	11	172	16
17*	RE	392	159	188	204	175	16	329	170
18	LE	383	120	318	65	98	22	142	22
19	RE	358	90	273	85	79	11	158	68
20*	RE	387	120	251	136	156	36	289	169
21	RE	400	125	264	136	164	39	272	147
MEAN		371.54	140.08	263.38	108.92	138.85	23.54	248.42	108.35
SD		24.42	28.93	54.16	62.72	31.78	15.90	57.32	56.99
RANGE		323–405	90–199	167–349	11–204	79–190	0–56	142–359	11–199

RE: right eye. LE: left eye. *Eyes with intrastromal tunnel created using femtosecond laser. SD: Standard Deviation.

wrong depth. Corneal thickness is conventionally measured using ultrasound pachymetry, which entails taking multiple measurements along the hypothetical tunnel area and can result in large interexaminer/intraexaminer variability in keratoconic corneas [15]. Tunnel depth may differ from that intended when a manual technique, or even femtosecond laser technology, is used for creating the tunnel [16] because technique accuracy may be reduced in the deep stroma [17–19].

In this study, the tunnel depth for Keraring implantation was planned using the pachymetry map created in RTVue 100. With a single and no-contact examination, it provides reliable pachymetric mapping over a corneal area 6 mm in diameter [13]. This area of analysis includes the tunnel area for implantation of the Keraring SI-5 and SI-6 models (inner diameter of 4.40 mm and 5.40 mm, resp.). Using this method, we were able to safely implant the ICRS in all patients.

After surgery, the measurements of Keraring distance from the anterior and the posterior corneal surface were highly reproducible. The interexaminer difference in measurements of the distance from the apex to the anterior surface and the distance from the inner and the outer corner to the posterior surface was small. This finding indicates that the method may be useful for assessing the ICRS position over time in reference to the anterior and the posterior cornea.

The distance of the inner corner from the posterior surface showed the best agreement with the intended distance (mean 138.85 ± 31.78 versus 140.08 ± 28.93 μm; $p = 0.83$). The mean absolute difference with respect to the intended

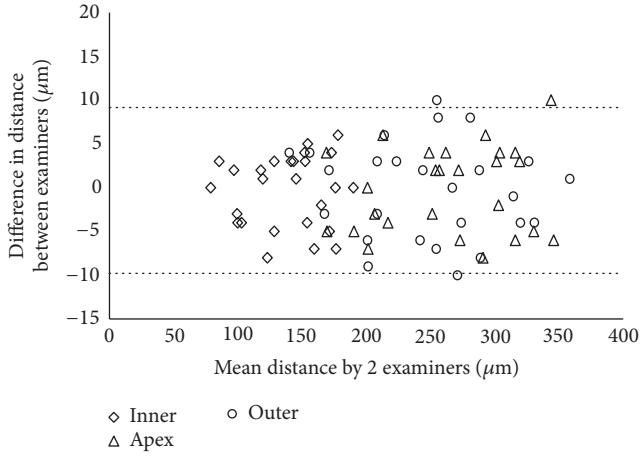

Figure 4: Scatterplot showing the differences between examiners' measurements of the distance from apex to anterior corneal surface (△), from inner corner to posterior corneal surface (◊), and from outer corner to posterior corneal surface (○). Individual differences between examiners are plotted against the mean value obtained by both examiners together. The 95% LoA interval is represented with dotted lines.

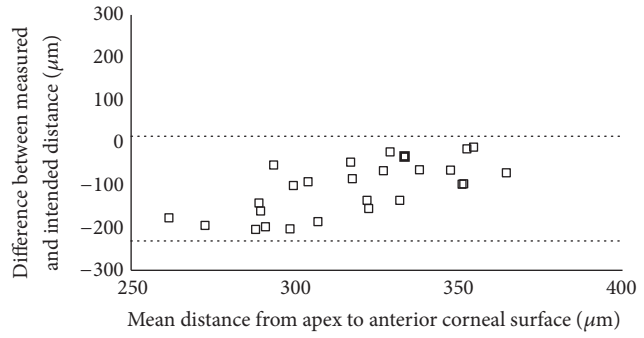

Figure 5: Scatterplot showing the differences between the measured and the intended distance from the Keraring apex to the anterior corneal surface. Individual differences between the measured and the intended distance are plotted against the mean value of the measured and the intended distance. The 95% LoA interval is represented with dotted lines.

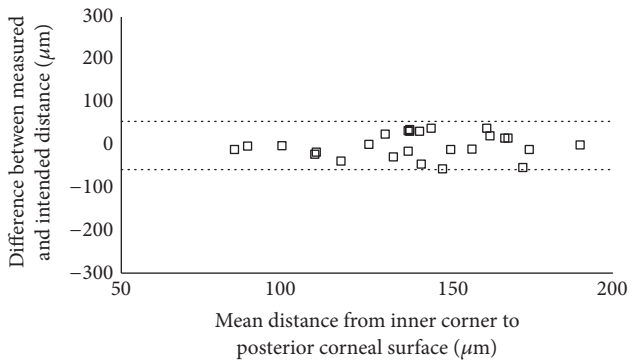

Figure 6: Scatterplot showing the differences between the measured and the intended distance from the Keraring inner corner to the posterior corneal surface. Individual differences between the measured and the intended distance are plotted against the mean value of the measured and the intended distance. The 95% LoA interval is represented with dotted lines.

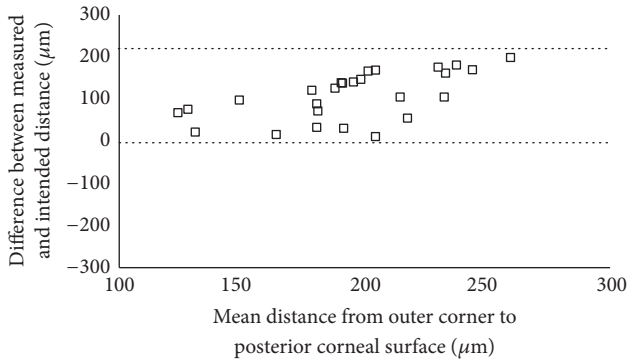

Figure 7: Scatterplot showing the differences between the measured and the intended distance from the Keraring outer corner to the posterior corneal surface. Individual differences between the measured and the intended distance are plotted against the mean value of the measured and the intended distance. The 95% LoA interval is represented with dotted lines.

distance (23.54 ± 15.90 μm) was significantly lower ($p < 0.001$) than that found for the other measurements and was within 25 μm and 50 μm in 57.7% and 92.3% of cases, respectively. The good agreement found for this measurement may be explained by the architecture and biomechanical properties of the posterior cornea [20, 21]. The posterior cornea has a low tensile strength and opposes low resistance to the pushing effect of the segment [22]. As a consequence, the posterior lamellae are slightly compressed behind the Keraring base, and the distance from the inner corner to the posterior surface is close to the intended distance.

The distance from the Keraring outer corner to the posterior corneal surface showed poor agreement with the intended distance. It was greater than intended, on average, by 108.35 μm ($p < 0.001$). As compared with the inner corner, the outer corner was farther from the posterior corneal surface, on average, by 109.58 μm. Using an IntraLase femtosecond laser, Gorgun et al. obtained similar results in 17 keratoconic eyes [9]. In their study, the outer corner was farther from the posterior surface, on average, by 88.0–111.7 μm as compared with the inner corner. These findings show that the Keraring base is positioned obliquely with respect to the posterior corneal surface. It is unlikely that this position results from the creation of an oblique intrastromal tunnel. A tunnel created with the IntraLase should run parallel to the corneal surfaces because it is prepared while the cornea is applanate by the optical interface. The greater distance from the outer corner to the posterior corneal surface may be due to two factors. First, the outer corner might move forward during segment insertion into the tunnel or during the early postoperative period. Pérez-Merino et al. found that the Keraring base was tilted forward with respect to the iris plane, on average, by 6.8° ± 2.6 at 7 days after surgery; small changes of tilt were observed between 7 and 90 days after surgery [11]. Second, the distance from the

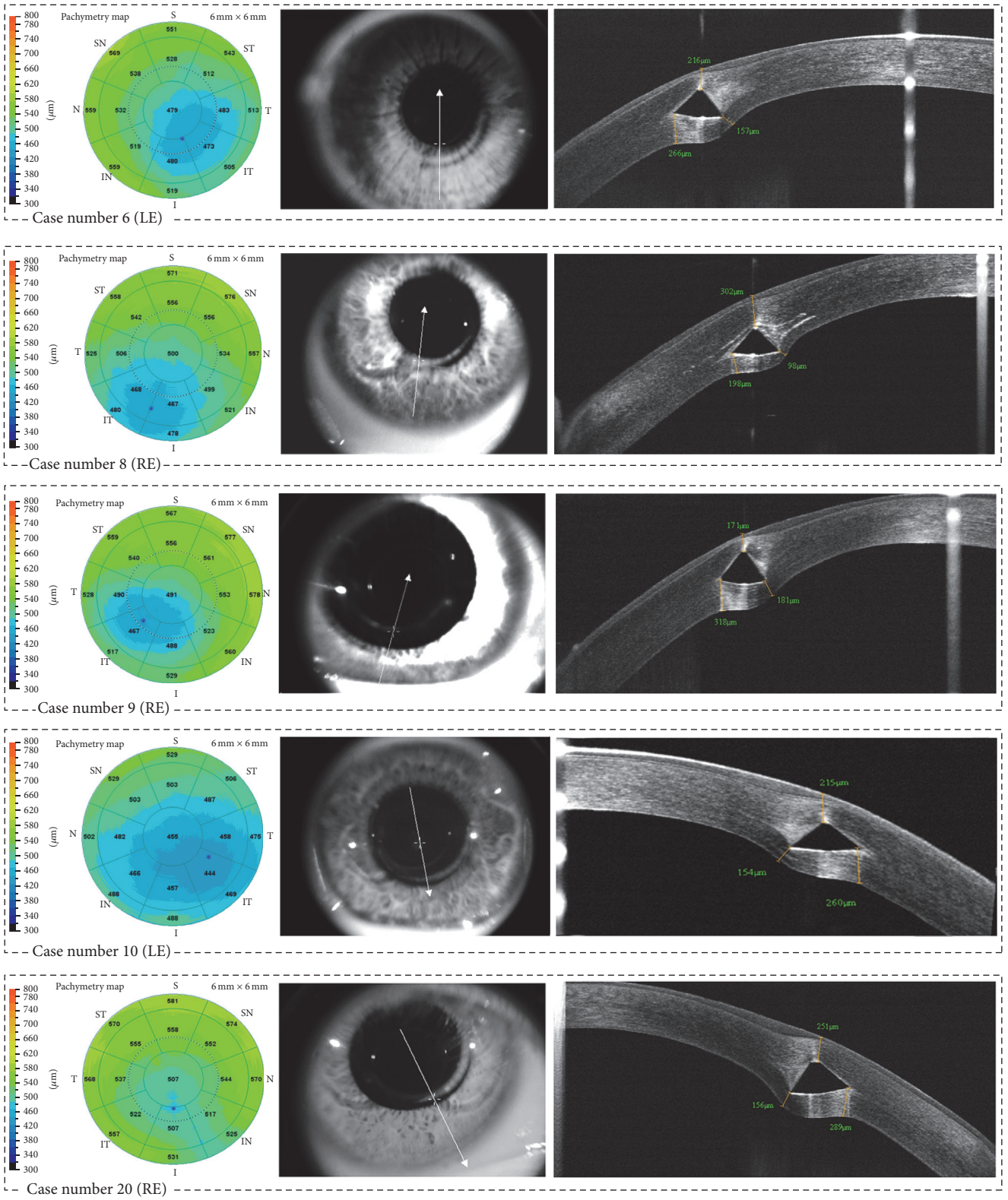

Figure 8: The pachymetry map and the Keraring OCT images (enface and high definition line) of cases # 6, # 8–10, and # 20. LE = left eye; RE = right eye.

outer corner to the posterior surface might be overestimated due to the refractive distortion generated by the implant. The dewarp calculation of the instrument software uses a 1.337 refractive index for the cornea, but it does not take into account the fact that the implant refractive index is 1.487. As a consequence, the higher optical path difference through the implant increases the thickness in the peripheral areas of the corneas. Ortiz et al. reported that this refractive distortion may increase by up to 35 μm the estimated corneal thickness [23]. In the OCT images, the refractive distortion generates a bulging of the posterior cornea. However, this artifact should be lower behind the inner corner as compared with the outer corner (Figure 8). The inner corner is closer to the central cornea, and the laser beam path through the implant is short when the distance from the inner corner to the posterior surface is evaluated. However, a distortion-corrected calculation is needed to determine the impact of this factor on the measurements taken behind the implant.

The distance from the apex to the anterior corneal surface is routinely measured to monitor the risk of complications such as ring migration and exposure. This measurement, however, agrees poorly with the intended distance. In the present study, the apex was closer to the anterior corneal surface than intended, on average, by more than 90 μm. These findings are consistent with those reported previously [9, 10]. Probably, the apex depth is shallower than intended because the stromal lamellae above the Keraring are highly compressed. Compression of the anterior lamellae derives from the pushing effect of the apex and from the high rigidity of the most anterior part of the stroma that tends to maintain the anterior curvature and shape [20–24].

In 10 eyes operated for keratoconus, Pérez-Merino et al. measured the distance between the center of mass of the Keraring and the anterior corneal surface [11]. They found good agreement between measurements and incision depth; the absolute difference was 23.93 ± 23.49 μm. This variability is comparable with the variability we noted for the distance from the inner corner to the posterior corneal surface. However, a comparative study is needed to establish the relationship between these measurements and to determine if they can be combined to verify whether the Keraring depth matches the intended depth in reference to the anterior and the posterior corneal surface.

The present study has several limitations. The Keraring depth was analyzed 3 months after surgery to minimize any effect of postoperative edema and inflammation on measurements. Nonetheless, the results might have been influenced by a slight change in implant depth in the first weeks after surgery. The tunnel was prepared using a manual technique in the majority of cases. The predictability of tunnel depth may be lower with the manual technique as compared with femtosecond laser technology. This factor might have inflated the differences between the measured and the intended distance. When we analyzed the 5 eyes operated on with femtosecond laser separately, the absolute difference with respect to the intended distance dropped to 19.40 ± 10.04 μm for the measurements taken at the inner corner. Finally, the study did not investigate the agreement between the measured distance and the intended distance on the proximal and distal parts of the segment, where it might differ from that found on the central part. In any case, the difference should be small. Naftali and Jabaly-Habib found that segment depth does not change significantly on the proximal and distal parts as compared with the central part [10].

In conclusion, reproducible measurements of Keraring distance from the anterior and the posterior corneal surface were obtained with spectral-domain OCT. These measurements may be useful for assessing implant stability over time. The distance from the inner corner to the posterior corneal surface showed good agreement with the intended distance. This measurement may be used to determine whether, in reference to the posterior corneal surface, segment depth matches intended depth.

Disclosure

Part of the study was presented at the Congress of the European Cataract and Refractive Surgery, Copenhagen, Denmark, September 2016.

Competing Interests

The authors have no financial or proprietary interest in a product, method, or material to declare.

References

[1] J. Colin, B. Cochener, G. Savary, and F. Malet, "Correcting keratoconus with intracorneal rings," *Journal of Cataract and Refractive Surgery*, vol. 26, no. 8, pp. 1117–1122, 2000.

[2] J. G. Bromley and J. B. Randleman, "Treatment strategies for corneal ectasia," *Current Opinion in Ophthalmology*, vol. 21, no. 4, pp. 255–258, 2010.

[3] D. P. Piñero and J. L. Alio, "Intracorneal ring segments in ectatic corneal disease—a review," *Clinical and Experimental Ophthalmology*, vol. 38, no. 2, pp. 154–167, 2010.

[4] S. Patel, J. Marshall, and F. W. Fitzke III, "Model for deriving the optical performance of the myopic eye corrected with an intracorneal ring," *Journal of Refractive Surgery*, vol. 11, no. 4, pp. 248–252, 1995.

[5] T. A. Silvestrini, M. L. Mathis, B. E. Loomas, and T. E. Burris, "A geometric model to predict the change in corneal curvature from the intrastromal corneal ring (ICR)," *Investigative Ophthalmology & Visual Science*, vol. 35, p. 2023, 1994.

[6] T. E. Burris, C. T. Ayer, D. A. Evensen, and J. M. Davenport, "Effects of intrastromal corneal ring size and thickness on corneal flattening in human eyes," *Refractive and Corneal Surgery*, vol. 7, no. 1, pp. 46–50, 1991.

[7] J. Ruckhofer, J. Stoiber, E. Alzner, and G. Grabner, "One year results of European multicenter study of intrastromal corneal ring segments. Part 2: complications, visual symptoms, and patient satisfaction," *Journal of Cataract and Refractive Surgery*, vol. 27, no. 2, pp. 287–296, 2001.

[8] M. M. Lai, M. Tang, E. M. M. Andrade et al., "Optical coherence tomography to assess intrastromal corneal ring segment depth in keratoconic eyes," *Journal of Cataract and Refractive Surgery*, vol. 32, no. 11, pp. 1860–1865, 2006.

[9] E. Gorgun, R. B. Kucumen, N. M. Yenerel, and F. Ciftci, "Assessment of intrastromal corneal ring segment position with anterior segment optical coherence tomography," *Ophthalmic Surgery Lasers and Imaging*, vol. 43, no. 3, pp. 214–221, 2012.

[10] M. Naftali and H. Jabaly-Habib, "Depth of intrastromal corneal ring segments by OCT," *European Journal of Ophthalmology*, vol. 23, no. 2, pp. 171–176, 2013.

[11] P. Pérez-Merino, S. Ortiz, N. Alejandre, I. Jiménez-Alfaro, and S. Marcos, "Quantitative OCT-based longitudinal evaluation of intracorneal ring segment implantation in keratoconus," *Investigative Ophthalmology & Visual Science*, vol. 54, no. 9, pp. 6040–6051, 2013.

[12] V. Westphal, A. M. Rollins, S. Radhakrishnan, and J. A. Izatt, "Correction of geometric and refractive image distortions in optical coherence tomography applying Fermat's principle," *Optics Express*, vol. 10, no. 9, pp. 397–404, 2002.

[13] Y. Li, R. Shekhar, and D. Huang, "Corneal pachymetry mapping with high-speed optical coherence tomography," *Ophthalmology*, vol. 113, no. 5, pp. 792.e2–799.e2, 2006.

[14] J. M. Bland and D. G. Altman, "Statistical methods for assessing agreement between two methods of clinical measurement," *Lancet*, vol. 1, no. 8476, pp. 307–310, 1986.

[15] U. de Sanctis, A. Missolungi, B. Mutani, L. Richiardi, and F. M. Grignolo, "Reproducibility and repeatability of central corneal thickness measurement in keratoconus using the rotating scheimpflug camera and ultrasound pachymetry," *American Journal of Ophthalmology*, vol. 144, no. 5, pp. 712.e1–718.e1, 2007.

[16] F.-X. Kouassi, C. Buestel, B. Raman et al., "Comparison of the depth predictability of intra corneal ring segment implantation by mechanical versus femtosecond laser-assisted techniques using optical coherence tomography (OCT Visante®)," *Journal Français d'Ophtalmologie*, vol. 35, no. 2, pp. 94–99, 2012.

[17] H. K. Soong, S. Mian, O. Abbasi, and T. Juhasz, "Femtosecond laser-assisted posterior lamellar keratoplasty: initial studies of surgical technique in eye bank eyes," *Ophthalmology*, vol. 112, no. 1, pp. 44–49, 2005.

[18] Y. J. Jones, K. M. Goins, J. E. Sutphin, R. Mullins, and J. M. Skeie, "Comparison of the femtosecond laser (IntraLase) versus manual microkeratome (Moria ALTK) in dissection of the donor in endothelial keratoplasty initial study in eye bank eyes," *Cornea*, vol. 27, no. 1, pp. 88–93, 2008.

[19] P. M. Phillips, L. J. Phillips, H. A. Saad et al., ""Ultra-thin" DSAEK tissue prepared with a low-pulse energy, high-frequency femtosecond laser," *Cornea*, vol. 32, no. 1, pp. 81–86, 2013.

[20] D. M. Maurice and F. Monroe, "Cohesive strength of corneal lamellae," *Experimental Eye Research*, vol. 50, no. 1, pp. 59–63, 1990.

[21] Y. Komai and T. Ushiki, "The three-dimensional organization of collagen fibrils in the human cornea and sclera," *Investigative Ophthalmology and Visual Science*, vol. 32, no. 8, pp. 2244–2258, 1991.

[22] J. B. Randleman, D. G. Dawson, H. E. Grossniklaus, B. E. McCarey, and H. F. Edelhauser, "Depth-dependent cohesive tensile strength in human donor corneas: implications for refractive surgery," *Journal of Refractive Surgery*, vol. 24, no. 1, pp. S85–S89, 2008.

[23] S. Ortiz, P. Pérez-Merino, N. Alejandre, E. Gambra, I. Jimenez-Alfaro, and S. Marcos, "Quantitative OCT-based corneal topography in keratoconus with intracorneal ring segments," *Biomedical Optics Express*, vol. 3, no. 5, pp. 814–825, 2012.

[24] L. J. Müller, E. Pels, and G. F. J. M. Vrensen, "The specific architecture of the anterior stroma accounts for maintenance of corneal curvature," *British Journal of Ophthalmology*, vol. 85, no. 4, pp. 437–443, 2001.

Hindawi
Journal of Ophthalmology
Volume 2017, Article ID 9678041, 9 pages
https://doi.org/10.1155/2017/9678041

Research Article

Quantitative Assessment of the Impact of Blood Pulsation on Intraocular Pressure Measurement Results in Healthy Subjects

Robert Koprowski[1] and Lei Tian[2]

[1]*Department of Biomedical Computer Systems, University of Silesia, Faculty of Computer Science and Materials Science, Institute of Computer Science, Ul. Będzińska 39, 41-200 Sosnowiec, Poland*
[2]*Beijing Institute of Ophthalmology, Beijing Tongren Eye Center, Beijing Tongren Hospital, Capital Medical University, Beijing Ophthalmology & Visual Sciences Key Laboratory, Beijing 100730, China*

Correspondence should be addressed to Lei Tian; tianlei0131@163.com

Received 8 October 2016; Accepted 5 January 2017; Published 30 January 2017

Academic Editor: Rachel W. Kuchtey

Background. Blood pulsation affects the results obtained using various medical devices in many different ways. *Method*. The paper proves the effect of blood pulsation on intraocular pressure measurements. Six measurements for each of the 10 healthy subjects were performed in various phases of blood pulsation. A total of 8400 corneal deformation images were recorded. The results of intraocular pressure measurements were related to the results of heartbeat phases measured with a pulse oximeter placed on the index finger of the subject's left hand. *Results*. The correlation between the heartbeat phase measured with a pulse oximeter and intraocular pressure is 0.69 ± 0.26 ($p < 0.05$). The phase shift calculated for the maximum correlation is equal to $60 \pm 40^{\circ}$ ($p < 0.05$). When the moment of measuring intraocular pressure with an air-puff tonometer is not synchronized, the changes in IOP for the analysed group of subjects can vary in the range of ± 2.31 mmHg ($p < 0.3$). *Conclusions*. Blood pulsation has a statistically significant effect on the results of intraocular pressure measurement. For this reason, in modern ophthalmic devices, the measurement should be synchronized with the heartbeat phases. The paper proposes an additional method for synchronizing the time of pressure measurement with the blood pulsation phase.

1. Introduction

Today, it is difficult to imagine a physician of any specialization without complicated equipment designed to perform different types of measurements in patients. It would be difficult or even impossible to perform a contemporary diagnosis without a series of measurements. On the one hand, doctors have more and more confidence in the results obtained from medical devices. On the other hand, there often exist simple methods for obtaining more accurate results and reducing measurement errors. These methods take into consideration blood pulsation phases. The impact of this element on measurements is strongly dependent on the anatomical and functional links between the blood pulsation and the measured parameter [1]. One of these groups of methods and medical devices includes Diaton transpalpebral tonometer, Dynamic contour tonometer, Goldmann applanation tonometer, and noncontact tonometers: Ocular Response Analyzer (ORA), Corvis ST, for measuring intraocular pressure (IOP), and other additional parameters [2, 3]. Corvis ST, owing to the Ultra-High-Speed Scheimpflug camera, can record corneal deformation which is the response to an air puff. The change in the blood pulsation phase during measurement affects the results in different ways. Moreover, measurement errors occur which result from nonsynchronization of the measurement moment with the blood pulsation phase [4]. The effect of blood pulsation on the results obtained in IOP measurement is well known [5–7]. The authors of work [6], in particular, showed that the ocular pulse amplitude readings measured with dynamic contour tonometry in healthy subjects were not associated with blood pressure levels nor amplitude. It appears that the ocular pulse amplitude is strongly dependent on the time-course of the cardiac contraction. Both regulating mechanisms in the carotid system and

scleral rigidity may be responsible for dampening the direct effect of blood pressure variations. Similarly the authors of work [7] confirmed, by means of experiments, that pulse amplitude, fundus pulsation amplitude, and pulsatile ocular blood flow depend on ocular volume and indicated that there is no reduction in the pulsatile component of ocular blood flow in the case of myopic patients. Accordingly, the relationship between axial eye length and pulsatile ocular blood flow seems to result from different ocular volumes. The research carried out by the authors in work [7] has important implications for the studies relating to pulse amplitude or pulsatile ocular blood flow. However, the dependence of the results obtained for a specific device, for example, the Corvis tonometer, is unknown. Currently, the Corvis tonometer allows for the measurement of a number of biomechanical characteristics of corneal deformation. These characteristics, whose dependence on the blood pulsation phase can vary, include the location of the first and second applanation, the size of flattening for the first and second applanation, the maximum corneal deformation, the maximum amplitude, and frequency of corneal vibration. On the other hand, the accuracy of measurement of these characteristics associated with the adopted image analysis and processing method is also vital. Various types of devices designed for detecting the corneal edge on a sequence of images from the Corvis tonometer can be applied here, ranging from Roberts, Sobel, or Prewitt filters to the Canny method or other profiled edge detection methods. The blood pulsation phase measurement itself can be also carried out with the use of various types of pulse oximeters corresponding to different types of absorption of radiation of two different wavelengths (red and infrared) by red blood cells in the capillaries. A variable component describes arterial blood absorbance and thus it is possible to calculate the degree of saturation of haemoglobin with oxygen. Therefore, the measurement of changes in the skin colour can be performed remotely without contact by means of laser light [8] or by analysing the skin image coming from the camera in visible light [9–11].

Considering all of the above factors, the analysis of the impact of blood pulsation phases on the results obtained from the Corvis tonometer is practically interesting. In particular, the following issues are of interest:

(i) confirmation of the dependence of IOP on the blood pulsation phase,

(ii) quantitative assessment of the dependence of IOP on the blood pulsation phase,

(iii) quantitative assessment of the dependence of 1st and 2nd applanation point, maximum corneal deformation, and amplitude of corneal vibrations for the frequency >100 Hz on the blood pulsation phase,

(iv) indication of the scope of variation in IOP measurement for the lack of measurement synchronization,

(v) creation of new analysis methods for images and signals from the Corvis tonometer and pulse oximeter allowing for automatic and reproducible measurement of the above parameters.

The obtained results of synchronization of IOP measurement moment and other corneal deformation parameters with the blood pulsation phase are shown in this paper.

2. Material

Eight thousand and four hundred corneal deformation images of the eyes of 10 healthy subjects were analysed as part of the study. The subjects ranged in age from 27 to 36 years and women accounted for 66% of the whole study group. Six IOP measurements using the Corvis ST (software ver. 1.2, Oculus Optikgeräte GmbH, Wetzlar, Germany; resolution of 0.1 mmHg, measurement range from 1 to 60 mmHg) were performed for each eye (5 left and 5 right eyes) in different blood pulsation phases. For each series of 6 measurements per one patient, an attempt was made to carry them out evenly in the full range from 0° to 360° of the blood pulsation phase. A total of 60 results of IOP measurement were acquired (6 measurements for each of the 10 subjects). The exclusion criterion concerned patients who had ophthalmic surgery, heart surgery, hypertension, ocular hypertension, cardiac arrhythmias, bypass, and other diseases of the heart or were pregnant. A sequence of images of corneal deformation resulting from an air puff was acquired from the Corvis tonometer. The Ultra-High-Speed Scheimpflug camera, which is an integral part of the Corvis tonometer, enables us to register, within the time $I = 140$, images with a resolution $M \times N = 200 \times 576$ pixels. Each ith image was recorded every 231 μs. The blood pulsation measurement was made with the Mindray PM-8000 Express (measurement range: from 0 to 100%, resolution of 1%, and pulse rate: from 20 to 254 beats/minute). The pulse oximeter was placed on the index finger of the subject's left hand. Multiple measurements of the same subject were carried out with minimum time intervals between successive measurements to prevent differentiation of the subject's pulse. All tests were carried out according to the Declaration of Helsinki on healthy subjects with their free and informed consent at the Beijing Tongren Hospital. The ophthalmologist during tests started the measurement (and at the same time triggered an air puff) which was recorded and saved together with the blood pulsation phase (in the data from the pulse oximeter). Further analysis of signals and images was carried out in software designed by the author in Matlab (Version 7.11.0.584, R2010b, Java VM Version: Java 1.6.0_17-b04 with Sun Microsystems Inc.) with Image Processing Toolbox (Version 7.1) and Signal Processing (Version 7.2) on a PC running Windows 7 Professional, 64-bit with the Intel Core i7-4960X CPU @ 3.60 GHz and HDD 3.5″ SATA III 2 TB.

3. Method and Results

The measurement method proposed by the authors consists of two phases:

(i) analysis and processing of images from the Corvis tonometer, which enables us to calculate biomechanical characteristics of the deformed cornea and IOP,

Table 1: Examples of measured values of features w (obtained from the Corvis tonometer) for a single healthy subject, for one right eye ($v = 1$), and 6 measurements.

Measurement number	$w(1)$ [ms]	$w(2)$ [ms]	$w(3)$ [mm]	$w(4)$ [Hz]	$w(5)$ [mmHg]
1	7.363	21.444	1.015	432	15
2	7.331	21.646	1.039	421	14.5
3	7.64	21.468	1.091	407	15
4	7.693	21.672	1.069	409	16
5	7.365	21.574	1.02	420	15
6	7.46	21.394	1.024	432	16

Table 2: Mean values of individual features w for 10 subjects ($p < 0.3$).

	Eye	$w(1)$	$w(2)$	$w(3)$	$w(4)$	$w(5)$
$v = 1$	Right	7.41 ± 0.15	21.54 ± 0.11	1.03 ± 0.03	416 ± 1.7	15.25 ± 0.6
$v = 2$	Right	7.38 ± 0.22	21.86 ± 0.51	1.04 ± 0.03	430 ± 3.1	14.9 ± 2.31
$v = 3$	Right	7.25 ± 0.32	22.05 ± 0.09	1.08 ± 0.033	444 ± 3.7	12.41 ± 0.49
$v = 4$	Right	7.30 ± 0.11	21.78 ± 0.18	1.08 ± 0.04	401 ± 2.0	14.33 ± 1.08
$v = 5$	Right	6.61 ± 0.08	22.81 ± 0.15	1.17 ± 0.03	399 ± 4.7	7.9 ± 0.63
$v = 6$	Left	6.71 ± 0.06	22.63 ± 0.09	1.11 ± 0.02	409 ± 3.1	8.08 ± 0.73
$v = 7$	Left	6.91 ± 0.03	22.13 ± 0.05	1.15 ± 0.01	434 ± 5.1	10.08 ± 0.28
$v = 8$	Left	6.91 ± 0.06	22.13 ± 0.15	1.16 ± 0.02	421 ± 1.4	10.08 ± 0.76
$v = 9$	Left	7.29 ± 0.13	21.94 ± 0.3	1.03 ± 0.045	409 ± 2.2	13.9 ± 1.5
$v = 10$	Left	7.09 ± 011	22.43 ± 0.2	1.15 ± 0.06	389 ± 3.7	12.1 ± 1.08

(ii) quantitative assessment of correlation between the blood pulsation phase and measured parameters (mainly IOP).

3.1. Analysis of Corneal Deformation Images. The analysis of corneal deformation images is related to an original method involving a series of operations performed on images from the Corvis tonometer. The input data, a sequence of images $L_{\mathrm{GRAY}}(m, n)$ (where m is row and n is image column) with a resolution $M \times N = 200 \times 576$ pixels, are loaded into Matlab in $*.jpg$ or $*.avi$ format. Image preprocessing involves median filtering with a mask sized $M_h \times N_h = 3 \times 3$ pixels, the output image $L_{\mathrm{MED}}(m, n)$. The filter mask size was selected based on the maximum size of a single noise (artefact) present in a 2D image L_{GRAY} that did not exceed 4 pixels. The next step is edge detection with the use of the Canny filter followed by joining the relevant parts of the contour. The issue of joining the edges entails a few problems associated with maintaining the corneal contour continuity. These problems include discontinuous edges and blank spaces between the detected contour portions. They are solved by using 5th-degree polynomial approximation. The polynomial degree was selected taking into account the anthropometric data of corneal curvature. Thus performed analysis for each ith image provides the image $L_C(n, i)$. On this basis, the corneal reaction $L_{HC}(n, i)$ is calculated (it is separated from the constant component, the corneal curvature at rest, and from the eyeball response). Based on preliminary studies and measurements, as well as biomechanical evidence and knowledge of ophthalmologists, the following features (which were measured) were selected:

$w(1)$: 1st applanation point (momentary corneal flattening),

$w(2)$: 2nd applanation point,

$w(3)$: maximum corneal deformation,

$w(4)$: frequency of corneal vibrations for the frequency >100 Hz,

$w(5)$: intraocular pressure (read from the tonometer).

The block diagrams of the proposed image analysis and processing methods and feature measurement idea are shown in Figure 1. Examples of values calculated for the features w for different blood pulsation phases are shown in Table 1.

As is apparent from the presented table (Table 1), the smallest changes and the smallest values of standard deviation of the mean (std) are visible for the feature $w(2)$ (the mean value of 21.54 ± 0.11 ms, ±0.51%, for a confidence interval $p < 0.3$) and for the other features: $w(1)$: 7.47 ± 0.16 ms (±2.1%), $w(3)$: 1.04 ± 0.03 mm (±2.8%), $w(4)$: 416 ± 10.7 Hz (±2.5%), and $w(5)$: 15.25 ± 0.61 mmHg (±4.0%) for $p < 0.3$ Student's t-distribution (an IOP unit was adopted in accordance with the units in tonometers). Detailed mean values of individual features for 10 subjects are shown in Table 2. The second measurement concerns correlation of the measured features w with the subject's pulse phase (feature $w(6)$).

3.2. Correlation between the Blood Pulsation Phase and Measured Parameters w. Blood pulsation measurement with the use of a pulse oximeter enables us to determine amplitudes

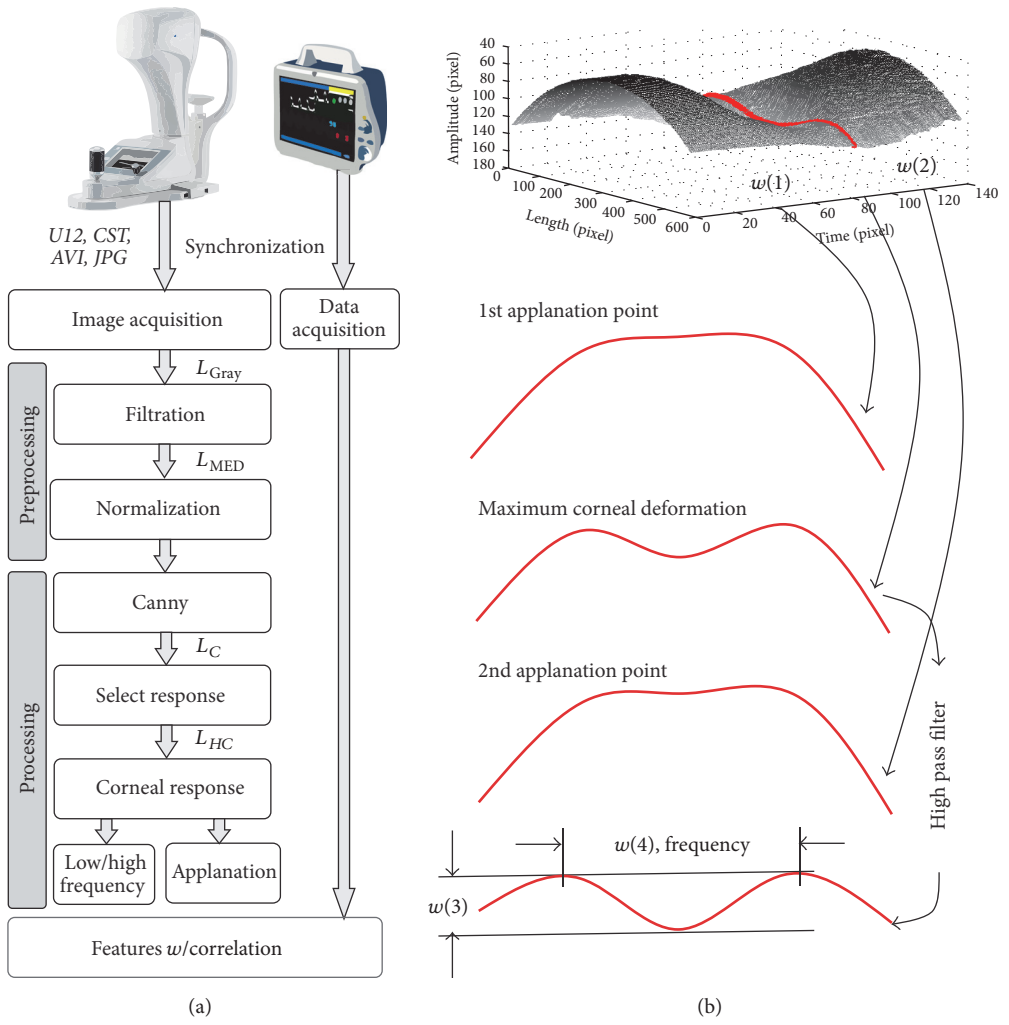

FIGURE 1: Block diagram of the idea of measuring the features w and the different phases of the analysis and processing of images from the Corvis tonometer (a) and the graph of corneal deformation for successive time sequences together with three characteristic waveforms (1st and 2nd applanation as well as the maximum corneal deformation) being the basis for calculating the features $w(1)$, $w(2)$, $w(3)$, and $w(4)$, respectively (b).

of pulse changes with a resolution of 1%. The impact of blood pulsation (the phase impact) on corneal biomechanical measurements performed using the Corvis tonometer was measured on the index finger of the subject's left hand. This corresponds to the typical placement of the pulse oximeter during hospitalization or when testing patients. Figure 2 shows the conventional coordinate system. The coordinate origin is the moment of measuring IOP for some of the 12 areas occurring every 30°. It means that the measurements were performed for 0°, 30°, 60°, 90°, and so forth. The adopted values and the analysis step result from simplification of analyses and measurement accuracy limitations (of the parameter and tonometer). The accuracy enables us to carry out a meaningful and repeatable measurement of the correlation for the same blood pulsation frequency. For 6 measurements performed for a single patient, the discrepancy in blood pulsation frequency was not more than 4%. The determined value of the blood pulsation phase was referred to as the feature $w(6)$. From a practical point of view, it is important to indicate the correlation between the feature $w(6)$ and the other features (from $w(1)$ to $w(5)$). The correlation $r_v(j)$ was measured using the formula below where k is the number of the measurement for one subject ($k \in (1, 6)$), v is the subject number ($v \in (1, 10)$), and j is the feature number ($j \in (1, 5)$); that is,

$$r_v(j) = \frac{\sum_{k=1}^{K} \left(w_{k,v}(j) - \overline{w_{k,v}(j)}\right) \cdot \left(w_{k,v}(6) - \overline{w_{k,v}(6)}\right)}{\sqrt{\sum_{k=1}^{K} \left(w_{k,v}(j) - \overline{w_{k,v}(j)}\right)^2 \cdot \sum_{k=1}^{K} \left(w_{k,v}(6) - \overline{w_{k,v}(6)}\right)^2}}, \quad (1)$$

where $r_v(j)$ is correlation for jth feature and vth subject for $j \in (1, 5)$, $w_{k,v}(j)$ is jth feature of the vth subject of the kth measurement, and K is the total number of measurements.

The natural phase shift in blood pulsation between the heart, the index finger (the measurement point), and the eye depends on the distance and subject's anatomical features.

Table 3: Results of the minimum and maximum correlation between the features $w(5)$ and $w(6)$ for 10 subjects (outliers are in italic font).

	$\min(r_v(j=5))$	ϕ	$\max(r_v(j=5))$	ϕ
$v=1$	−0.95	230	0.95	50
$v=2$	−0.91	250	0.91	70
$v=3$	−0.95	220	0.95	40
$v=4$	*−0.48*	*340*	*0.48*	*160*
$v=5$	−0.88	130	0.88	310
$v=6$	*−0.16*	*50*	*0.16*	*230*
$v=7$	*−0.51*	*100*	*0.5*	*160*
$v=8$	−0.99	150	0.99	330
$v=9$	−0.66	200	0.66	20
$v=10$	−069	230	0.69	50

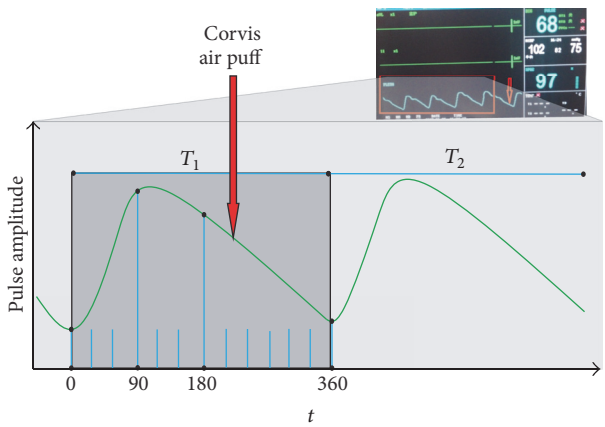

Figure 2: Graph of changes in the blood pulsation amplitude over time. A sample moment of starting the measurement with the Corvis tonometer and the conventionally adopted angular measurement scales are marked in red.

For the analysed data, correlation is determined according to formula (1) for subsequent, artificially added, phase shifts ϕ of the feature $w_{k,v}(j)$. The results of changes in correlation for the artificially added phase shifts ϕ are shown in Figure 3. The values of phase shift ϕ for which the correlation $r_v(j)$ reaches the maximum and minimum values are given in Table 3 for the feature $w(5)$ ($j = 5$). Further calculations were performed *under* the assumption of *the null hypothesis Ho* that there is a statistical relationship between the features $w(1)$ to $w(5)$ and $w(6)$ and under the assumption of the alternative hypothesis H_1 that this relationship does not exist. The calculated correlation for all the analysed subjects indicates statistical significance ($p < 0.05$ for Student's t-distribution) only for the feature $w(5)$. Therefore, there is a significant correlation between the intraocular pressure and heartbeat phase (between the features $w(5)$ and $w(6)$). For the measured group of subjects, this correlation is high (it is in the range from 0.48 to 0.99; the measurement for $v = 6$ was considered a thick error and rejected) and its mean value is 0.78 ± 0.19 (see Table 3). The results presented in Table 3 for the features $w(5)$ and $w(6)$ are extremely important in practice. Low values of mean std of changes in the features from $w(1)$ to $w(4)$ can here result from two elements. The first one is the limited resolution of the analysed image. For the image resolution $M \times N = 200 \times 576$ pixels, there is, on average, 20 μm per one pixel. This means that the accuracy of measuring the feature $w(1)$ as well as features $w(2)$, $w(3)$, and $w(4)$ is limited to the resolution of $\pm 20\,\mu$m. So, if, for example, the amplitude for the first applanation changes by less than 20 μm for the next i frames (images in a sequence), the measurement error of the feature $w(1)$ will be 231 μs. The other element influencing the low values of mean std of changes in the features from $w(1)$ to $w(4)$ is the lack of correlation with the heartbeat phases. For subjects $v = \{1, 2, 3, 4, 5, 7, 8, 9, 10\}$, there was a close relationship between the heartbeat phase and IOP. According to the diagram shown in Figure 3, the highest values of IOP are obtained for the phase shift of 60°. Minimum IOP values are obtained for the phase shift of 240° (60° + 180°); see Figure 4. The correlation for these angular values is 0.69 ± 0.26 ($p < 0.05$). The changes in mean correlation $r_v(j = 5)$ for individual subjects (after removing thick errors, outliers) as a function of phase shift ϕ presented in Figure 4 clearly indicate a strong correlation (0.69 ± 0.26) between IOP and the heartbeat phase.

4. Discussion

The impact of blood pulsation and its phases on measurements performed in medicine is known primarily from electrocardiogram (ECG). A lot of interesting publications have been written in this area [12–26]. In the first one [16] related to continuous cuffless blood pressure estimation using the pulse transit time and photoplethysmogram intensity ratio, the authors presented an algorithm which was validated on 27 healthy subjects with continuous Finapres blood pressure as a reference. The results showed that the mean std for the estimated systolic, diastolic, and mean blood pressure with the proposed method against reference was −0.37 and 5.21 mmHg, −0.08 and 4.06 mmHg, and −0.18 and 4.13 mmHg, and the mean absolute differences were 4.09 mmHg, 3.18 mmHg, and 3.18 mmHg, respectively. In the next work [20], the authors referred to the pulse transit time as a predictor of the efficacy of a celiac plexus block in patients suffering from chronic intractable abdominal pain. A celiac plexus block was successful in 9 out of 12 cases; the pulse transit time of the success group was 6.84 ± 5.04% versus

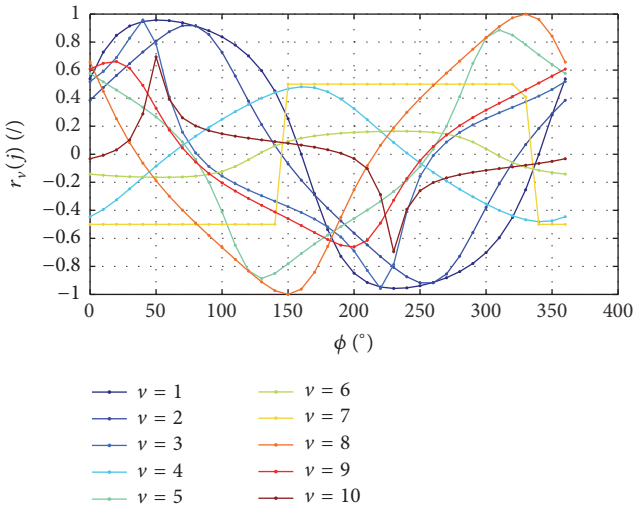

FIGURE 3: Graph of changes in the correlation $r_v(j = 5)$ of feature $w_{k,v}(j = 5)$ for individual subjects ($v \in (1, 10)$) as a function of phase shift ϕ.

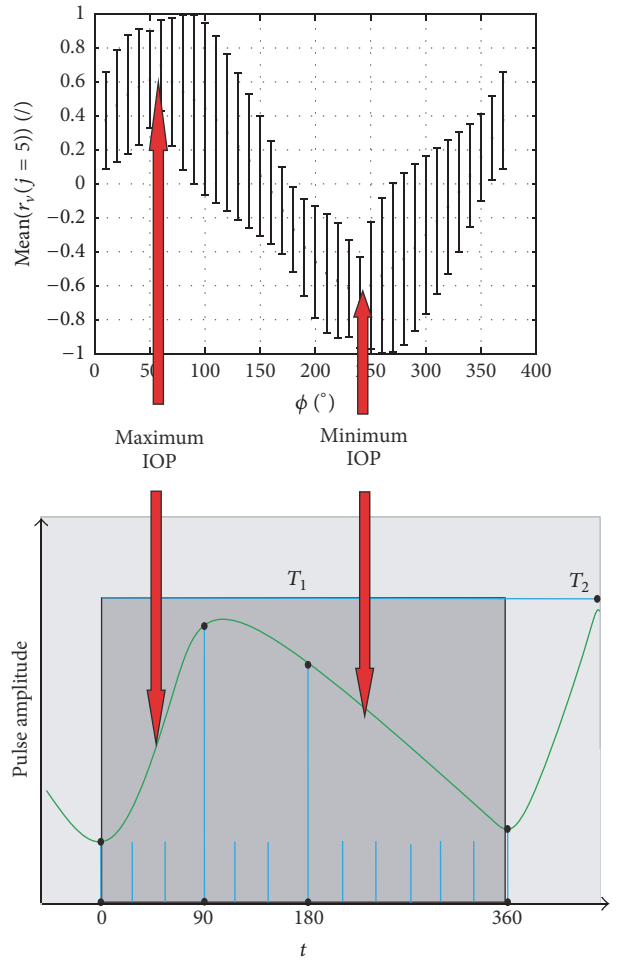

FIGURE 4: Graph of changes in mean correlation $r_v(j = 5)$ of the feature $w_{k,v}(j = 5)$ for individual subjects (after removing thick errors, outliers) as a function of phase shift ϕ. Additionally, the graph shows the position of the minimum and maximum IOP values relative to the blood pulsation phase. Minimum and maximum values of IOP are marked with red arrows. Blue lines on the x-axis indicate the arbitrarily adopted measurement times.

0.72 ± 0.78% in the failure group ($p = 0.021$). In turn, in work [14], the pulse transit time was calculated for each ECG R-wave and the corresponding steepest upstroke slope in the photoplethysmogram and was transformed to a continuous blood pressure estimate using multipoint nonlinear regression calibration based on the individual subject's sphygmomanometer readings. Bland-Altman limits of agreement between pulse transit time-derived systolic blood pressure estimates and sphygmomanometer values were −24.7 to 24.1 mmHg and between Portapres and sphygmomanometer systolic blood pressure values were −42.0 to 70.1 mmHg. For beat-to-beat systolic blood pressure estimation during exercise, pulse transmit measurement combined with multipoint nonlinear regression calibration based on intermittent sphygmomanometry can constitute an alternative to volume clamp devices. In work [17], the authors showed that the PTT-based blood pressure estimation may not be accurate enough since the regulation of blood pressure within the human body is a complex, multivariate physiological process. Taking into consideration the negative feedback mechanism in the blood pressure control, the authors introduced the heart rate (HR) and the blood pressure estimate in the previous step to obtain the current estimate. They validated this method by using the clinical database. Authors' results show that the pulse transit time, HR, and previous estimate reduce the estimated error significantly when compared to the conventional pulse transit time estimation approach ($p < 0.05$). There are also other interesting solutions relating to, for example, a wearable vital signs monitor at the ear [18], measuring short-term blood pressure variability: a comparison with the Finometer [23], comparison of ubiquitous blood pressure monitoring via pulse transit time [25], and others [12, 15, 19, 21]. Decision trees [26] or a new measurement system BioWatch described in work [13] were also used in the beat-to-beat and phase shift analysis. However, the authors of the above-mentioned publications did not make any reference to the analysis of the impact of blood pulsation phase on measurements in ophthalmology, in particular, measurements that are carried out using small and also relatively affordable devices (such as Corvis).

In the group of publications devoted to image analysis and processing, there are a lot of interesting works on ophthalmology, starting with those on the biomechanics of the eye associated with the Corvis tonometer [27–30], which show the effect of keratoconus, glaucoma, or diabetes on the results obtained, and ending with those on the analysis and processing of corneal edge images [31–35], which examine various methods of edge detection and measurement of additional biomechanical parameters. One of the few approaches to analysis of blood pulsation presented in the literature and related to the eye concerns the measurement of pupil size changes resulting from blood pulsation [36]. However, none of the presented methods of both image analysis and analysis of results takes into account the impact of blood

pulsation on the obtained results of biomechanics of the eye (including IOP), which is presented in this paper. It should be emphasized that the presented image analysis and processing methods are one possible solution to this problem. There are also approaches described in the literature which are based on a fast Fourier transform (FFT) [37–41], computational intelligence systems [42–44], or fuzzy algorithms, used in other fields of life (for other applications).

Blood pulsation in ophthalmology is generally known (for other devices than Corvis) and its influence on measurement results is still under examination. It should be specifically noted that the impact of parameter changes on the results obtained is of high clinical importance. In the case of the impact of blood pulsation or the effect of other parameters (such as patient positioning during examination), different measurement results are obtained (in this case IOP). The so-called sensitivity to changing parameters enables us to clarify and define medical procedures. It indicates to what extent a given parameter may distort the result. Moreover, it indicates how the parameters such as patient positioning, head position, or, as in the discussed case, blood pulsation affect (quantitatively) the results. According to the authors, these procedures should be carried out for each medical device. Usefulness and reliability of such procedures should be verified both with ophthalmologists and with technicians operating the devices used in ophthalmology. Therefore, the issues described in this paper are current and important for both engineering and practical diagnostic usefulness in everyday work of ophthalmologists.

5. Conclusions

The study confirmed the correlation between the heartbeat phase and IOP measurement result. This correlation is high and amounts to 0.69 ± 0.26 ($p < 0.05$). The phase shift for the analysed cases (after 6 measurements per subject using the pulse oximeter placed on the index finger of the left hand) is $60 \pm 40^{\circ}$ ($p < 0.05$) for the maximum correlation. In the range of minimum and maximum correlation values, the mean std of IOP changes is even ± 2.31 mmHg ($p < 0.3$). It should be noted that the sources of errors include alternating rhythm (pulse) of the heart. For the performed measurements, heart rate variability was in the range of 4% (typically 84 beats/minute). Therefore, it was at the level of other errors resulting from the finite image resolution and algorithm errors (range of ±1 pixel when detecting the corneal contour during its deformation). In summary, the paper

(1) proposes a reproducible and fully automated method for measuring the features w based on the sequence of images obtained from the Corvis tonometer;

(2) indicates which features w are dependent on the blood pulsation phase, in particular feature $w(5)$;

(3) confirms the dependence of IOP on the blood pulsation phase for the Corvis tonometer;

(4) shows the reproducibility of the method for the discussed subjects.

The authors in subsequent works intend to carry out further studies on the impact of heartbeat rate changes or the anatomy of patients on the results of IOP and repeatability of measurements. In particular, the relationship between individual anatomical characteristics of patients and the obtained phase shift values will be explored. The presence of correlation between the heartbeat phase and IOP confirmed in this study led the authors to propose a system for connecting heartbeat phase measurement with triggering the measurement in the Corvis tonometer. In its current form, the heartbeat measurement is carried out using a CCD camera which is placed on the forehead support of the Corvis tonometer. The camera records changes in absorption of red radiation by red blood cells in the capillaries. The camera complements the modified system for measuring intraocular pressure patented by the author [37]. Currently, the method is being tested at the Beijing Institute of Ophthalmology, Beijing Tongren Hospital in China.

Competing Interests

The authors declare that they have no competing interests.

Authors' Contributions

Robert Koprowski suggested the idea and the article and wrote the paper together with the figures; Lei Tian performed tests on subjects and obtained consent for their conduct and publication. All authors approved the final manuscript.

Acknowledgments

This research was supported by grants from the National Natural Science Foundation of China (81271052, 3160040136) and the priming scientific research foundation for the junior researcher in Beijing Tongren Hospital, Capital Medical University (2015-YJJ-ZZL-008) and Beijing Key Laboratory of Ophthalmology and Visual Science (2016YKSJ02).

References

[1] K. Willekens, R. Rocha, K. Van Keer et al., "Review on dynamic contour tonometry and ocular pulse amplitude," *Ophthalmic Research*, vol. 55, no. 2, pp. 91–98, 2016.

[2] A. Z. Jiwani, D. J. Rhee, S. C. Brauner et al., "Effects of caffeinated coffee consumption on intraocular pressure, ocular perfusion pressure, and ocular pulse amplitude: a randomized controlled trial," *Eye*, vol. 26, no. 8, pp. 1122–1130, 2012.

[3] S. Moghimi, H. Torabi, G. Fakhraie, N. Nassiri, and M. Mohammadi, "Dynamic contour tonometry in primary open angle glaucoma and pseudoexfoliation glaucoma: factors associated with intraocular pressure and ocular pulse amplitude," *Middle East African Journal of Ophthalmology*, vol. 20, no. 2, pp. 158–162, 2013.

[4] P. B. Knecht, L. M. Bachmann, M. A. Thiel, K. Landau, and C. Kaufmann, "Ocular pulse amplitude as a diagnostic adjunct in giant cell arteritis," *Eye*, vol. 29, no. 7, pp. 860–866, 2015.

[5] M. E. Langham, *Ischemia and Loss of Vascular Autoregulation in Ocular and Cerebral Diseases*, Springer, New York, NY, USA, 2009.

[6] M. C. Grieshaber, R. Katamay, K. Gugleta, A. Kochkorov, J. Flammer, and S. Orgül, "Relationship between ocular pulse amplitude and systemic blood pressure measurements," *Acta Ophthalmologica*, vol. 87, no. 3, pp. 329–334, 2009.

[7] F. Berisha, O. Findl, M. Lasta, B. Kiss, and L. Schmetterer, "A study comparing ocular pressure pulse and ocular fundus pulse in dependence of axial eye length and ocular volume," *Acta Ophthalmologica*, vol. 88, no. 7, pp. 766–772, 2010.

[8] D. Bouget, F. Lalys, and P. Jannin, "Surgical tools recognition and pupil segmentation for cataract surgical process modeling," *Studies in Health Technology & Informatics*, vol. 173, pp. 78–84, 2012.

[9] R. Koprowski, S. Wilczyński, Z. Wróbel, S. Kasperczyk, and B. Błońska-Fajfrowska, "Automatic method for the dermatological diagnosis of selected hand skin features in hyperspectral imaging," *BioMedical Engineering Online*, vol. 13, no. 1, article no. 47, 2014.

[10] R. Koprowski, S. Wilczyński, Z. Wróbel, and B. Błońska-Fajfrowska, "Calibration and segmentation of skin areas in hyperspectral imaging for the needs of dermatology," *Biomedical Engineering Online*, vol. 13, article 113, 2014.

[11] D. Y. Tam and I. I. K. Ahmed, "The phaco hemi-flip: a method of lens removal in nuclei of soft to moderate density," *Ophthalmic Surgery Lasers & Imaging*, vol. 42, no. 2, pp. 170–174, 2011.

[12] C.-S. Kim, A. M. Carek, R. Mukkamala, O. T. Inan, and J.-O. Hahn, "Ballistocardiogram as proximal timing reference for pulse transit time measurement: potential for cuffless blood pressure monitoring," *IEEE Transactions on Biomedical Engineering*, vol. 62, no. 11, pp. 2657–2664, 2015.

[13] S. S. Thomas, V. Nathan, C. Zong et al., "BioWatch—a wrist watch based signal acquisition system for physiological signals including blood pressure," in *Proceedings of the 36th Annual International Conference of the IEEE Engineering in Medicine and Biology Society (EMBC '14)*, pp. 2286–2289, Chicago, Ill, USA, August 2014.

[14] T. Wibmer, C. Denner, C. Fischer et al., "Blood pressure monitoring during exercise: comparison of pulse transit time and volume clamp methods," *Blood Pressure*, vol. 24, no. 6, pp. 353–360, 2015.

[15] A. Patzak, Y. Mendoza, H. Gesche, and M. Konermann, "Continuous blood pressure measurement using the pulse transit time: comparison to intra-arterial measurement," *Blood Pressure*, vol. 24, no. 4, pp. 217–221, 2015.

[16] X.-R. Ding, Y.-T. Zhang, J. Liu, W.-X. Dai, and H. K. Tsang, "Continuous cuffless blood pressure estimation using pulse transit time and photoplethysmogram intensity ratio," *IEEE Transactions on Biomedical Engineering*, vol. 63, no. 5, pp. 964–972, 2016.

[17] R. Wang, W. Jia, Z.-H. Mao, R. J. Sclabassi, and M. Sun, "Cuff-free blood pressure estimation using pulse transit time and heart rate," in *Proceedings of the 12th IEEE International Conference on Signal Processing (ICSP '14)*, pp. 115–118, HangZhou, China, October 2014.

[18] D. Da He, E. S. Winokur, and C. G. Sodini, "An ear-worn vital signs monitor," *IEEE Transactions on Biomedical Engineering*, vol. 62, no. 11, pp. 2547–2552, 2015.

[19] M. Forouzanfar, H. R. Dajani, V. Z. Groza, M. Bolic, S. Rajan, and I. Batkin, "Oscillometric blood pressure estimation: past, present, and future," *IEEE Reviews in Biomedical Engineering*, vol. 8, pp. 44–63, 2015.

[20] Y. U. Kim, D. H. Kim, Y. Cheong et al., "Pulse transit time as a predictor of the efficacy of a celiac plexus block in patients with chronic intractable abdominal pain," *Clinical Journal of Pain*, vol. 32, no. 6, pp. 522–526, 2016.

[21] S. Umesh, S. Padma, S. Ambastha, A. Kalegowda, and S. Asokan, "Pulse transit time differential measurement by fiber Bragg grating pulse recorder," *Journal of Biomedical Optics*, vol. 20, no. 5, Article ID 057005, 2015.

[22] F. S. Hu, Y. L. Zhang, Z. C. Ma et al., "A region-matching method for pulse transit time estimation: potential for improving the accuracy in determining carotid femoral pulse wave velocity," *Journal of Human Hypertension*, vol. 29, no. 11, pp. 675–682, 2015.

[23] L. S. Manning, T. G. Robinson, and R. B. Panerai, "The SOMNOtouch device as a novel method for measuring short-term blood pressure variability: a comparison with the Finometer," *Blood Pressure Monitoring*, vol. 20, no. 6, pp. 361–368, 2015.

[24] D. Buxi, J.-M. Redouté, and M. R. Yuce, "A survey on signals and systems in ambulatory blood pressure monitoring using pulse transit time," *Physiological Measurement*, vol. 36, no. 3, pp. R1–R26, 2015.

[25] R. Mukkamala, J.-O. Hahn, O. T. Inan et al., "Toward ubiquitous blood pressure monitoring via pulse transit time: theory and practice," *IEEE Transactions on Biomedical Engineering*, vol. 62, no. 8, pp. 1879–1901, 2015.

[26] X. Zhou, R. Peng, H. Ding, N. Zhang, and P. Li, "Validation of new and existing decision rules for the estimation of beat-to-beat pulse transit time," *BioMed Research International*, vol. 2015, Article ID 306934, 13 pages, 2015.

[27] W. Wang, S. Du, and X. Zhang, "Corneal deformation response in patients with primary open-angle glaucoma and in healthy subjects analyzed by corvis ST," *Investigative Ophthalmology and Visual Science*, vol. 56, no. 9, pp. 5557–5565, 2015.

[28] R. Lee, R. T. Chang, I. Y. H. Wong, J. S. M. Lai, J. W. Y. Lee, and K. Singh, "Novel parameter of corneal biomechanics that differentiate normals from glaucoma," *Journal of Glaucoma*, vol. 25, no. 6, pp. e603–e609, 2016.

[29] F. J. Bao, M. L. Deng, Q. M. Wang et al., "Evaluation of the relationship of corneal biomechanical metrics with physical intraocular pressure and central corneal thickness in ex vivo rabbit eye globes," *Experimental Eye Research*, vol. 137, pp. 11–17, 2015.

[30] A. Frings, S. J. Linke, E. L. Bauer, V. Druchkiv, T. Katz, and J. Steinberg, "Effects of laser in situ keratomileusis (LASIK) on corneal biomechanical measurements with the Corvis ST tonometer," *Clinical Ophthalmology*, vol. 9, pp. 305–311, 2015.

[31] C. Ji, J. Yu, T. Li et al., "Dynamic curvature topography for evaluating the anterior corneal surface change with Corvis ST," *BioMedical Engineering Online*, vol. 14, article 53, pp. 1–16, 2015.

[32] R. Koprowski and R. Ambrósio, "Quantitative assessment of corneal vibrations during intraocular pressure measurement with the air-puff method in patients with keratoconus," *Computers in Biology and Medicine*, vol. 66, pp. 170–178, 2015.

[33] R. Koprowski, "Open source software for the analysis of corneal deformation parameters on the images from the Corvis tonometer," *BioMedical Engineering Online*, vol. 14, no. 1, article 31, pp. 1–15, 2015.

[34] R. Koprowski, R. Ambrósio, and S. Reisdorf, "Scheimpflug camera in the quantitative assessment of reproducibility of

high-speed corneal deformation during intraocular pressure measurement," *Journal of Biophotonics*, vol. 8, no. 11-12, pp. 968–978, 2015.

[35] R. Koprowski, "Automatic method of analysis and measurement of additional parameters of corneal deformation in the Corvis tonometer," *BioMedical Engineering Online*, vol. 13, no. 1, article 150, 2014.

[36] R. Koprowski, M. Szmigiel, H. Kasprzak, Z. Wróbel, and S. Wilczyński, "Quantitative assessment of the impact of blood pulsation on images of the pupil in infrared light," *Journal of the Optical Society of America A*, vol. 32, no. 8, pp. 1446–1453, 2015.

[37] H. Kasprzak and R. Koprowski, "Tonometer for contact measurement such as cornea pressure and visco elasticity of eye, has two filters connected to subtractor, and analog-to-digital converter connected to microprocessor, where one of filter is connected to microprocessor," Patent Number: PL406553-A1, Patent Assignee: Politechnika Wroclawska, 2014.

[38] R. Koprowski, S. Teper, Z. Wróbel, and E. Wylegala, "Automatic analysis of selected choroidal diseases in OCT images of the eye fundus," *BioMedical Engineering Online*, vol. 12, no. 1, article no. 117, 2013.

[39] S. Wilczyński, B. Pilawa, R. Koprowski et al., "EPR studies of free radicals decay and survival in gamma irradiated aminoglycoside antibiotics: sisomicin, tobramycin and paromomycin," *European Journal of Pharmaceutical Sciences*, vol. 45, no. 3, pp. 251–262, 2012.

[40] R. Koprowski, S. Wilczyński, A. Samojedny, Z. Wróbel, and A. Deda, "Image analysis and processing methods in verifying the correctness of performing low-invasive esthetic medical procedures," *BioMedical Engineering Online*, vol. 12, no. 1, article 51, 2013.

[41] A. Glowacz and Z. Glowacz, "Diagnostics of stator faults of the single-phase induction motor using thermal images, MoASoS and selected classifiers," *Measurement: Journal of the International Measurement Confederation*, vol. 93, pp. 86–93, 2016.

[42] A. Byrski and M. Kisiel-Dorohinicki, "Agent-based model and computing environment facilitating the development of distributed computational intelligence systems," in *Computational Science—ICCS 2009: 9th International Conference Baton Rouge, LA, USA, May 25–27, 2009 Proceedings, Part II*, vol. 5545 of *Lecture Notes in Computer Science*, pp. 865–874, Springer, Berlin, Germany, 2009.

[43] D. Krzywicki, Ł. Faber, A. Byrski, and M. Kisiel-Dorohinicki, "Computing agents for decision support systems," *Future Generation Computer Systems*, vol. 37, pp. 390–400, 2014.

[44] A. Byrski, R. Schaefer, M. Smolka, and C. Cotta, "Asymptotic guarantee of success for multi-agent memetic systems," *Bulletin of the Polish Academy of Sciences: Technical Sciences*, vol. 61, no. 1, pp. 257–278, 2013.

Hindawi Publishing Corporation
Journal of Ophthalmology
Volume 2016, Article ID 9640643, 8 pages
http://dx.doi.org/10.1155/2016/9640643

Clinical Study

Evaluation of Monocular Treatment for Meibomian Gland Dysfunction with an Automated Thermodynamic System in Elderly Chinese Patients: A Contralateral Eye Study

Yinying Zhao,[1,2] Jialu Xie,[1,2] Junhua Li,[1,2] Yana Fu,[1,2] Xiaolei Lin,[1,2] Shangrong Wang,[1,2] Jiling Ma,[1,2] and Yune Zhao[1,2]

[1]*School of Ophthalmology and Optometry, Eye Hospital, Wenzhou Medical University, Wenzhou, Zhejiang, China*
[2]*Key Laboratory of Vision Science, Ministry of Health, Wenzhou, Zhejiang, China*

Correspondence should be addressed to Yune Zhao; zyehzeye@126.com

Received 24 August 2016; Revised 24 November 2016; Accepted 30 November 2016

Academic Editor: László Módis

Purpose. To investigate the safety and efficacy of monocular treatment for elderly Chinese patients with meibomian gland dysfunction (MGD) with an automated thermodynamic system. *Methods.* This study was a prospective, examiner-masked, contralateral eye clinical trial. The eye perceived by the patient to be worse (test eye) received a 12-minute LipiFlow treatment, while the other eye served as control. All patients were examined before treatment and one week, one month, and three months after treatment. Clinical parameters included dry eye symptoms, lipid layer thickness (LLT), partial blink (PB) ratio, invasive tear breakup time (ITBUT) and cornea staining, Schirmer I test, meibomian glands yielding liquid secretion (MGYLS), and meibomian gland dropout. *Results.* A total of 29 patients were examined during the three-month follow-up. At each posttreatment visit, they had a significant reduction in dry eye symptoms accompanied by an increase of ITBUT and MGYLS and a reduction in corneal staining compared with the baseline parameters. There was a significant improvement in MGYLS and ITBUT in the test eye compared with the control eye. Other clinical parameters were not statistically significant. *Conclusion.* LipiFlow is an effective treatment for patients with MGD. Monocular treatment with LipiFlow may be a cost-effective treatment option to those afflicted with MGD in the developing world.

1. Introduction

In 2011, the International Workshop on Meibomian Gland Dysfunction announced a new definition of MGD: "a chronic, diffuse abnormality of the meibomian glands, commonly characterized by terminal duct obstruction and/or qualitative/quantitative changes in the glandular secretion. It may result in alteration of the tear film, symptoms of eye irritation, clinically apparent inflammation, and ocular surface disease [1]."

Today, numerous clinical approaches are being undertaken to relieve meibomian gland obstruction. The most effective and well-known treatment is warm compress combined with lid massage, which heats the glands and alleviates gland obstruction [2, 3]. However, for this treatment to be effective, an intensive treatment regimen is required to be performed by the patient, making patient compliance low [4, 5].

A promising new instrument called LipiFlow (TearScience Inc., Morrisville, NC) has been specifically designed to partially or possibly completely alleviate meibomian gland obstruction. This instrument combines the benefits of both heat therapy and physical expression while accurately controlling the temperature, pressure, and technique.

Several studies [6–8] have reported the improvement in meibomian gland secretion after one 12-minute treatment by LipiFlow and the effects last up to one year. Tear film breakup time (TBUT) and symptom scores also showed improvement compared with traditional therapies [9–11]. Previous studies were performed with concurrent binocular therapy, which

may be cost prohibitive in developing countries and may introduce statistical errors in the analysis of the study. This is the first study to evaluate the effect of monocular therapy by LipiFlow. Overall, the objective of this study was to determine the efficacy of monocular treatment with LipiFlow, with the contralateral eye as a control, in elderly Chinese patients with MGD.

2. Patients and Methods

This prospective, examiner-masked, clinical trial was performed at Wenzhou University, Zhejiang, China, and was approved by the Institutional Review Board/Ethics Committee of Wenzhou Medical University. Informed consent to participate in this research study was obtained from each patient. Practices and researches were conducted in accordance with the tenets of the Declaration of Helsinki. The study was registered at www.clinicaltrials.gov and the clinical trial accession number is NCT02481167.

2.1. Patients. Patients who completed a comprehensive baseline ocular surface evaluation were enrolled in accordance with the inclusion criterion. Eligible patients were recruited. The eye which the patient perceived as worse was selected as the test eye. The test eye received a 12-minute LipiFlow treatment. The contralateral eye served as the control eye. Data from both eyes were recorded before treatment as baseline and were reexamined at one week, one month, and three months posttreatment. Patients who met the following criteria were eligible for the study.

2.1.1. Inclusion Criteria

(1) Age from 55 to 75 years old

(2) Reported dry eye symptoms with a standard patient evaluation for eye dryness (SPEED) score greater than 6 at the baseline

(3) Meibomian gland atrophy less than fifty percent

(4) Evidence of functional meibomian gland (clear liquid secretion) number being 6 or less

(5) Informed consent given to participate in the study

(6) Ability to complete an initial evaluation and the follow-up visits after treatment (one week, one month, and three months)

2.1.2. Exclusion Criteria

(1) Ocular trauma, surgery, or active infection in either eye within three months of the baseline examination

(2) Being determined to have dry eye symptoms that were not secondary to MGD, such as a systemic autoimmune disease

(3) Abnormalities that may potentially affect the integrity of the cornea or lid function in either eye

(4) Involvement in other ophthalmic drug or medical device clinical trials within 30 days of the baseline examination

(5) Treatment with lacrimal plugs or canaliculoplasty in either eye within three months of the baseline examination or the potential of requiring new treatment during the follow-up period

2.2. Methods. Before the initial clinical examination, patients were asked to report their clinical history and general physical condition. Meibography was only recorded at the baseline and three-month visit. The following clinical tests were performed at each follow-up visit in this order: dry eye questionnaire, best corrected visual acuity (BCVA), Lipiview Interferometer examination, slit-lamp examination, TBUT, corneal staining, Schirmer I test, and extrusion of meibomian glands. In order to control for examiner variability, the same experienced masked clinical investigator conducted all examinations. During the follow-up period, ocular lubricants and warm compress treatments were not restricted for humanitarian reasons.

2.3. Investigated Parameters

2.3.1. Dry Eye Symptoms. Two questionnaires, Standard Patient Evaluation of Eye Dryness (SPEED) [12] and the Ocular Surface Disease Index (OSDI), were used to assess dry eye symptoms.

2.3.2. Lipid Layer Thickness (LLT) and Partial Blink (PB). Lipiview Interferometer (TearScience Inc., Morrisville, NC) was used to determine the lipid layer thickness (LLT) and blink pattern (BP). A 20-second video of each eye was captured to record the interference pattern of the tear film. The software uses an algorithm which converts the value in interferometric color units (ICUs) into nanometers of lipid layer thickness (LLT) (1 ICU approximately reflects 1 nm of the LLT). Additionally, partial blinks (PB) and total blinks were also recorded. The partial blink (PB) ratio equals the number of partial blinks/the number of total blinks.

2.3.3. Invasive Tear Breakup Time (ITBUT) and Corneal Staining [13]. To evaluate the TBUT and corneal staining, strips of fluorescein sodium (containing 1.0 mg fluorescein sodium) (Jing Ming New Technological Development Co., Ltd., Tianjin, China) were used. To perform this, patients were told to look up while the tip of the strip quickly touched the inferior conjunctiva. ITBUT was calculated by calculating the average of three consecutive breakup times, as determined manually by a stopwatch.

Three minutes after fluorescein instillation slit-lamp biomicroscopy cobalt blue illumination was used to evaluate corneal staining. The cornea was divided into four quadrants (supertemporal, inferotemporal, supernasal, and inferonasal). Superficial punctate keratopathy in the cornea was scored from 0 to 3 in each quadrant: 0, no staining in the cornea; 1, <5 punctuate staining; 2, >5 punctuate staining

but <10; and 3, >10 punctuate staining. A sum of the staining scores ranged from 0 to 12.

2.3.4. Schirmer I Test without Anesthesia. The Schirmer I test was performed without anesthesia. Schirmer Tear Test Strips (Jing Ming New Technological Development Co., Ltd., Tianjin, China) were placed between the lateral and middle third of the lower eyelid and patients were instructed to close their eyelids for five minutes.

2.3.5. Meibomian Gland Assessment. To assess meibomian gland function, the number of functional glands was counted. A gland was considered functional if it yielded a clear liquid secretion, which represents both the quantity and the quality of meibomian gland secretions. The number of meibomian gland orifices was quantified using the Meibomian Gland Evaluator (TearScience Inc.). Using this handheld instrument, a defined pressure (a consistent force of 1.25 g/mm^2, similar to that experienced with a deliberate or forced blink) was applied to the nasal, central, and temporal regions of the lower eyelid. Each region contained five consecutive meibomian gland orifices. A total of 15 glands were evaluated along the lower eyelid margin. Finally, the number of glands secreting clear liquid was counted.

2.3.6. Meibomian Gland Dropout [14]. The Keratograph 5M (Oculus, Wetzlar, Germany) is an advanced corneal topographer that can be used for meibography. Infrared meibography with high-contrast images of the meibomian glands was employed to observe upper and lower everted eyelids of each eye. A meiboscore was given according to calculations assigned by ImageJ software (Ver. 1.50b, National Institutes of Health, USA) for each eyelid corresponding to the percentage of meibomian gland affected by atrophy. The overall percentage of abnormalities of each lid was described as 0% (grade 0), less than 33% (grade 1), 33 to 67% (grade 2), or greater than 67% (grade 3) [15]. The higher the score, the more severe the meibomian atrophy.

2.3.7. Additional Clinical Parameters. Several additional parameters were assessed to evaluate the safety of LipiFlow instrument. These included adverse events (during the study period) and an ocular health exam (eyelid marginal hyperemia and pachyblepharosis).

2.4. Statistical Analysis. Statistical analysis was performed using SPSS 19.0 for Microsoft Windows (Chicago, Illinois, USA). To compare the baseline and posttreatment outcomes for the test group, paired two-tailed t-test was used where the normal distribution was confirmed using the Kolmogorov–Smirnov test, $p > 0.05$). The Wilcoxon signed-rank test was used for nonparametric distributed data (Kolmogorov–Smirnov test, $p < 0.05$). A repeated measures analysis of variance (ANOVA) test was performed for comparison of test group and control group at all time points. A difference was considered statistically significant if a value of $p = 0.05$ was reached.

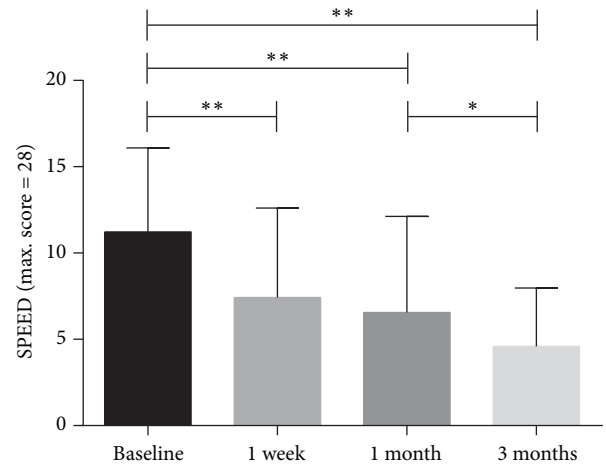

Figure 1: The mean value of test-eye Standard Patient Evaluation of Eye Dryness (SPEED) score measured at baseline, at one week, at one month, and at three months ($^*p < 0.05$, $^{**}p < 0.001$).

3. Results

Thirty subjects were initially enrolled; however, 29 subjects (58 eyes, 56.90 ± 7.07 years old, 20 (69%) women and 9 (31%) men) completed the study. One patient enrolled in the study had to be excluded after the baseline examination due to treatment for meningeal gliomatosis.

3.1. Comparison of the Test Eye at Baseline and after Treatment

3.1.1. Subjective Symptoms. There was a significant improvement in SPEED scores at the one-week visit (7.43 ± 5.18, $p < 0.0001$) compared with the baseline scores (11.22 ± 4.87) and this improvement was maintained at the one-month time point (6.55 ± 5.57, $p < 0.001$). Similarly, at the three-month time point (4.59 ± 3.40, $p < 0.001$), the observed improvement was still significant. However, the difference between the one-week and the one-month visits was not statistically significant ($p = 0.343$, $p > 0.05$). SPEED scores continued to decrease from the one-month visit to the three-month visit ($p = 0.017$, $p < 0.05$) (Figure 1). A significant improvement of dry eye symptoms was observed in both one-week and one-month follow-ups. Also, a further improvement was found in the three-month follow-up. Results of OSDI score were consistent with SPEED scores (Figure 2).

3.1.2. Changes of Tear Film. No statistically significant change in the average, maximum, or minimum in the lipid layer thickness (LLT) was observed from preprocedure time point to one week, one month, and three-month postprocedure visits (Figure 3). Partial blink (PB) ratios held a similar trend as no statistical difference between the initial evaluation and any of the follow-up visits after treatment was recorded (Figure 4).

A statistically significant increase in TBUT from the preprocedure time point (2.48 ± 0.83) to the one-week postprocedure visit (3.24 ± 1.02; $p = 0.003$) was reported.

Table 1: Baseline parameters.

	Lipiview (ave.)	Lipiview (max.)	Lipiview (min.)	Partial blink*	BUT*	Schirmer*	Meibomian gland orifices*	Corneal stain*
Test	62.07 ± 23.98	75.76 ± 21.61	54.24 ± 23.79	0.65 ± 0.35	2.48 ± 0.83	8.17 ± 6.96	1.79 ± 1.78	1.21 ± 0.62
Control	68.90 ± 23.32	77.93 ± 20.03	59.59 ± 22.61	0.70 ± 0.33	2.79 ± 1.01	8.76 ± 6.42	2.34 ± 1.90	1.55 ± 0.74
Significance	0.052	0.516	0.194	0.778	0.119	0.560	0.130	0.309

*Wilcoxon signed-rank test.
There were no significant differences for all of these measured parameters between the test and control eyes before treatment ($p > 0.05$).

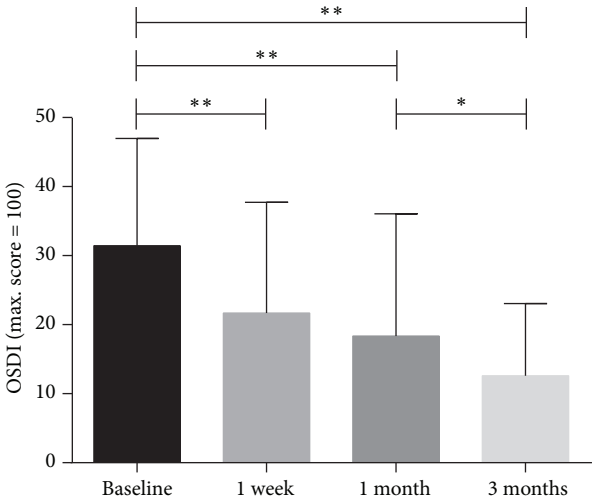

Figure 2: The mean value of test-eye Ocular Surface Disease Index (OSDI) at baseline, at one week, at one month, and at three months (*$p < 0.05$, **$p < 0.001$).

This increase remained significant at the one-month (3.62 ± 1.15; $p = 0.001$) and the three-month (3.52 ± 1.43; $p = 0.004$) postprocedure visits. The difference between one-week and one-month visits was also statistically significant ($p = 0.033$, $p < 0.05$). However, the difference between one-month and three-month visits was not statistically significant ($p = 0.687$, $p > 0.05$) (Figure 5). An increase of TBUT was observed at all follow-up visits; however, further improvement was not observed at the three-month follow-up visit.

Total score of the four corneal regions examined was on a scale of 0 to 12 at the baseline, one-week, one-month, and three-month examinations. The total sodium fluorescein staining scores of the corneal epithelium were reduced from baseline (2.34 ± 1.77) to one week (1.63 ± 1.50, $p = 0.002$). There was a statistically significant reduction in the fluorescein staining scores when comparing baseline visit data to one-month (1.50 ± 1.41, $p < 0.0001$) and three-month (1.31 ± 1.49, $p < 0.0001$) posttreatment visit data (Figure 6).

There was a statistically significant decrease in Schirmer I test without anesthesia from the preprocedure time point (8.17 ± 6.96) compared to the one-week postprocedure visit (6.03 ± 4.38; $p = 0.040$, <0.05). A nonsignificant decrease was observed at the one-month postprocedure visit (6.90 ± 7.09; $p = 0.086$), However, at the three-month postprocedure visit, a significant decrease compared to baseline (4.90 ± 6.56; $p = 0.004$, <0.05) was observed. The difference between one-week and one-month visits was not statistically significant ($p = 0.680$, >0.05). The difference between one-month and three-month visits was also not statistically significant ($p = 0.120$, $p > 0.05$) (Figure 7).

3.2. Improvements of Meibomian Gland Function

3.2.1. Meibomian Glands Yielding Liquid Secretion (MGYLS). A significant increase was seen in MGYLS from preprocedure levels (1.78 ± 1.78) to the postprocedure one-week visit (3.75 ± 2.82, $p < 0.0001$). The improvement at one month remained significant (4.56 ± 2.85, $p < 0.0001$). Improvement was maintained at the three-month postprocedure visit (4.75 ± 3.08, $p < 0.0001$). There was no statistically significant difference between the one-week and the one-month visits ($p = 0.687$). Likewise, no difference was observed between the one-month and the three-month visits ($p = 0.635$) (Figure 8).

3.2.2. Meibomian Gland Dropout. There were no statistical differences in meibomian gland dropout between baseline and three-month posttreatment of both the upper eyelid ($p = 0.655$) and the lower eyelid ($p = 0.414$). This suggests that treatment may not have an effect on the atrophic meibomian gland.

3.2.3. Comparison of the Test Eye and the Control Eye. Binocular baseline parameters are listed in Table 1. At baseline, there was no statistically significant difference for all measurements between control and test eyes ($p > 0.05$). After the treatment period, there were statistically significant changes in TBUT (Figure 9) and MGYLS (Figure 10).

During the posttreatment period, eight (28%) patients stopped using artificial tears and 11 (38%) patients reduced the frequency in which they use artificial tears. At the end of the three-month follow-up, only three patients reported that their subjective dry eye symptoms had not been improved. The remaining patients all reported improvements in their clinical symptoms at differing degrees.

4. Discussion

The goal of this study was to assess the safety and effectiveness of a 12-minute LipiFlow monocular treatment on elderly

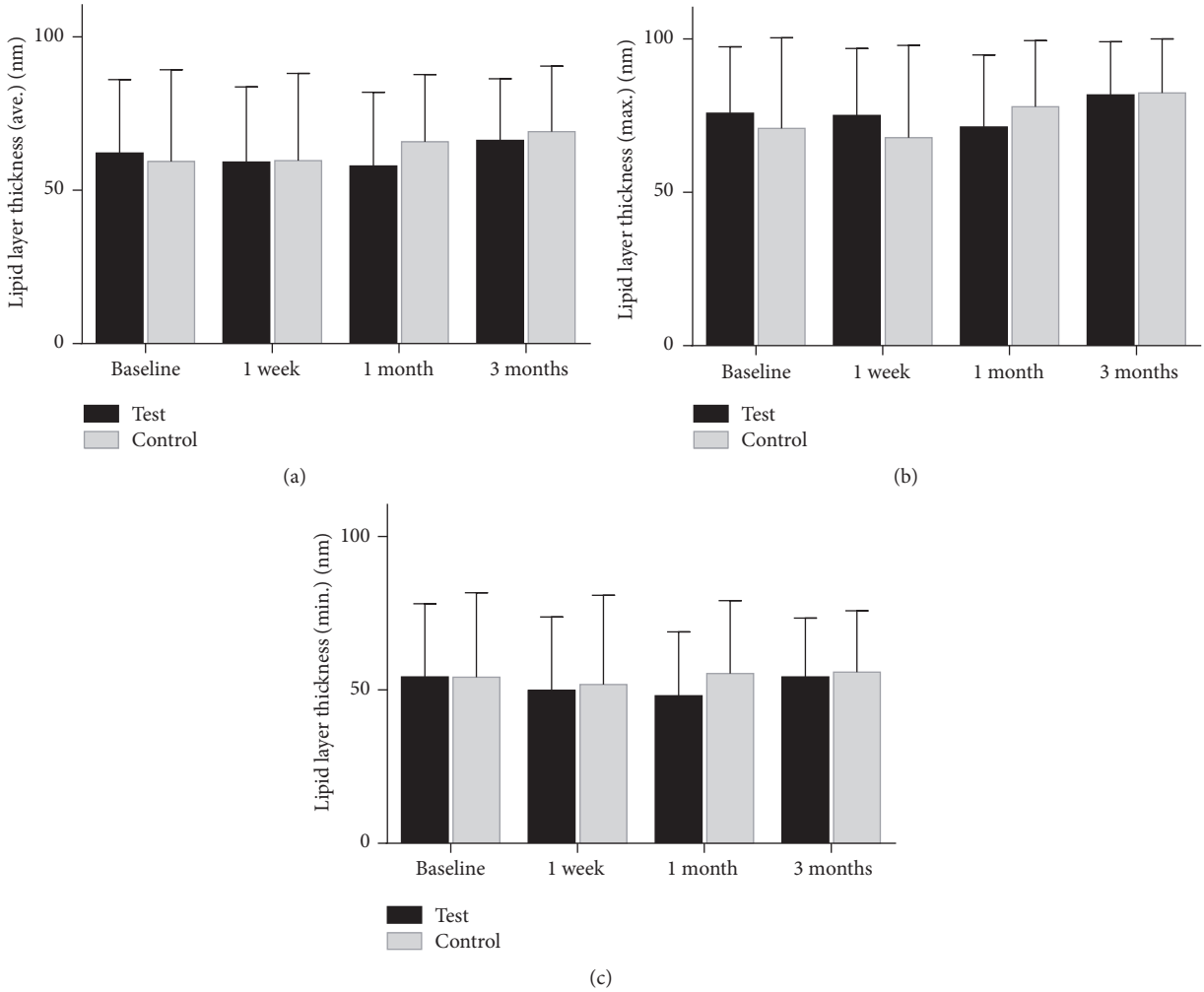

Figure 3: The mean value of test-eye lipid layer thickness (LLT) at baseline, at one week, at one month, and at three months. (a) The average of LLT. (b) The maximum of LLT. (c) The minimum of LLT.

Chinese patients with MGD. Previous studies reported that a single LipiFlow 12-minute treatment improved meibomian gland secretion, TBUT, and symptom scores at one month, nine months, 12 months, and even three years posttreatment compared with traditional or new-style warm compress therapies and common clinical methods of physical expression of meibomian gland obstruction [16].

Previous studies evaluated the efficacy of LipiFlow by treatment of both eyes. Treatment of both eyes considerably increases the cost for patients in developing countries. This is the first study to report the results of monocular treatment with LipiFlow with the contralateral eye as a control.

The primary clinical parameters used to assess the effectiveness of LipiFlow indicated significant improvement of meibomian gland function and tear film stability in the test eye. These results demonstrate that treatment restored the function of previously blocked dysfunctional meibomian glands and an increase in gland function improved tear film stability, which may directly influence other objective and subjective measures of ocular surface health. Briefly, the prolonged TBUT, reduced corneal staining, and improved subjective symptoms provide strong evidence of the efficiency of LipiFlow.

However, significant changes of LLT were not observed. Previous studies report the repeatability and reliability of LLT measured by Lipiview [17]. Finis et al. [18] found that LLT increased significantly six months after treatment with LipiFlow. During the follow-up period, we observed that the consistency of meibum secreted from the meibomian gland greatly influenced LLT. Unhealthy meibum, which has a high LLT value, may have altered the results of our study. We plan to focus on the relationship between the consistency of meibum and LLT in future studies. Interestingly, we observed that Schirmer I test results, which represents tear fluid secretion, began to decrease at one week and continued to decrease at the three-month posttreatment examination. We speculate that the reopening of the meibomian glands stabilizes the tear film, making the tear fluid reflexively decrease to maintain homeostasis at the ocular surface. The existence of a homeostatic state of the tear film was proposed by Dartt and Willcox [19] where components of the tear film may compensate for deficiencies in others. Arita et al. [20]

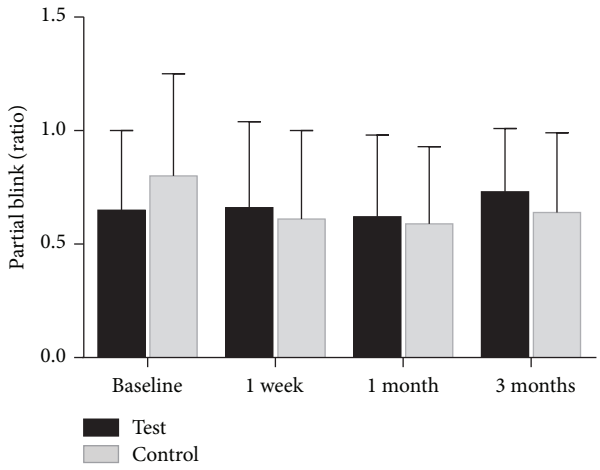

Figure 4: The mean value of test-eye partial blink (PB) ratios at baseline, at one week, at one month, and at three months.

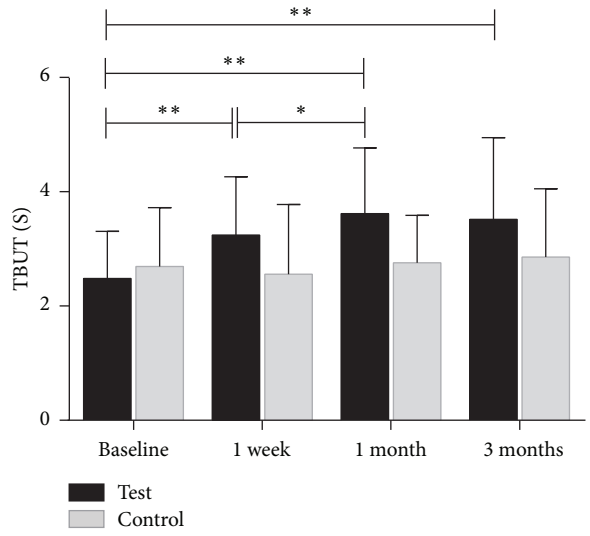

Figure 5: The mean value of test-eye tear breakup time (TBUT) measured at baseline, at one week, at one month, and at three months ($^{*}p < 0.05$, $^{**}p < 0.001$).

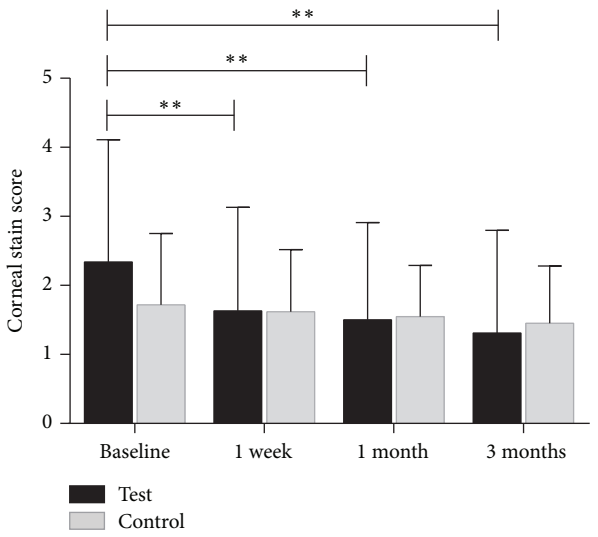

Figure 6: The mean value of test-eye cornea staining score measured at baseline, at one week, at one month, and at three months ($^{*}p < 0.05$, $^{**}p < 0.001$).

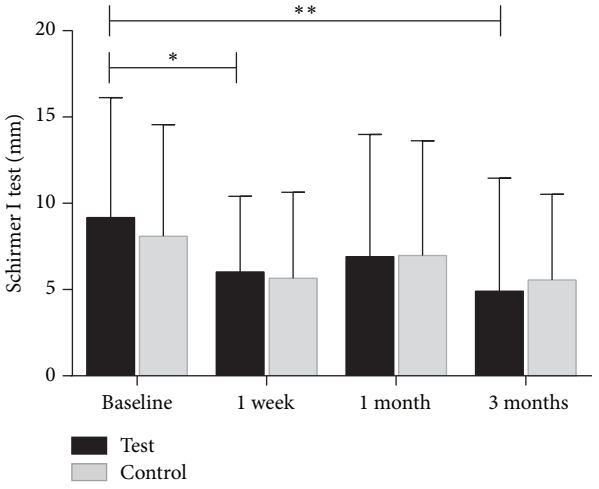

Figure 7: The mean value of test-eye Schirmer I test without anesthesia measured at baseline, at one week, at one month, and at three months ($^{*}p < 0.05$, $^{**}p < 0.001$).

reported that an increase in tear fluid production likely compensates for loss of meibomian glands in MGD patients. Our results support the hypothesis of the homeostatic nature of the tear film.

Blink is an action associated with consciousness [21]; this behavior is difficult to change in a short time. Furthermore, during the examination of the partial blink by Lipiview, there is a strong flicker which could disturb the patients blink in nature. These may explain why partial blink was unchanged before and after treatment. We will make further explorations about the association between blink and dry eye.

Our study reports improvement in the subjective symptoms of control eye, which did not receive treatment, after three months of the monocular treatment. We speculate that this could be attributed to the placebo effect. Placebos are known to have an effect on the immune system [22]. It has been suggested that the effectiveness of a treatment or placebo is shaped by the subjects' expectations [23]. For example, patients with dry eye have increased incidence of depression and anxiety [24, 25]. Treatment, even placebo, may improve their clinical outcome and may explain why treatment in one eye has an effect on both eyes.

In this study, we excluded patients with severe meibomian gland atrophy (more than fifty percent) as they may respond poorly to treatment. Consistent with previously published studies, meibomian gland morphology had no obvious change posttreatment. This might also explain why patients with early stage of MGD are more likely to respond positively to this treatment. It is also possible that three months may

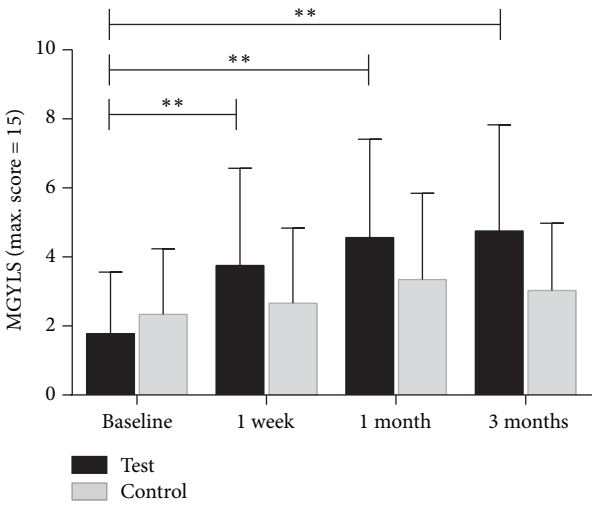

Figure 8: The mean value of test-eye meibomian glands yielding liquid secretion (MGYLS) measured at baseline, at one week, at one month, and at three months ($^{**}p < 0.001$).

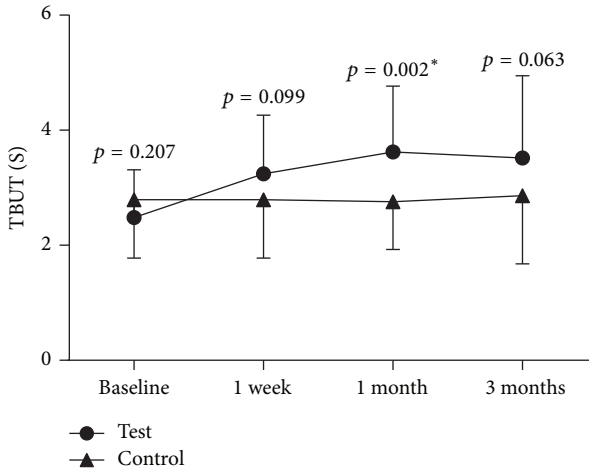

Figure 9: Time course of tear film breakup time (TBUT). Circle: test eye; triangle: control eye. There was a significant change between the test and control eye ($p = 0.045$). Differences of each point (one week, one month, and three months) posttreatment visit were labeled above the line ($^{*}p < 0.05$).

not be long enough to detect changes in meibography as the regrowth of new glands and ducts may take longer.

In conclusion, our study suggests that the eyes treated by LipiFlow improved dramatically in objective parameters compared with contralateral eye in patients with MGD. Furthermore, monocular treatment can be beneficial to improve the subjective symptoms of those afflicted with MGD. Monocular treatment with LipiFlow may be a cost-effective alternative for treatment of MGD in developing countries.

Ethical Approval

This prospective study was approved by the Research Review Board at Wenzhou Medical University. Practices and research

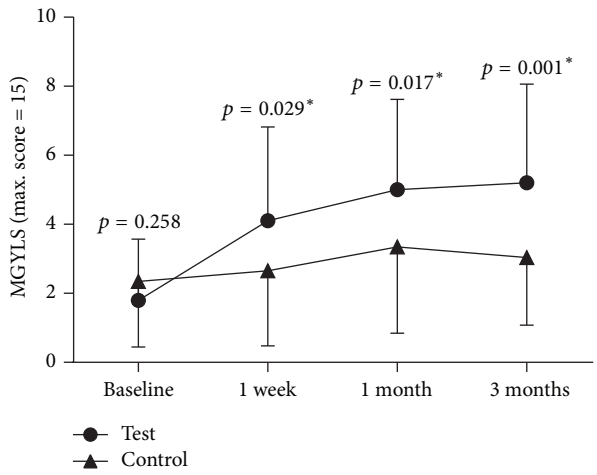

Figure 10: Time course of meibomian glands yielding liquid secretion (MGYLS). Circle: test eye; triangle: control eye. There was a significant change between the test and control eye ($p = 0.019$). Differences of each point (one week, one month, and three months) posttreatment visit were labeled above the line ($^{*}p < 0.05$).

were in accordance with the tenets of the Declaration of Helsinki.

Consent

Written informed consent was obtained from all the patients after explanation.

Competing Interests

All authors declare that the mentioned received grant did not lead to any competing interests regarding the publication of this manuscript and there is not any other possible conflict of interests in the manuscript.

Authors' Contributions

Design of the study was carried out by Yune Zhao and Yinying Zhao. Yune Zhao, Yinying Zhao, Jialu Xie, and Junhua Li conducted the study. Collection of data was done by Yinying Zhao, Jialu Xie, Yana Fu, Shangrong Wang, and Jiling Ma. Interpretation of the data was carried out by Yinying Zhao, Jialu Xie, Junhua Li, and Yana Fu. Yinying Zhao, Jialu Xie, Xiaolei Lin, and Yune Zhao prepared the manuscript. Yune Zhao approved the final version of the manuscript. Yinying Zhao and Jialu Xie contributed equally to this work.

Acknowledgments

The LipiFlow activator was supplied at no cost by TearScience Inc. Company. This study was supported by research grants from the Provincial Construction Project of Zhejiang (Grant no. 201647538) and the Innovation Discipline of Zhejiang Province (lens disease in children). The authors thank Terry

G. Coursey, Ph.D. (Baylor College of Medicine), for providing editing services for this manuscript.

References

[1] K. K. Nichols, "The international workshop on meibomian gland dysfunction: introduction," *Investigative Ophthalmology & Visual Science*, vol. 52, no. 4, pp. 1917–1921, 2011.

[2] S. Yeo, J. H. Tan, U. R. Acharya, V. K. Sudarshan, and L. Tong, "Longitudinal changes in tear evaporation rates after eyelid warming therapies in meibomian gland dysfunction," *Investigative Opthalmology & Visual Science*, vol. 57, no. 4, pp. 1974–1981, 2016.

[3] C. A. Blackie, J. D. Solomon, J. V. Greiner, M. Holmes, and D. R. Korb, "Inner eyelid surface temperature as a function of warm compress methodology," *Optometry and Vision Science*, vol. 85, no. 8, pp. 675–683, 2008.

[4] D. K. Murakami, C. A. Blackie, and D. R. Korb, "All warm compresses are not equally efficacious," *Optometry and Vision Science*, vol. 92, no. 9, pp. e327–e333, 2015.

[5] A. R. Thode and R. A. Latkany, "Current and emerging therapeutic strategies for the treatment of meibomian gland dysfunction (MGD)," *Drugs*, vol. 75, no. 11, pp. 1177–1185, 2015.

[6] R. Arita, N. Morishige, R. Shirakawa, Y. Sato, and S. Amano, "Effects of eyelid warming devices on tear film parameters in normal subjects and patients with Meibomian gland dysfunction," *The Ocular Surface*, vol. 13, no. 4, pp. 321–330, 2015.

[7] D. Finis, J. Hayajneh, C. König, M. Borrelli, S. Schrader, and G. Geerling, "Evaluation of an automated thermodynamic treatment (Lipiflow®) system for meibomian gland dysfunction: a prospective, randomized, observer-masked trial," *The Ocular Surface*, vol. 12, no. 2, pp. 146–154, 2014.

[8] J. V. Greiner, "A single LipiFlow® thermal pulsation system treatment improves meibomian gland function and reduces dry eye symptoms for 9 months," *Current Eye Research*, vol. 37, no. 4, pp. 272–278, 2012.

[9] J. V. Greiner, "Long-term (12-month) improvement in meibomian gland function and reduced dry eye symptoms with a single thermal pulsation treatment," *Clinical & Experimental Ophthalmology*, vol. 41, no. 6, pp. 524–530, 2013.

[10] D. R. Korb and C. A. Blackie, "Meibomian gland diagnostic expressibility: correlation with dry eye symptoms and gland location," *Cornea*, vol. 27, no. 10, pp. 1142–1147, 2008.

[11] D. R. Korb and C. A. Blackie, "Case report: a successful lipiflow treatment of a single case of meibomian gland dysfunction and dropout," *Eye & Contact Lens*, vol. 39, no. 3, pp. e1–e3, 2013.

[12] D. R. Korb, J. P. Herman, J. V. Greiner et al., "Lid wiper epitheliopathy and dry eye symptoms," *Eye & Contact Lens*, vol. 31, no. 1, pp. 2–8, 2005.

[13] Y. Feng, Z. Gao, K. Feng, H. Qu, and J. Hong, "Meibomian gland dropout in patients with dry eye disease in China," *Current Eye Research*, vol. 39, no. 10, pp. 965–972, 2014.

[14] R. Arita, J. Suehiro, T. Haraguchi, R. Shirakawa, H. Tokoro, and S. Amano, "Objective image analysis of the meibomian gland area," *The British Journal of Ophthalmology*, vol. 98, no. 6, pp. 746–755, 2014.

[15] R. Arita, K. Itoh, K. Inoue, and S. Amano, "Noncontact infrared meibography to document age-related changes of the meibomian glands in a normal population," *Ophthalmology*, vol. 115, no. 5, pp. 911–915, 2008.

[16] J. V. Greiner, "Long-term (3 Year) effects of a single thermal pulsation system treatment on meibomian gland function and dry eye symptoms," *Eye & Contact Lens*, vol. 42, no. 2, pp. 99–107, 2016.

[17] D. Finis, N. Pischel, S. Schrader, and G. Geerling, "Evaluation of lipid layer thickness measurement of the tear film as a diagnostic tool for Meibomian gland dysfunction," *Cornea*, vol. 32, no. 12, pp. 1549–1553, 2013.

[18] D. Finis, C. König, J. Hayajneh, M. Borrelli, S. Schrader, and G. Geerling, "Six-month effects of a thermodynamic treatment for MGD and implications of meibomian gland atrophy," *Cornea*, vol. 33, no. 12, pp. 1265–1270, 2014.

[19] D. A. Dartt and M. D. P. Willcox, "Complexity of the tear film: importance in homeostasis and dysfunction during disease," *Experimental Eye Research*, vol. 117, pp. 1–3, 2013.

[20] R. Arita, N. Morishige, T. Fujii et al., "Tear interferometric patterns reflect clinical tear dynamics in dry eye patients," *Investigative Ophthalmology & Visual Science*, vol. 57, no. 8, pp. 3928–3934, 2016.

[21] J. C. Elliott, B. Baird, and B. Giesbrecht, "Consciousness isn't all-or-none: evidence for partial awareness during the attentional blink," *Consciousness and Cognition*, vol. 40, pp. 79–85, 2016.

[22] K. B. Thomas, "The placebo in general practice," *The Lancet*, vol. 344, no. 8929, pp. 1066–1067, 1994.

[23] C. Marchesi, C. De Panfilis, M. Tonna, and P. Ossola, "Is placebo useful in the treatment of major depression in clinical practice?" *Neuropsychiatric Disease and Treatment*, vol. 9, pp. 915–920, 2013.

[24] A. Labbé, Y. X. Wang, Y. Jie, C. Baudouin, J. B. Jonas, and L. Xu, "Dry eye disease, dry eye symptoms and depression: the Beijing eye study," *The British Journal of Ophthalmology*, vol. 97, no. 11, pp. 1399–1403, 2013.

[25] M. Kawashima, M. Uchino, N. Yokoi et al., "Associations between subjective happiness and dry eye disease: a new perspective from the Osaka study," *PLoS ONE*, vol. 10, no. 4, Article ID e0123299, 2015.

Hindawi Publishing Corporation
Journal of Ophthalmology
Volume 2016, Article ID 4041767, 8 pages
http://dx.doi.org/10.1155/2016/4041767

Research Article

Biocompatibility and Biomechanical Effect of Single Wall Carbon Nanotubes Implanted in the Corneal Stroma: A Proof of Concept Investigation

Alfredo Vega-Estrada,[1,2,3] Joaquin Silvestre-Albero,[4] Alejandra E. Rodriguez,[1,2,3] Francisco Rodriguez-Reinoso,[4] Jose A. Gomez-Tejedor,[5] Carmen M. Antolinos-Turpin,[5] Laurent Bataille,[1,2,3] and Jorge L. Alio[1,2,3]

[1]*Keratoconus Unit, Vissum Corporation, Alicante, Spain*
[2]*Research and Development Department, Vissum Corporation, Alicante, Spain*
[3]*Division of Ophthalmology, Universidad Miguel Hernández, Alicante, Spain*
[4]*Departamento de Química Inorgánica, Universidad de Alicante, Alicante, Spain*
[5]*Center for Biomaterials and Tissue Engineering, Universitat Politècnica de València, Valencia, Spain*

Correspondence should be addressed to Alfredo Vega-Estrada; alfredoivega@yahoo.com

Received 26 September 2016; Accepted 8 December 2016

Academic Editor: László Módis

Corneal ectatic disorders are characterized by a progressive weakening of the tissue due to biomechanical alterations of the corneal collagen fibers. Carbon nanostructures, mainly carbon nanotubes (CNTs) and graphene, are nanomaterials that offer extraordinary mechanical properties and are used to increase the rigidity of different materials and biomolecules such as collagen fibers. We conducted an experimental investigation where New Zealand rabbits were treated with a composition of CNTs suspended in balanced saline solution which was applied in the corneal tissue. Biocompatibility of the composition was assessed by means of histopathology analysis and mechanical properties by stress-strain measurements. Histopathology samples stained with blue Alcian showed that there were no fibrous scaring and no alterations in the mucopolysaccharides of the stroma. It also showed that there were no signs of active inflammation. These were confirmed when Masson trichrome staining was performed. Biomechanical evaluation assessed by means of tensile test showed that there is a trend to obtain higher levels of rigidity in those corneas implanted with CNTs, although these changes are not statistically significant ($p > 0.05$). Implanting CNTs is biocompatible and safe procedure for the corneal stroma which can lead to an increase in the rigidity of the collagen fibers.

1. Introduction

Corneal debilitating disorders are characterized by progressive changes of the geometry of the tissue that leads to an irregular astigmatism that negatively impacts the patient's visual system [1]. There are basically two types of corneal ectatic disorders; the first one is comprised of those pathologies of primary origin, such as keratoconus and pellucid marginal degeneration, and the other kind of pathologies, that appear secondary to a corneal photoablative procedure, is known as Ectasia post-LASIK or Iatrogenic Keratectasia [2]. The underlying mechanism responsible for the corneal weakening that induces the aforementioned abnormalities is the biomechanical alterations of the collagen fibers within the corneal stroma [3–5]. Contact lens wearing, intracorneal ring segment implantation, thermokeratoplasty procedures, cornea transplant, and corneal collagen cross-linking have been described as treatment alternatives to manage such a pathological condition [6–11]. Until the date, riboflavin/UV light exposure corneal collagen cross-linking is the only treatment option that has proved to stop the progressive nature of the corneal ecstatic disorders [12]. However, it is

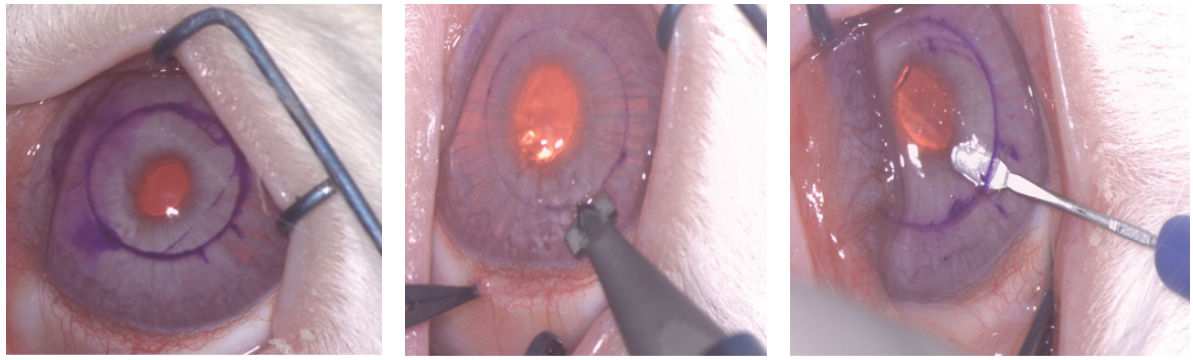

Figure 1: Rabbit eye at the moment of the surgical procedure showing the different steps for the creation of the pocket in the corneal stroma.

a long and uncomfortable surgical procedure for both the patient and the surgeon and it is also a technique not exempt of complications [12].

Carbon nanostructures, mainly carbon nanotubes (CNTs) and graphene, have attracted great attention in the last few years due to their small size and their extraordinary physicochemical properties (they are the stiffest and strongest materials known). Whereas graphene is a flat monolayer of carbon atoms tightly packed into a two-dimensional (2D) honeycomb lattice, carbon nanotubes can be visualized as rolled sheets of graphene built from sp2-carbon units. Previous studies described in the literature have shown that carbon nanomaterials (mainly CNTs) offer potential structural reinforcement in hydrogels to be used in regenerative medicine due to their high mechanical strength and good biocompatibility [13–15]. Furthermore, CNTs have shown promising biochemical properties, such as strong cell adhesion in multiwall carbon nanotube-coated collagen sponge and protein absorption [16–18].

The purpose of the present investigation was to assess if carbon nanomaterials are safe and compatible with the ocular tissues. We also aimed to evaluate the mechanical properties of the corneal stroma after implantation of the CNTs. To the best of our knowledge, this is the first time that carbon nanomaterials influence on corneal rigidity is reported and also the first to evaluate the corneal tolerance of such nanostructures.

2. Materials and Methods

2.1. Experimental Animals. White New Zealand rabbits were used in this study as reference animal models (internationally homologated) for the safety evaluation of new ocular concepts. Animal care and treatment procedures were in accordance with the standards of the EU Directive 2010/63/EU for animal experiments, in conformity to National Guidelines for animal usage in research and with the regular rules (Real Decreto 53/2013) of the Animal Experimentation Service of the Miguel Hernandez University, Alicante, Spain and after the Ethics Experimental Animal Committee approval.

Twenty-four eyes of white New Zealand rabbits were included in this study. The animals were anesthetized with subcutaneous injections of a mixture of ketamine hydrochloride 20 mg/kg (Imalgene 1000; Merial, Lyon, France) and xylazine hydrochloride 4 mg/kg (Xilagesic 2%; Laboratorios Calier, Barcelona, Spain), and ocular topic double anesthetic (tetracaine 0.1% and oxibuprocaine 0.4%, Colircusi; Alcon Cusi SA, Barcelona, Spain). The study was designed based on four experimental animal groups as follows: Group 1 (Control group): 5 eyes in which no surgical procedure was performed; Group 2 (Pocket group): 5 eyes in which a space (pocket) was created in the middle of the corneal stroma. In order to create the pocket, we first marked a 6 mm diameter circle on the surface of the cornea. Then a vertical incision of 300 microns in depth was performed using a calibrated diamond knife. Finally, the dissection of the corneal stroma through an area of 6 mm and at 300 microns in depth was performed using a minicrescent surgical knife (Figure 1). Group 3 (Reference 1 group) was 7 eyes in which a pocket was created and a dispersion composed of carbon nanotubes (CNTs) mixed with saline solution was injected inside the pocket. The concentration of this composition was 0.1 mg/mL. Group 4 (Reference 2 group) was 7 eyes in which a pocket was created and a dispersion composed of CNTs mixed with saline solution was injected inside the pocket. The concentration of this composition was 1 mg/mL (Figure 2).

Antibiotic prophylaxis was topically applied using Tobramycin/Dexamethasone (Tobradex, Alcon) and Chloramphenicol ointment (Oftalmolosa Cusi, Alcon) twice a day for 7 days. Subcutaneous Buprenorphine (0.05 mg/kg) and Paracetamol in drinking water (100 mg/mL) were also used as analgesic for the first days after surgery.

After the injection of the composition containing CNTs, the rabbits were kept under observation for a period of 3 months.

Afterwards, euthanasia was performed in rabbits and a corneoscleral rim of approximately 15 mm in diameter was dissected for histopathology and biomechanical evaluations.

2.2. Preparation of Carbon Nanotubes. Single wall carbon nanotubes (SWCNTs) were used in the current experimental protocol. SWCNTs were prepared by laser ablation of a graphite rod in the presence of Cobalt (Co) and Nickel (Ni) according to previous recipes reported in the literature [19, 20].

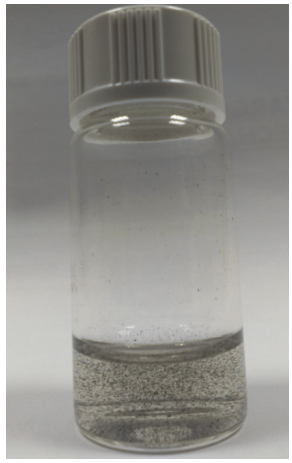

Figure 2: Appearance of the dispersion composed of carbon nanotubes (CNTs) mixed with saline solution in which concentration is 1 mg/mL.

Synthesized SWCNTs were purified using 15% hydrogen peroxide solution under reflux at 100°C for 5 hours to remove the amorphous carbons. The residual catalysts of Ni and Co were removed by 1 M hydrogen chloride solution, followed by a washing step using double distilled water. Synthesized SWCNTs were dissolved in physiological solution (buffer saline solution) before being incorporated in the cornea using a final concentration of 0.1 mg/mL and 1 mg/mL (see Figure 2).

2.3. Histopathology Evaluation. After euthanasia, a piece of the corneal bottoms was dissected and fixed in 10% phosphate buffered formaldehyde until tissue processing. The safety and biocompatibility of the CNTs dispersion composition in the corneal tissue were assessed by means of histopathology examination of the samples 3 months after the surgery. Histological sections were obtained with a thickness of 3 microns and were stained with Hematoxylin and Eosin, blue Alcian, and Masson's trichrome.

2.4. Biomechanical Evaluation. Mechanical properties of the cornea were analyzed by performing stress-strain measurements in order to determine the modulus of elasticity of the corneal tissue. For this purpose, we dissected a strip of corneoscleral tissue with a dimension of 5 × 15 mm that then was clamped into a Microtest SCM 3000 95 universal testing machine in tensile mode (Microtest SA, Madrid, Spain) with load cell of 15 N at room temperature. By means of strain control, samples underwent deformation in a ramp with a constant speed of 1 mm/min. The equipment registered the force that was necessary to perform this deformation, and then with the data that was obtained, stress/strain graphics were drawn. Young's modulus of the samples was obtained as the slope of the linear region in the stress-strain curve at approximately 10% strain. Yield strength was calculated as the stress at which this linear behaviour is finished; that is, it began to deform plastically. Failure strain was calculated at the point at which the sample started to break. Between five and seven measurements were performed for each group. Results are given as the average plus/minus standard deviation.

2.5. Statistical Analysis. The statistical analysis was carried out using the one-way analysis of variance (ANOVA) with R 3.1.0 software. The level of statistical significance was $p < 0.05$ in all cases.

3. Results

3.1. Clinical Evaluation. The present investigation was performed by means of an experimental protocol where 24 eyes of New Zealand white rabbits were implanted with CNTs in the corneal stroma and were kept under observation during a period of 3 months. Figure 3 corresponds to a series of images showing the rabbit's eyes at the moment of the surgical procedure, 7 days after CNTs implantation, and at 3 months during the last follow-up. At the moment of the surgery, the CNTs can be appreciated, using the surgical microscope under high magnification, as small black dots distributed along the previously performed corneal pocket. One week after the procedure, the corneal tissue is completely transparent, with no epithelial defect, without corneal edema and no signs of stromal or anterior chamber inflammation. At three months, the corneal tissue remains transparent, with the small black dots corresponding to the CNTs implanted and no clinical signs of ocular inflammation. There were no complications in any of the 14 eyes implanted with the CNTs and there was no need of an early euthanasia in any of the rabbits during the follow-up period.

3.2. Histopathology Evaluation. Figure 4 shows a sample of corneal stroma, where the collagen fibers are oriented vertically and stained with blue Alcian to illustrate that there are no fibrous scaring and no alterations in the mucopolysaccharides of the corneal stroma. It also shows that there are no signs of active inflammation after the procedure. The latest is confirmed when the Masson trichrome staining is performed (Figure 5: solid red arrows showing the carbon nanotubes within the corneal tissue). Figure 6 illustrates another sample, again vertically oriented, stained with Masson trichrome to show that there is no inflammation and no foreign body giant cell reaction against the CNTs implanted. It also shows a stronger adhesion of the tissue in the area surrounding the CNTs. Other interesting findings that were observed in the pathology report were the absence of neovascularization and that there was no apoptosis of the keratocytes on the samples examined.

3.3. Biomechanical Evaluation. Figure 7 shows a typical stress-strain curve, where several regions can be observed. On one hand, the so-called toe region can be observed, typical in most soft tissues, where the relation between stress and strain is not linear, and the slope increases with stress. On the other hand, the elastic region can be observed, where the relation between the stress and the strain is almost linear. In this region, Young's modulus is calculated as the slope of the straight line (red line in Figure 7). When the stress

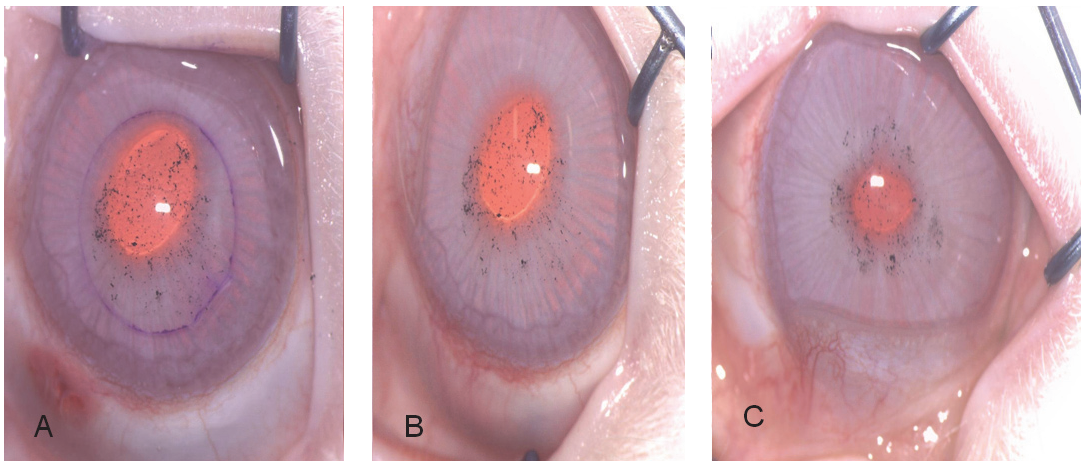

Figure 3: Same eye of a rabbit at the moment of the surgical procedure (A), 7 days after CNTs implantation (B) and at 3 months after the surgery (C).

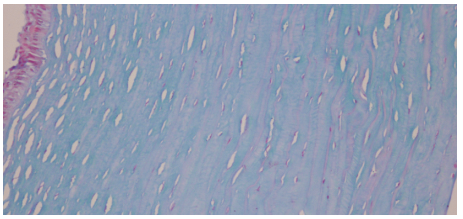

Figure 4: Corneal stroma sample in vertical orientation stained with blue Alcian.

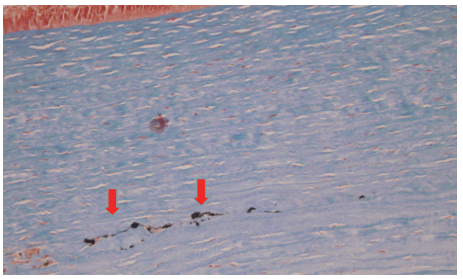

Figure 5: Corneal stroma sample in horizontal orientation stained with Masson trichrome. Solid red arrows showing the CNTs within the corneal tissue.

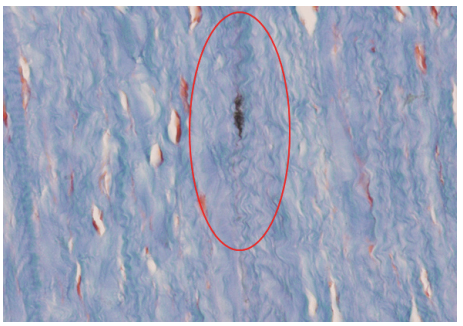

Figure 6: Corneal stroma sample vertically oriented with Masson trichrome staining. Red circle showing the strong adhesion of the tissue around the CNTs.

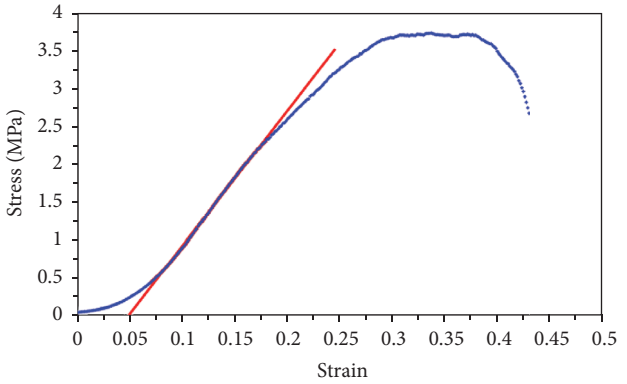

Figure 7: Typical stress-strain curve. Blue points represent the experimental data, and red straight line, the linear fitting used to obtain Young's modulus.

is increased above the elastic region, the shape of the curve changes and the plastic regions begin. In this region the tissue suffers nonreversible changes. The tissue is not able to recover its original shape in case the force is removed. Finally, the breakdown point of the tissue is reached [21].

Table 1 shows Young's modulus, yield stress, and failure strain obtained for each one of the samples. It can be seen from Young's modulus that there was a trend towards a higher rigidity for the Reference 2 sample (CNTs 1 mg/mL), although this difference was not statistically significant ($p > 0.05$). The yield stress increased for References 1 and 2 compared to the Control sample. However, this difference was only statistically significant for Reference 1 ($p < 0.05$). Also, for Reference 2 there was an increase of the failure strain, but again it was not statistically significant ($p > 0.05$).

4. Discussion

The present study evaluates the safety and biocompatibility of carbon nanotubes (CNTs) in ocular tissues. It also assesses the

Table 1: Number of sample data sets (n), Young's modulus, yield stress, and failure strain obtained in each one of the samples.

Group	n	Young's modulus (MPa)	Yield stress (MPa)	Failure strain
Control	5	12.1 ± 2.5	1.4 ± 0.3	0.40 ± 0.06
Pocket	6	12.0 ± 4.2	1.9 ± 1.0	0.39 ± 0.08
Reference 1	5	11.8 ± 1.3	2.3 ± 0.3	0.47 ± 0.05
Reference 2	7	13.0 ± 3.9	1.9 ± 0.6	0.41 ± 0.07

capability of the nanomaterials to increase the biomechanical properties in the corneal stroma. To the best of our knowledge, this is the first scientific investigation that evaluates the behaviour of carbon nanomaterials in ocular tissues.

The unique characteristics of CNTs have kept the attention in many areas within the scientific arena, such as electronics, physics, and mechanics. Also, in nanomedicine the interest for these materials has significantly grown during the last decade as advances in technology allow isolating and developing pure forms of carbon nanostructures. As nanotechnology is defined by the size of a material (generally 1–100 nm) or manipulation on the molecular level, it involves a broad range of nanoscaled materials used in various fields of biology and medicine [22]. Nanotechnology offers promising perspectives in biomedical research as well as in clinical practice. The high versatility of carbon nanomaterials brings many opportunities as therapeutic agents in the field of nanomedicine. Among the different interesting and unique properties that characterized carbon nanostructures, its biocompatibility, optical transparency, and mechanical properties make these structures an excellent option to develop new alternatives of personalized medicine and treat several pathologies in the ophthalmology field.

Corneal ectatic disorders are characterized by a progressive corneal thinning that induces alterations in the morphology of the cornea, which negatively impacts the patient's visual function. The mechanical stability of the cornea is primarily determined by the structure of the collagen molecules and their spatial arrangement, which is orthogonal in normal patients. However, the equilibrium of this architecture is lost in eyes with ectatic corneal pathologies, which leads to biomechanical alterations that are responsible for the instability and weakness of the tissue in these diseases [3]. To this day, the only surgical technique that has demonstrated to stabilize and stop the progressive nature of these disorders is riboflavin UV-A light corneal collagen cross-linking (CXL) [12]. This procedure increases the stiffness of the cornea by a photo oxidative reaction that creates covalent bonds between the collagen fibers of the corneal tissue [12]. However, it is a very long surgical procedure, which makes it uncomfortable for both the surgeon and the patient. Additionally, because of the phototoxic effect of the UV light, it cannot be performed in thin corneas, which is characteristic in ectatic disorders and may present some complications related to the epithelial debridement as well as alterations in the transparency of the tissue. Therefore, using carbon nanomaterials in order to reinforce the corneal stroma will have several advantages as an alternative therapeutic option for such pathological conditions due to the excellent mechanical properties that characterized these nanostructures and also because most of the limitations related to the current treatment options can be avoided.

In the present investigation, biocompatibility of CNTs in ocular tissues was assessed by means of histopathology evaluation. It was found that carbon nanomaterials do not induce any inflammatory or foreign body reaction in the corneal stroma. Biocompatibility of CNTs has been previously reported in other fields of biology and medicine, for example, tissue engineering, regenerative medicine, drug delivery systems, and reinforcement of biological tissues [22–24]. Zhao et al. specifically evaluated the cytocompatibility and hemocompatibility of CNTs by cell adhesion assays and hemolytic rate experiments [23]. They concluded that CNTs did not interfere with the viability, metabolic activity, morphology, and spreading of either of the cell types analyzed. In the same way, Koyama and colleagues observed low toxicity and stable (almost inert) biological response by analyzing the systematic study of T-cells in peripheral blood in in vivo experimental animals [24]. In another study, Tan et al. evaluated the biocompatibility of CNTs composites by seeding these nanomaterials together with pulmonary arterial endothelial cells. Results from this study demonstrated high levels of cell viability and adhesion, thus showing excellent biocompatibility of the CNTs [17]. In addition, there are several authors that have analyzed the biological response of these materials in different types of cells and they have found that CNTs are biologically inert and do not show toxicity on the tissues that were evaluated and also that these nanomaterials are cleared by circulation when injected intravenously [25–29].

In the current study, the mechanical properties of the cornea after being implanted with CNTs were also evaluated. The module of elasticity was assessed by means of stress-strain measurements in order to determine which of the samples under analysis showed the most rigid behaviour. Even though a trend towards stiffer results in those samples treated with the higher concentration of CNTs was found, the differences were not statistically significant when compared with those samples untreated. Therefore, if we want to introduce a reinforced material to another material, it is clear that an interaction must exist between the materials involved.

In the present study, interactions between the CNTs and the collagen fibers of the corneal stroma were not assessed. Nevertheless, there are some investigations that have demonstrated the adsorption and interaction that is present when combining carbon nanomaterials and collagen fibers by means of theoretical models. Using molecular dynamics simulation, Cazorla characterized the quantum interaction that exists between carbon based nanostructures and collagen-like peptides [30]. In addition, other authors

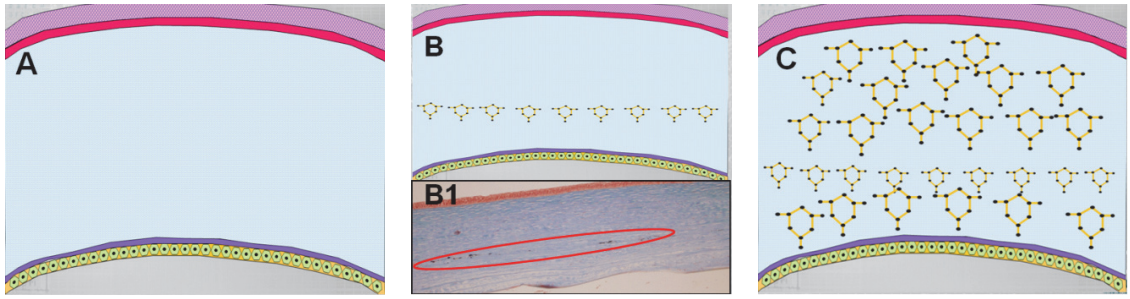

Figure 8: Schematic representation of a cross section of the cornea. (A) Cornea without carbon nanostructures. (B) Cornea with carbon nanostructures in the area where the pocket was created as it was performed in the current study. (B1) Histopathology sample stained with Masson trichrome corresponding to one of the corneas analyzed in the present work where carbon nanostructures can be found just in the area where the stromal pocket was created (red circle). (C) Schematic representation of the cross section of the cornea with an increased distribution of carbon nanomaterials.

have reported the interaction and adsorption that is present between collagen fibers and carbon nanomaterials by using finite elements analysis and density functional theory [31]. In the same way, aggregation between the collagen fibers and the CNTs has also been demonstrated by measuring the turbidity of the suspension [32]. There are other investigations in which qualitative and chemical assessment have been carried out in order to evaluate the interaction between collagen fibers and carbon nanostructures. Akasaka and col. evaluated the interaction between CNTs and collagen using scanning electron microscopy (SEM) [33]. The authors concluded that CNTs interact strongly and blend with collagen fibers. In the same way, Tosun and McFetridge performed qualitative analysis using SEM and also found an increase in adsorption between the single wall carbon nanotubes and collagen hydrogels [34]. Moreover, this interaction between CNTs and collagen fiber has also been studied using a chemical approach. In the aforementioned study performed by Tan and colleagues, the relationship between CNTs and collagen fibers was also analyzed by spectrometry analysis [17]. Additionally, Cao et al. also evaluated the chemical interaction by means of Fourier transform infrared spectroscopy and they specifically observed that the carboxylic and hydroxyl groups present on the surface of CNTs form covalent and hydrogen bonds with the amino groups of the collagen fibers [16]. As we can see, there is enough scientific evidence published in the literature that has demonstrated the interaction that exists between the CNTs and the collagen by means of theoretical, qualitative, and quantitative assessment. Finally, some of these reports observed that this interaction leads to an increase of the mechanical properties in the collagen. Cao et al. specifically found an increase of the static tensile modulus and strength of the collagen with the addition of CNTs [16]. Tosun and McFetridge also reported that the collagen gels treated with CNTs displayed a significant increase in material stiffness when evaluated by unconfined compression analysis [34]. Nevertheless, as previously mentioned, in the current investigation, even when we observed a trend towards increasing the mechanical properties of the samples treated with CNTs, these changes were not statistically significant. There are some variables, like the small sample under analysis and the methodology used in order to evaluate the mechanical properties, which could have been related to this behaviour. However, we consider that the most important factor that could explain the limited enhancement of the mechanical properties of the samples in our study is that CNTs were inducing their effect on just a small area of the cornea, specifically where the pocket was created (Figure 8). Hence, it is our hypothesis that it is necessary to obtain a more homogeneous distribution of the carbon nanomaterials all over the stroma in order to achieve a significant increase of the mechanical properties in the cornea (Figure 8).

Optimized alternatives including other types of carbon nanomaterials, such as graphene, incorporating drug delivery systems to enhance the penetration and distribution of carbon nanomaterials along the corneal stroma and increasing their chemical properties via functionalization are now being developed by our research group. This will certainly improve the biocompatibility, the optical transparency, and the capacity of these materials to conjugate and interact with other biomolecules, such as corneal collagen fibers.

5. Conclusions

In conclusion, histopathology evaluation shows the biotolerance and biocompatibility of carbon nanostructures after being implanted in the corneal stroma. The corneal biomechanical evaluation, as performed in this investigation, shows that there is a trend to obtain more rigidity of the corneal tissue after carbon nanostructures implantation, although these changes were not statistically significant. To the best of our knowledge, this is the first study that aims to assess the biocompatibility and biomechanical properties of the cornea after being implanted with carbon nanomaterials. Thus, further research is necessary in order to comprehend and improve the biomechanical assessment of the present investigation and also to understand the potentials use of these materials and this novel technology for the development of new applications of nanomedicine in visual sciences.

Disclosure

The products and technologies discussed hereinafter were described and claimed in Patent Cooperation Treaty (PCT)

Appl. no. PCT/GB2014/050217, which derives priority from US provisional Appl. no. 61758294.

Competing Interests

The authors declare that they have no competing interests.

Acknowledgments

The authors would like to acknowledge Professor K. Kaneko for the supply of the SWCNTs. They will also like to acknowledge the support of the Spanish Ministerio de Economía y Competitividad (MINECO) and FEDER funds under the project MAT2012-38359-C03-01. This publication has been sponsored in part with the funding of the framework of the Red Temática de Investigación Cooperativa en Salud (RETICS), Reference no. RD12/0034/0007, financed by the Instituto Carlos III-General Subdirection of Networks and Cooperative Investigation Centers (R&D&I National Plan 2008–2011) and the European Regional Development Fund (Fondo Europeo de Desarrollo Regional FEDER).

References

[1] Y. S. Rabinowitz, "Keratoconus," *Survey of Ophthalmology*, vol. 42, no. 4, pp. 297–319, 1998.

[2] W. J. Dupps Jr., "Biomechanical modeling of corneal ectasia," *Journal of Refractive Surgery*, vol. 21, no. 2, pp. 186–190, 2005.

[3] A. Daxer and P. Fratzl, "Collagen fibril orientation in the human corneal stroma and its implication in keratoconus," *Investigative Ophthalmology and Visual Science*, vol. 38, no. 1, pp. 121–129, 1997.

[4] I. S. Nash, P. R. Greene, and C. S. Foster, "Comparison of mechanical properties of keratoconus and normal corneas," *Experimental Eye Research*, vol. 35, no. 5, pp. 413–424, 1982.

[5] T. T. Andreassen, A. Hjorth Simonsen, and H. Oxlund, "Biomechanical properties of keratoconus and normal corneas," *Experimental Eye Research*, vol. 31, no. 4, pp. 435–441, 1980.

[6] M. Garcia-Lledo, C. Feinbaum, and J. L. Alió, "Contact lens fitting in keratoconus," *Comprehensive Ophthalmology Update*, vol. 7, no. 2, pp. 47–52, 2006.

[7] G. Wollensak, E. Spoerl, and T. Seiler, "Riboflavin/ultraviolet-A-induced collagen crosslinking for the treatment of keratoconus," *American Journal of Ophthalmology*, vol. 135, no. 5, pp. 620–627, 2003.

[8] A. Vega-Estrada, J. L. Alió, A. B. Plaza Puche, and J. Marshall, "Outcomes of a new microwave procedure followed by accelerated cross-linking for the treatment of keratoconus: a pilot study," *Journal of Refractive Surgery*, vol. 28, no. 11, pp. 787–792, 2012.

[9] D. P. Piñero and J. L. Alio, "Intracorneal ring segments in ectatic corneal disease—a review," *Clinical and Experimental Ophthalmology*, vol. 38, no. 2, pp. 154–167, 2010.

[10] A. Vega-Estrada, J. L. Alió, L. F. Brenner, and N. Burguera, "Outcomes of intrastromal corneal ring segments for treatment of keratoconus: five-year follow-up analysis," *Journal of Cataract and Refractive Surgery*, vol. 39, no. 8, pp. 1234–1240, 2013.

[11] G. Sutton, C. Hodge, and C. N. J. Mcghee, "Rapid visual recovery after penetrating keratoplasty for keratoconus," *Clinical and Experimental Ophthalmology*, vol. 36, no. 8, pp. 725–730, 2008.

[12] K. M. Meek and S. Hayes, "Corneal cross-linking—a review," *Ophthalmic and Physiological Optics*, vol. 33, no. 2, pp. 78–93, 2013.

[13] Y. Chen, B. Bilgen, R. A. Pareta et al., "Self-assembled rosette nanotube/hydrogel composites for cartilage tissue engineering," *Tissue Engineering Part C: Methods*, vol. 16, no. 6, pp. 1233–1243, 2010.

[14] Y. S. Song, "A passive microfluidic valve fabricated from a hydrogel filled with carbon nanotubes," *Carbon*, vol. 50, no. 3, pp. 1417–1421, 2012.

[15] A. A. Rodrigues, N. A. Batista, V. P. Bavaresco et al., "Polyvinyl alcohol associated with carbon nanotube scaffolds for osteogenic differentiation of rat bone mesenchymal stem cells," *Carbon*, vol. 50, no. 2, pp. 450–459, 2012.

[16] Y. Cao, Y. M. Zhou, Y. Shan, H. X. Ju, and X. J. Xue, "Preparation and characterization of grafted collagen-multiwalled carbon nanotubes composites," *Journal of Nanoscience and Nanotechnology*, vol. 7, no. 2, pp. 447–451, 2007.

[17] W. Tan, J. Twomey, D. Guo, K. Madhavan, and M. Li, "Evaluation of nanostructural, mechanical and biological properties of collagen-nanotube composites," *IEEE Transactions on NanoBioscience*, vol. 9, no. 2, pp. 111–120, 2010.

[18] R. Gopalakrishnan and V. Subramanian, "Interaction of collagen with carbon nanotube: a molecular dynamics investigation," *Journal of Biomedical Nanotechnology*, vol. 7, no. 1, pp. 186–187, 2011.

[19] S. Gotovac, H. Honda, Y. Hattori, K. Takahashi, H. Kanoh, and K. Kaneko, "Effect of nanoscale curvature of single-walled carbon nanotubes on adsorption of polycyclic aromatic hydrocarbons," *Nano Letters*, vol. 7, no. 3, pp. 583–587, 2007.

[20] M. Arai, S. Utsumi, M. Kanamaru et al., "Enhanced hydrogen adsorptivity of single-wall carbon nanotube bundles by one-step C_{60}-pillaring method," *Nano Letters*, vol. 9, no. 11, pp. 3694–3698, 2009.

[21] R. K. Korhonen and S. Saarakkala, "Biomechanics and modeling of skeletal soft tissues," in *Theoretical Biomechanics: Orthopedics, Physical Medicine and Rehabilitation*, V. Klika, Ed., InTech, Rijeka, Croatia, 2011, http://www.intechopen.com/books/theoretical-biomechanics/biomechanics-and-modeling-of-skeletal-soft-tissues.

[22] Š. Kubinová and E. Syková, "Nanotechnologies in regenerative medicine," *Minimally Invasive Therapy and Allied Technologies*, vol. 19, no. 3, pp. 144–156, 2010.

[23] M. L. Zhao, D. J. Li, L. Yuan, Y. C. Yue, H. Liu, and X. Sun, "Differences in cytocompatibility and hemocompatibility between carbon nanotubes and nitrogen-doped carbon nanotubes," *Carbon*, vol. 49, no. 9, pp. 3125–3133, 2011.

[24] S. Koyama, H. Haniu, K. Osaka et al., "Medical application of carbon-nanotube-filled nanocomposites: the microcatheter," *Small*, vol. 2, no. 12, pp. 1406–1411, 2006.

[25] S. Garibaldi, C. Brunelli, V. Bavastrello, G. Ghigliotti, and C. Nicolini, "Carbon nanotube biocompatibility with cardiac muscle cells," *Nanotechnology*, vol. 17, no. 2, pp. 391–397, 2006.

[26] N. Aoki, A. Yokoyama, Y. Nodasaka et al., "Strikingly extended morphology of cells grown on carbon nanotubes," *Chemistry Letters*, vol. 35, no. 5, pp. 508–509, 2006.

[27] L. W. Zhang, L. Zeng, A. R. Barron, and N. A. Monteiro-Riviere, "Biological interactions of functionalized single-wall carbon nanotubes in human epidermal keratinocytes," *International Journal of Toxicology*, vol. 26, no. 2, pp. 103–113, 2007.

[28] A. Bianco, K. Kostarelos, and M. Prato, "Applications of carbon nanotubes in drug delivery," *Current Opinion in Chemical Biology*, vol. 9, no. 6, pp. 674–679, 2005.

[29] M. Davoren, E. Herzog, A. Casey et al., "*In vitro* toxicity evaluation of single walled carbon nanotubes on human A549 lung cells," *Toxicology in Vitro*, vol. 21, no. 3, pp. 438–448, 2007.

[30] C. Cazorla, "Unrave lingthe quantum inter actions of collagen-like peptides with carbon-based nano structures in aqueous media," Science and Super computing in Europe-Research Highlights, 2010–6.

[31] R. Gopalakrishnan, K. Balamurugan, E. R. A. Singam, S. Sundaraman, and V. Subramanian, "Adsorption of collagen onto single walled carbon nanotubes: a molecular dynamics investigation," *Physical Chemistry Chemical Physics*, vol. 13, no. 28, pp. 13046–13057, 2011.

[32] Y. Kuboki, M. Terada, Y. Kitagawa, S. Abe, M. Uo, and F. Watari, "Interaction of collagen triple-helix with carbon nanotubes: Geometric property of rod-like molecules," *Bio-Medical Materials and Engineering*, vol. 19, no. 1, pp. 3–9, 2009.

[33] T. Akasaka, K. Nakata, M. Uo, and F. Watari, "Modification of the dentin surface byusing carbon nano tubes," *Bio-Medical Materials and Engineering*, vol. 19, no. 2-3, pp. 179–185, 2009.

[34] Z. Tosun and P. S. McFetridge, "A composite SWNT–collagen matrix: characterization and preliminary assessment as a conductive peripheral nerve regeneration matrix," *Journal of Neural Engineering*, vol. 7, no. 6, Article ID 066002, 2010.

Hindawi Publishing Corporation
Journal of Ophthalmology
Volume 2016, Article ID 5742346, 7 pages
http://dx.doi.org/10.1155/2016/5742346

Clinical Study

Active Pedicle Epithelial Flap Transposition Combined with Amniotic Membrane Transplantation for Treatment of Nonhealing Corneal Ulcers

Ting Zhang,[1,2] Yuexin Wang,[2] Yanni Jia,[1,2] Dongle Liu,[2] Suxia Li,[2] Weiyun Shi,[2] and Hua Gao[2]

[1]*Qingdao University, 308 Ningxia Road, Qingdao 266071, China*
[2]*Shandong Eye Hospital, Shandong Eye Institute, Shandong Academy of Medical Sciences, 372 Jingsi Road, Jinan 250021, China*

Correspondence should be addressed to Hua Gao; gaohua100@126.com

Received 12 July 2016; Accepted 26 September 2016

Academic Editor: Anna Nowinska

Introduction. The objective was to evaluate the efficacy of active pedicle epithelial flap transposition combined with amniotic membrane transplantation (AMT) in treating nonhealing corneal ulcers. *Material and Methods*. Eleven patients (11 eyes) with nonhealing corneal ulcer who underwent the combined surgery were included. Postoperatively, ulcer healing time was detected by corneal fluorescein staining. Visual acuity, intraocular pressure, surgical complications, and recurrence were recorded. Corneal status was inspected by the laser scanning confocal microscopy and anterior segment optical coherence tomography (AS-OCT). *Results*. The primary diseases were herpes simplex keratitis (8 eyes), corneal graft ulcer (2 eyes), and Stevens-Johnson syndrome (1 eye). All epithelial flaps were intact following surgery, without shedding or displacement. Mean ulcer healing time was 10.8 ± 3.1 days, with a healing rate of 91%. Vision significantly improved from 1.70 to 0.82 log MAR ($P = 0.001$). A significant decrease in inflammatory cell infiltration and corneal stromal edema was revealed 2 months postoperatively by confocal microscopy and AS-OCT. Corneal ulcer recurred in 1 eye. None of the patients developed major complications. *Conclusion*. Active pedicle epithelial flap transposition combined with AMT is a simple and effective treatment for nonhealing corneal ulcers.

1. Introduction

A nonhealing corneal ulcer is defined as an ulcer which does not show any indication of healing within two weeks, despite the administration of proper medical treatment [1]. Suspicious causes of a nonhealing corneal ulcer include persistent infection, neurotrophic keratopathy, exposure keratopathy, dry eye, treatment toxicity, steroid use, and chronic conjunctival inflammation, such as ocular cicatricial pemphigoid [2]. Once a corneal ulcer occurs and is left unattended, corneal melting, descemetocele, and corneal perforation can subsequently develop, leading to devastating consequences [3]. Moreover, when a resistant corneal ulcer progressively develops, lamellar keratoplasty or penetrating keratoplasty is usually needed [4, 5]. Therefore, curing a resistant ulcer in its early stages is highly recommended.

Amniotic membrane transplantation (AMT) can be used to treat a superficial corneal ulcer. However, the efficacy of AMT, or even repeated AMT, in treating a nonhealing corneal ulcer is limited because the latter is usually associated with severe inflammatory response, which frequently causes corneal melting, earlier amniotic membrane dissolution, and deferred ocular surface epithelialization. Thus, reducing inflammatory cell infiltration and improving the local microenvironment may facilitate the healing of a resistant corneal ulcer.

Inspired by the significant anti-inflammation effects of the epithelial cells and the successful clinical application of laser-assisted subepithelial keratectomy (LASEK), which makes an epithelial flap with alcohol and significantly prevents haze formation in the subepithelial area [6], we attempted to treat nonhealing corneal ulcers in this study

with the use of active pedicle epithelial flap transposition combined with AMT.

2. Material and Methods

2.1. Patients. This study was approved by the Institutional Review Board of Shandong Eye Institute, Qingdao, China, and conformed to the guidelines of the Declaration of Helsinki. Patients provided informed consent to participate in the study. The medical records of patients who had undergone active pedicle epithelial flap transposition combined with AMT for a nonhealing corneal ulcer between 1 March 2012 and 1 July 2015 were reviewed.

All of the patients had a history of eye hyperemia associated with pain and decreased vision. The ulcers were from 2 to 5 mm in diameter and less than 1/3 of the corneal stroma in depth. All ulcers were associated with corneal stroma melting and remained unhealed for ≥4 weeks despite the administration of medical treatment. The study mainly focused on nonhealing sterile corneal ulcers, and all patients received corneal scraping, culture, and laser scanning confocal microscopy examination to exclude active infection, for example, a fungal, resistant bacterial, or *Acanthamoeba* corneal ulcer.

2.2. Surgical Technique. The amniotic membrane (AM) was prepared and preserved as previously reported [7], with minor modifications. The surgery was performed by the same surgeon. Necrotic corneal tissue was removed from the base and wall of the ulceration, and then thermal cautery was applied to the ulcer to dry out its surface. Thereafter, an epithelial flap was constructed from the transparent cornea at the edge of the ulcer, near the limbus. For this procedure, obtaining a flap from the edge of ulcer ensures easy transposition, and taking a flap from the cornea near the limbus guarantees rapid healing of the epithelial defect resulting from making a flap. In addition, a corneal epithelial scraper was used to create an epithelial flap without the use of alcohol to maintain epithelial cells activity. Briefly, the epithelial scraper was gently pressed onto the corneal surface to make a boundary of the flap shaped like the ulcer under the auxiliary arm of a caliper. A pedicle, like a sprout, was preserved in the lateral or nasal portion of the epithelial flap. The corneal epithelium was then carved following the boundary, with the depth confined to the epithelial layer. In this way, an epithelial flap was created by the corneal epithelial scraper. Next, the flap was rotated to cover the epithelial nonhealing region of the ulcer. To maintain flap adhesion, fluid on the ocular surface was cleaned with a sponge swab before covering it. Finally, a trephine was used to make an amniotic membrane of 14 mm in diameter, and the AM patch was sutured onto the surface to cover the entire cornea using a continuous 10-0 nylon suture within 1 mm of the limbus (Figure 1).

2.3. Postoperative Treatment. The primary diseases of nonhealing corneal ulcer in the study included herpes simplex keratitis (HSK), corneal graft ulcer, and Stevens-Johnson syndrome (SJS). Postoperatively, tobramycin and dexamethasone eye drops (Alcon, Puurs, Belgium) were used 4 times daily for 1-2 weeks and then replaced with 0.1% fluorometholone eye drops (Santen, Osaka, Japan) 4 times daily for approximately 1-2 months. For eyes with HSK, antiviral medication was applied topically and systemically with adjuvant corticosteroid eye drops [8, 9]. Acyclovir eye drops (Wuhan Wujing Pharmaceutical Co., Wuhan, China) were used 4 times every day. Ganciclovir ophthalmic gel (Hubei Keyi Pharmaceutical Co., Wuhan, China) was used every night. Acyclovir was administered orally (8 mg/kg) 3 times daily for 3 months. For eyes with prior corneal transplantation or Stevens-Johnson syndrome, 1% cyclosporine eye drops (Huabei Pharmaceutical Co., Shijiazhuang, China) were used 1–4 times daily.

The medical treatment was adjusted with the alleviation of symptoms and the dissolution of AM. Corneal fluorescein staining was performed daily and the sutures were removed 1–3 weeks postoperatively when the AM dissolved.

2.4. Postoperative Evaluation. Patients were examined daily for the first week, weekly for 4 weeks, and monthly thereafter. Ulcer healing time was observed by corneal fluorescein staining during the follow-up. The uncorrected visual acuity (UCVA), intraocular pressure (IOP), and corneal status were recorded. Laser scanning confocal microscopy was applied to determine the extent of local inflammation, and anterior segment optical coherence tomography (AS-OCT) was performed to visualize corneal tissue cicatrization proximal to the ulcer.

2.5. Statistical Analysis. The data were analyzed using SPSS® 11.5 software. UCVA before and after surgery was converted to the minimum angle of resolution (log MAR) for calculation purposes and compared with Student's t-test. A P value of <0.05 was considered to be statistically significant.

3. Results

3.1. General Information. Eleven patients (11 eyes) with a nonhealing corneal ulcer who underwent the combined surgery were included in the study. Of these, 7 were male and 4 were female, with an age range of 29–68 years (mean ± standard deviation, 58.1 ± 11.4). The etiologies of the corneal ulcers included HSK (8 eyes), corneal graft ulcer (2 eyes), and SJS (1 eye). The ulcers were less than 1/3 of the corneal stroma in depth and 2–5 mm in diameter and lasted for 1–6 months. The site of ulcer in the 11 cases was on the pupillary zone in 5 eyes, on the inferior cornea in 5 eyes, and at the superior cornea in one eye. Combined anterior chamber hypopyon of approximately 1–3 mm was noted in 4 eyes. These patients underwent various medical treatments (antibiotics, antiviral medication, corticosteroids, growth factor, and bandage contact lens) for ≥4 weeks. Of these, 5 eyes received AMT once and 1 eye received AMT twice, but the ulcers remained unhealed (Table 1). Thereafter, active pedicle epithelial flap transposition combined with AMT was performed, and patients were followed-up for 6–24 months (16.9 ± 9.9).

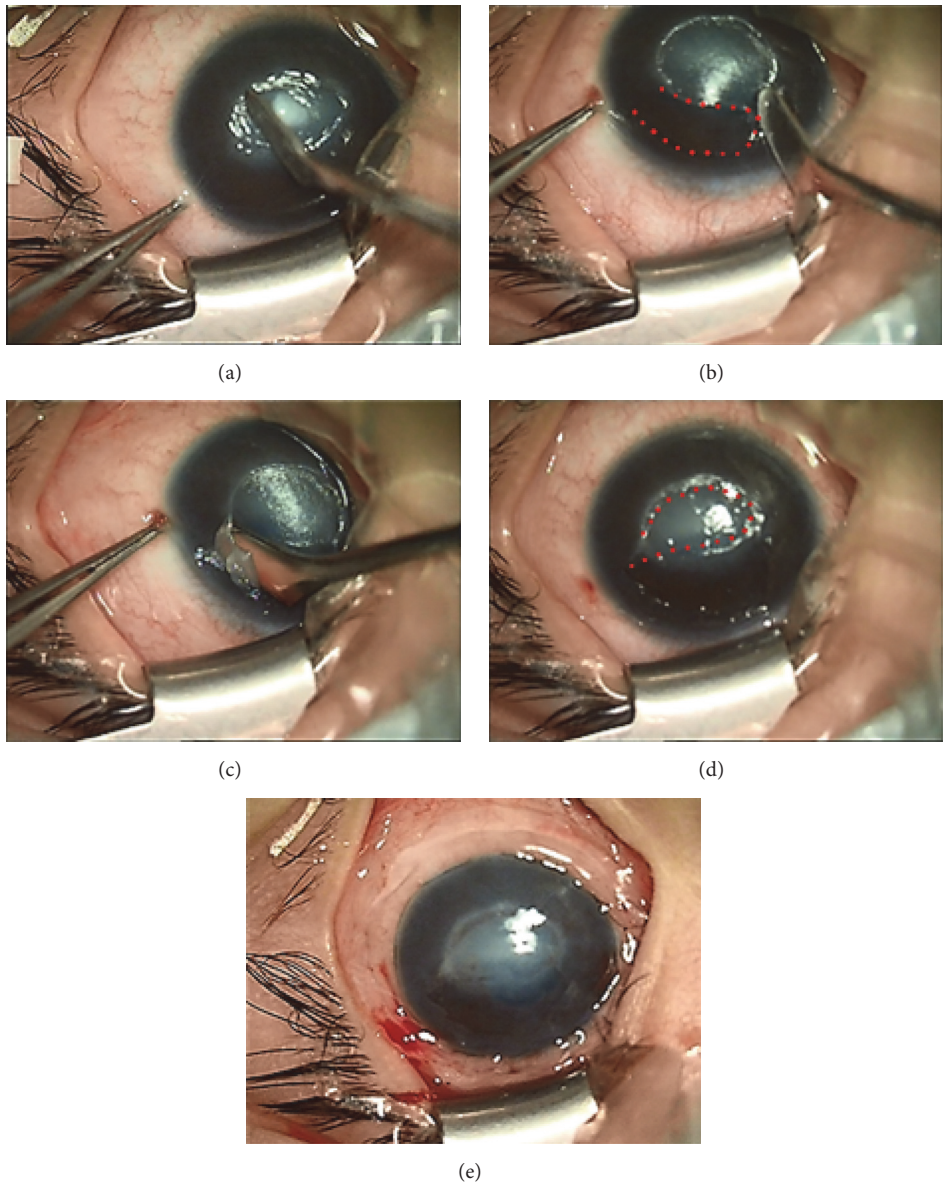

(a) (b) (c) (d) (e)

Figure 1: Photographs showing the procedures of epithelial flap transposition combined with amniotic membrane transplantation. (a) Cleaning the ulcer surface. (b) Constructing a flap boundary (the dotted line demonstrates the region from where the epithelial flap was obtained). (c) Obtaining an epithelial flap. (d) Transposing the epithelial flap (the dotted line demonstrates the translocated epithelial flap). (e) Suturing an amniotic membrane patch.

3.2. Clinical Examination. After surgery, all of the epithelial flaps were intact, without displacement or shedding. The corneal ulcers healed from 6 to 15 days (10.8 ± 3.1) postoperatively with negative fluorescein staining. The epithelial defect that resulted from the construction of flap healed within 1-2 days (1.45 ± 0.52). Following surgery, eye hyperemia decreased gradually. The hypopyon observed in 4 patients disappeared at 1-2 weeks. The corneal edema subsided within 2 weeks. The AM patch dissolved between 1 and 3 weeks postoperatively. Corneal opacity was alleviated during the follow-up, with variable effects on visual acuity (VA) (Figure 2). An elevated IOP (30 mmHg) was present in 1 eye and controlled by medication within 3 days. HSK recurrence was observed in 1 patient at 10 weeks and 14 months but without the occurrence of corneal ulcer. Corneal ulcer recurrence was noted in 1 eye (after penetrating keratoplasty) at 3 weeks postoperatively, resulting in a fungal infection and intractable corneal perforation. Finally, the eye was treated successfully with a second penetrating keratoplasty.

3.3. Recovery of Visual Acuity. The average preoperative and postoperative UCVA were 1.70 log MAR and 0.82 log MAR, respectively. The percentage of patients with UCVA of <0.05 decreased from 73% (8/11 eyes) preoperatively to 9% (1/11 eyes) postoperatively. The VA increased by at least one row (maximum, six rows) after surgery. The difference in UCVA pre- and postoperatively was statistically significant ($P = 0.001$) (Table 2).

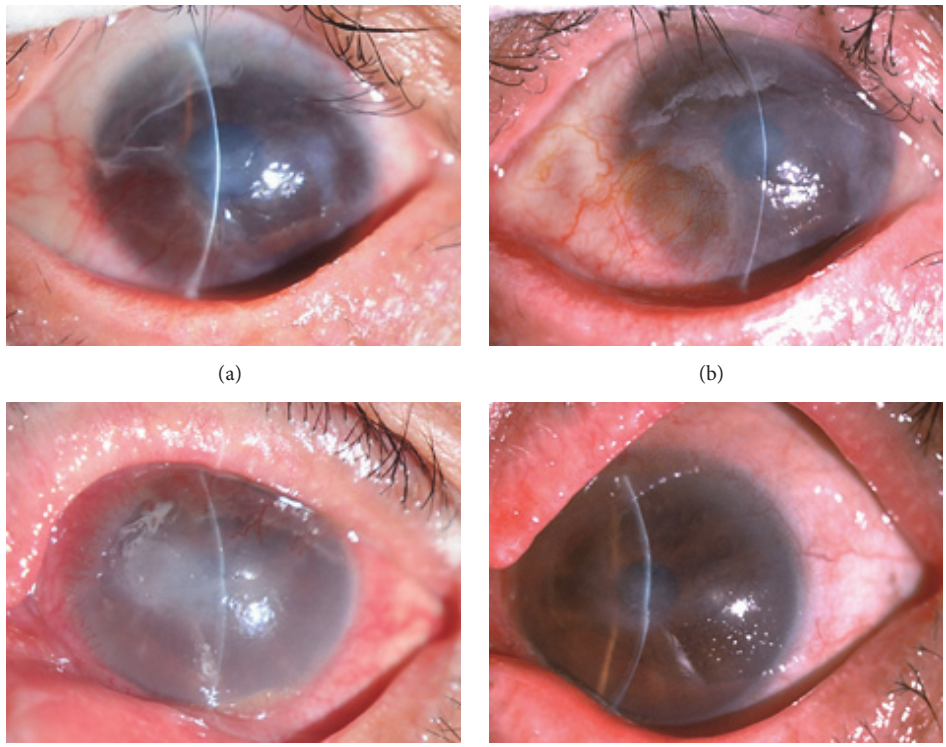

(a) (b) (c) (d)

Figure 2: Slit-lamp photographs showing the treatment course of nonhealing corneal ulcers. (a) *Patient 1*: the preoperative uncorrected visual acuity was finger counting. The size of the ulcer was approximately 4.0 × 3.0 mm. The surrounding tissue displayed infiltration and edema. (b) At 1 month after surgery, the corneal ulcer was completely cured, with the relief of corneal opacity, and the postoperative uncorrected visual acuity was 0.1 (1.0 log MAR). (c) *Patient 2*: the preoperative uncorrected visual acuity was hand motion. The ulcer was approximately 5.0 × 2.5 mm. Evident stromal necrosis, edema, and anterior chamber hypopyon were observed. (d) At 1 month after surgery, the corneal ulcer was healed, with the relief of corneal edema, and the postoperative uncorrected visual acuity was 0.1 (1.0 log MAR).

Table 1: Prior treatment for nonhealing corneal ulcers.

Etiology	Course (month)	Treatment
HSK	4	Medication and AMT
HSK	2.5	Medication and AMT
HSK	2	Medication and AMT
HSK	1	Medication and AMT
HSK	1	Medication and AMT
HSK	1.5	Medication
HSK	1	Medication
HSK	1	Medication
Corneal graft ulcer	1	Medication
Corneal graft ulcer	1	Medication and AMT
SJS	6	Medication

HSK: herpes simplex keratitis; SJS: Stevens-Johnson syndrome; AMT: amniotic membrane transplantation.

3.4. Confocal Microscopy Examination. The inflammatory cells were found to aggregate in the epithelium and basal membrane surrounding the epithelial nonhealing region of the ulcer by confocal microscopy prior to surgery. Inflammatory cell infiltration was noted to be greatly alleviated after surgery (Figure 3).

Table 2: The difference in uncorrected visual acuity (log MAR) before and after surgery.

Difference of UCVA					
Mean	SD	*N*	*t*	*P* value[a]	95% CI
0.88	0.60	11	4.91	0.001	0.48–1.28

UCVA: uncorrected visual acuity; SD: standard deviation; *N*: number of eyes; CI: confidence interval.
[a]Paired *t*-test.

3.5. Anterior Segment Optical Coherence Tomography Examination. AS-OCT revealed that the surgical treatment had healed the corneal ulcer. Postoperatively, corneal stromal edema decreased, leaving a semitransparent and highly reflective region in the cornea (Figure 4).

4. Discussion

The management of nonhealing corneal ulcers is one of the most difficult challenges faced by ophthalmologists because only a few resistant ulcers can be cured solely by medication. Once the nonhealing corneal ulcer tends toward expansion and aggravation, devastating complications can subsequently develop [3]. In the current study, the combination of active

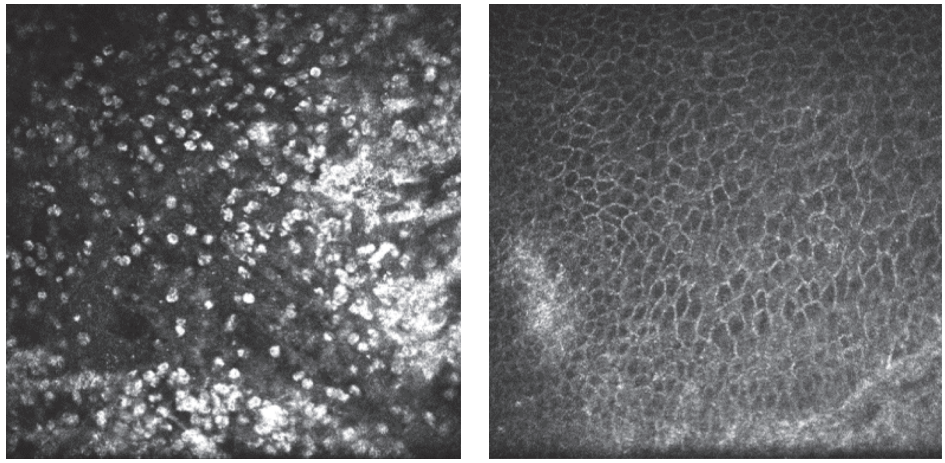

(a) (b)

Figure 3: (a) Abundant inflammatory cells were displayed in the epithelium and basal membrane surrounding the epithelial nonhealing region of the ulcer. (b) The number of inflammatory cells decreased significantly at 2 months after surgery.

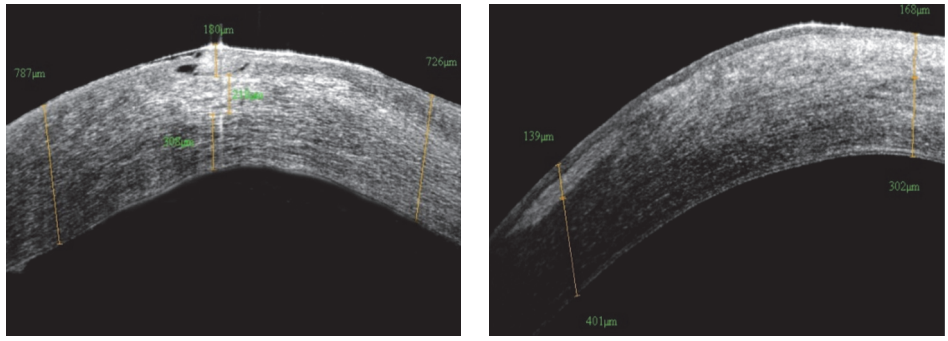

(a) (b)

Figure 4: (a) The ulcer was shown to involve approximately 1/3 of the corneal stroma, with stromal edema and infiltration. (b) The combined surgery healed the ulcer, leaving a semitransparent and highly reflective region in the cornea at 2 months postoperatively.

pedicle epithelial flap transposition and AMT was found to be effective in promoting ulcer healing and yielding a good cosmesis. Following the treatment, complete ocular surface epithelialization was achieved within an average of 10.8 days.

Initially understanding the underlying reasons for a deferred epithelial healing in this case series was necessary to achieve the most optimal therapeutic effect and recognize the involved mechanisms of the combined surgery in treating resistant corneal ulcers.

The deferred epithelial healing in this study could be attributed to several factors. Firstly, an abnormal or deficient basal membrane caused by corneal melting due to local inflammation hindered epithelial healing, resulting in defective cellular adhesion and recurrent breakdown of the epithelium [10]. Secondly, the inflammatory cells and stromal keratocytes in a distinct, preexisting inflammatory microenvironment restrained epithelial healing by secreting proinflammatory cytokines and proteolytic enzymes [3]. In this study, the primary diseases of corneal ulcer were HSK, corneal graft ulcer, and SJS. It is possible that many of the eyes affected by HSK or after keratoplasty had poor corneal sensation and the eyes with SJS had limbal stem cell pathology. Thus, the conditions of these eyes were predisposed to a deferred epithelial healing.

We believe that the mechanism behind the combined surgery in promoting ulcer healing is related to a comprehensive improvement in the corneal microenvironment through the use of an active epithelial flap. Since the introduction of LASEK to refractive surgery in recent decades, epithelial flaps have successfully been used in subepithelial keratectomy by covering the excimer laser ablation area to reduce inflammation and scarring caused by photorefractive keratectomy [11–13].

It was shown in previous studies that many mediators produced or expressed in the corneal epithelium were effective in regulating inflammatory response and maintaining the homeostasis of the ocular surface, such as Resolvin D1, Resolvin E1, IL1RA, Netrin-1, and UNC5B. These factors reduced the recruitment of inflammatory cells, enhanced phagocytosis, and suppressed the secretion of proinflammatory cytokines [14–18]. It has been demonstrated in previous researches that active epithelial cells can markedly reduce

ocular surface inflammation and relieve neurotrophic keratopathy [19–21].

The flap was obtained without the use of alcohol in the current study to preserve the activity of the epithelial flap as far as possible. The active epithelial flap inhibited inflammatory cell infiltration in the inflamed tissue and reduced the quantity of proteinases and cytokines released into the inflammatory cornea. Covering the ulcer with the active epithelial flap provided a relatively healthy substrate and microenvironment. This facilitated epithelial migration, reinforced basal epithelial adhesion, and promoted ocular surface healing. Meanwhile, a decrease in the number of inflammatory cells was detected on confocal microscopy. In addition, thermal cautery was helpful in astringing the melting tissue, gaining better adhesion of the epithelial flap, and ensuring a relative healthy basal membrane. Debridement of the necrotizing tissue around and on the ulcer base helped to improve the corneal microenvironment for ulcer healing. By contrast, a replicating virus and/or severe local inflammatory response could damage the corneal basal membrane and disturb the normal epithelium repair process [8, 22]. Following surgery, the topical administration of corticosteroids further suppresses the immune response, alleviating the stromal edema and improving the visual acuity [23].

The superiority of using the combined surgery over a single AMT treatment was marked. Of all the eyes, 5 eyes received AMT once and 1 eye received AMT twice. However, the corneal ulcers remained unhealed. After the application of a combination of active pedicle epithelial flap transposition and AMT, all of these ulcers were successfully cured within a short time. The results indicate that the epithelial flap might have a greater anti-inflammatory and prohealing effect than that of the amniotic membrane. We speculated that it was the collaborative effect of the epithelial flap and amniotic membrane which inhibited inflammatory cell infiltration and facilitated a relatively healthy microenvironment for ulcer healing. Meanwhile, AMT also ensured epithelial flap adhesion.

Adverse effects were not reported from the use of combined surgery in our study. Its use might also eliminate the need for keratoplasty in some cases. A high risk of immune rejection, epithelial defect, infection, graft melting, and corneal perforation is usually encountered when treating ulcers by corneal transplantation in patients with SJS or other immune diseases [24]. There is less possibility of the immune system being activated and more opportunity of gaining a favorable VA prognosis by employing autogenic epithelial flap transposition in combination with AMT, in addition to reconstructing the corneal surface at an early stage.

In the current study, it was a considerable concern of the clinician whether or not the construction of an epithelial flap would aggravate the primary ocular disease. The epithelial flap was obtained from the transparent cornea close to the limbus for all the eyes because the limbal stem cells are located in this position and taking a flap from here would assure rapid epithelialization. The epithelial defect that resulted from making the flap healed 1.45 days postoperatively and no new region of epithelial defect was identified. Thus, active pedicle epithelial flap transposition combined with AMT was a simple, safe, and effective treatment for nonhealing corneal ulcers.

The treatment of nonhealing sterile corneal ulcers was addressed in the current study but the same approach could not be expected to be effective in patients with recalcitrant corneal ulcers associated with active fungal or bacterial infection. Furthermore, the optimal time for this procedure remains unknown. It is unknown whether the method should be delayed until all conventional treatment has failed or instead be considered earlier. Although the outcome of combined surgery was good in the current study, a randomized, controlled study with a larger sample size is needed for further investigations.

5. Conclusion

The combination of active pedicle epithelial flap transposition and AMT can reduce inflammatory response, promote epithelial healing, and restore useful vision in cases of nonhealing corneal ulcers.

Competing Interests

The authors have no conflict of interests to declare.

Acknowledgments

The National Natural Science Foundation of China (nos. 81370989 and 81570821), National Basic Research Program of China (no. 2013CB967004), Taishan Scholars Program Phase II (no. 20081148), Innovation Project of Shandong Academy of Medical Sciences, and Shandong Provincial Excellent Innovation Team Program are acknowledged as sources of funding for the study.

References

[1] S. Mohan, I. Budhiraja, A. Saxena, P. Khan, and S. K. Sachan, "Role of multilayered amniotic membrane transplantation for the treatment of resistant corneal ulcers in North India," *International Ophthalmology*, vol. 34, no. 3, pp. 485–491, 2014.

[2] I. Livingstone, F. Stefanowicz, S. Moggach et al., "New insight into non-healing corneal ulcers: iatrogenic crystals," *Eye*, vol. 27, no. 6, pp. 755–762, 2013.

[3] P. Prabhasawat, N. Tesavibul, and W. Komolsuradej, "Single and multilayer amniotic membrane transplantation for persistent corneal epithelial defect with and without stromal thinning and perforation," *British Journal of Ophthalmology*, vol. 85, no. 12, pp. 1455–1463, 2001.

[4] E. E. Gabison, S. Doan, M. Catanese, P. Chastang, M. Ben M'hamed, and I. Cochereau, "Modified deep anterior lamellar keratoplasty in the management of small and large epithelialized descemetoceles," *Cornea*, vol. 30, no. 10, pp. 1179–1182, 2011.

[5] A. Medsinge, E. Gajdosova, W. Moore, and K. K. Nischal, "Management of inflammatory corneal melt leading to central perforation in children: a retrospective study and review of literature," *Eye*, vol. 30, no. 4, pp. 593–601, 2016.

[6] S. M. Li, S. Zhan, Y. Li et al., "Laser-assisted subepithelial keratectomy (LASEK) versus photorefractive keratectomy (PRK) for correction of myopia," *The Cochrane Database of Systematic Reviews*, no. 2, Article ID CD009799, 2016.

[7] S.-H. Lee and S. C. G. Tseng, "Amniotic membrane transplantation for persistent epithelial defects with ulceration," *American Journal of Ophthalmology*, vol. 123, no. 3, pp. 303–312, 1997.

[8] W. Shi, M. Chen, and L. Xie, "Amniotic membrane transplantation combined with antiviral and steroid therapy for herpes necrotizing stromal keratitis," *Ophthalmology*, vol. 114, no. 8, pp. 1476–1481, 2007.

[9] S. Dutt, M. Acharya, A. Gour, N. Sapra, L. Chauhan, and U. Mathur, "Clinical efficacy of oral and topical acyclovir in virus," *Indian Journal of Ophthalmology*, vol. 64, no. 4, pp. 292–295, 2016.

[10] R. R. Sayegh, P. B. Kouyoumjian, G. G. Vedula, J. M. Nottage, and V. S. Nirankari, "Cocaine-assisted epithelial debridement for the treatment of anterior basement membrane dystrophy," *Cornea*, vol. 32, no. 6, pp. 889–892, 2013.

[11] S. Taneri, R. Feit, and D. T. Azar, "Safety, efficacy, and stability indices of LASEK correction in moderate myopia and astigmatism," *Journal of Cataract and Refractive Surgery*, vol. 30, no. 10, pp. 2130–2137, 2004.

[12] L.-Q. Zhao, R.-L. Wei, J.-W. Cheng, Y. Li, J.-P. Cai, and X.-Y. Ma, "Meta-analysis: clinical outcomes of laser-assisted subepithelial keratectomy and photorefractive keratectomy in myopia," *Ophthalmology*, vol. 117, no. 10, pp. 1912–1922, 2010.

[13] S. Korkmaz, K. Bilgihan, S. Sul, and A. Hondur, "A clinical and confocal microscopic comparison of transepithelial PRK and LASEK for myopia," *Journal of Ophthalmology*, vol. 2014, Article ID 784185, 5 pages, 2014.

[14] C. N. Serhan, "Resolution phase of inflammation: novel endogenous anti-inflammatory and proresolving lipid mediators and pathways," *Annual Review of Immunology*, vol. 25, pp. 101–137, 2007.

[15] Y. Jin, M. Arita, Q. Zhang et al., "Anti-angiogenesis effect of the novel anti-inflammatory and pro-resolving lipid mediators," *Investigative Ophthalmology and Visual Science*, vol. 50, no. 10, pp. 4743–4752, 2009.

[16] L. V. Norling, J. Dalli, R. J. Flower, C. N. Serhan, and M. Perretti, "Resolvin D1 limits polymorphonuclear leukocyte recruitment to inflammatory loci: receptor-dependent actions," *Arteriosclerosis, Thrombosis, and Vascular Biology*, vol. 32, no. 8, pp. 1970–1978, 2012.

[17] Y. Han, Y. Shao, Z. Lin et al., "Netrin-1 simultaneously suppresses corneal inflammation and neovascularization," *Investigative Ophthalmology and Visual Science*, vol. 53, no. 3, pp. 1285–1295, 2012.

[18] P. Rosenberger, J. M. Schwab, V. Mirakaj et al., "Hypoxia-inducible factor-dependent induction of netrin-1 dampens inflammation caused by hypoxia," *Nature Immunology*, vol. 10, no. 2, pp. 195–202, 2009.

[19] J.-E. Lee, Y. Sun, P. Gjorstrup, and E. Pearlman, "Inhibition of corneal inflammation by the resolvin E1," *Investigative Ophthalmology and Visual Science*, vol. 56, no. 4, pp. 2728–2736, 2015.

[20] N. P. Ly, K. Komatsuzaki, I. P. Fraser et al., "Netrin-1 inhibits leukocyte migration in vitro and in vivo," *Proceedings of the National Academy of Sciences of the United States of America*, vol. 102, no. 41, pp. 14729–14734, 2005.

[21] J. E. Moore, T. C. B. McMullen, I. L. Campbell et al., "The inflammatory milieu associated with conjunctivalized cornea and its alteration with IL-1 RA gene therapy," *Investigative Ophthalmology and Visual Science*, vol. 43, no. 9, pp. 2905–2915, 2002.

[22] H. Gao, Y. Jia, S. Li, T. Wang, Y. Tan, and W. Shi, "Conjunctival flap covering combined with antiviral and steroid therapy for severe herpes simplex virus necrotizing stromal keratitis," *The Scientific World Journal*, vol. 2015, Article ID 565964, 6 pages, 2015.

[23] A. Heiligenhaus, H. Li, E. E. Hernandez Galindo, J. M. Koch, K.-P. Steuhl, and D. Meller, "Management of acute ulcerative and necrotising herpes simplex and zoster keratitis with amniotic membrane transplantation," *British Journal of Ophthalmology*, vol. 87, no. 10, pp. 1215–1219, 2003.

[24] F. Wang, S. Li, T. Wang, H. Gao, and W. Shi, "Modified tectonic keratoplasty with minimal corneal graft for corneal perforation in severe Stevens-Johnson syndrome: a case series study," *BMC Ophthalmology*, vol. 14, no. 97, 2014.

Hindawi Publishing Corporation
Journal of Ophthalmology
Volume 2016, Article ID 1965720, 11 pages
http://dx.doi.org/10.1155/2016/1965720

Research Article

A Novel Technique for Conjunctivoplasty in a Rabbit Model: Platelet-Rich Fibrin Membrane Grafting

Mehmet Erol Can,[1] Hasan Basri Çakmak,[2] Gamze Dereli Can,[3] Hatice Ünverdi,[4] Yasin Toklu,[3] and Sema Hücemenoğlu[4]

[1]*Department of Ophthalmology, Keçiören Training and Research Hospital, Ankara, Turkey*
[2]*Department of Ophthalmology, Hacettepe University Faculty of Medicine, Ankara, Turkey*
[3]*Department of Ophthalmology, Yıldırım Beyazıt University Faculty of Medicine, Ankara Atatürk Training and Research Hospital, Ankara, Turkey*
[4]*Department of Pathology, Ankara Training and Research Hospital, Ankara, Turkey*

Correspondence should be addressed to Mehmet Erol Can; drm.erolcan@gmail.com

Received 19 June 2016; Accepted 31 August 2016

Academic Editor: Anna Nowinska

Purpose. To investigate the effect of platelet-rich fibrin (PRF) membrane on wound healing. *Methods*. Twenty-four right eyes of 24 New Zealand rabbits equally divided into 2 groups for the study design. After the creation of 5 × 5 mm conjunctival damage, it was secured with PRF membrane, which was generated from the rabbit's whole blood samples in PRF membrane group, whereas damage was left unsutured in the control group. Three animals were sacrificed in each group on the 1st, 3rd, 7th, and 28th postoperative days. Immunohistochemical (IHC) stainings and biomicroscopic evaluation were performed and compared between groups. *Results*. PRF membrane generated significant expressions of vascular endothelial growth factor (VEGF), transforming growth factor-beta (TGF-β), and platelet-derived growth factor (PDGF) in the early postoperative period. However, the IHC evaluation allowed showing the excessive staining at day 28, in control group. Biomicroscopic evaluation revealed complete epithelialization in PRF membrane group, but none of the cases showed complete healing in the control group. *Conclusions*. This experimental study showed us the beneficial effects of the PRF membrane on conjunctival healing. Besides its chemical effects, it provides mechanical support as a scaffold for the migrating cells that are important for ocular surface regeneration. These overall results encourage us to apply autologous PRF membrane as a growth factor-enriched endogenous scaffold for ocular surface reconstruction.

1. Introduction

The conjunctiva, as an integral part of the ocular surface, has to be kept healthy and free of various disease processes that cause disruption in the integrity and function of the ocular surface. Minor conjunctival defects can be closed by primary intent; however, in the case of large tissue defects, the need for alternative covering materials for tension-free conjunctival closure is inevitable. Restoration of the ocular surface poses challenges following removal of lesions like pterygium, tumor, symblepharon, or conjunctivochalasis. In addition, complications resulting from a sequel of acute chemical burn or conjunctival scarring due to mucous membrane disorders, such as ocular cicatricial pemphigoid, Stevens-Johnson syndrome (SJS), or toxic epidermal necrolysis (TEN), necessitate conjunctival reconstruction, which requires large amounts of tissue replacement.

Human amniotic membrane is one of the most common biomaterials for ocular surface reconstruction in which condition the tissue defect is outsized. However, it has some disadvantages such as the risk of disease transmission, limited transparency, variable and unstable quality, and low mechanical strength. Other tissue substitutes include conjunctival autografts, oral mucosal grafts, nasal mucosal grafts, or *in vitro* limbal/mucous epithelial cell expansions employed with varying reported success rates [1–4]. All of these methods

have drawbacks due to their need for more complex surgery with intrinsic complications, thereby preventing optimal treatment success.

Platelet-rich fibrin (PRF) membrane is a second-generation platelet concentrate which was first developed for oral and maxillofacial applications by the French Choukroun et al. in 2006 [5, 6].

Many growth factors including platelet-derived growth factor (PDGF), vascular endothelial growth factor (VEGF), and transforming growth factor-beta (TGF-β), which are released by PRF membrane during a period of at least 7 days and up to 28 days, and matrix proteins such as thrombospondin-1, fibronectin, and vitronectin, which have key roles in hemostasis and wound healing, exist in the PRF membrane [7, 8]. Furthermore, PRF membrane provides mechanical support as a scaffold for the cell proliferation, differentiation, and migration which are important for ocular surface regeneration [9]. Several clinical applications of PRF membrane have been described in oral surgery [5, 10, 11], periodontal regeneration surgery [12–18], treatment of meniscus tearing [19], treatment of chronic lower-extremity ulcers [20], ear-nose-throat procedures [21], plastic surgery [22–24], and ophthalmic surgery [25]. The combination of mechanical and chemotactic support of autologous PRF membrane makes it suitable for reconstruction, improvement, and/or maintenance of the tissue function and might offer many potential clinical and biotechnological advantages for tissue engineering applications in ophthalmology.

The purpose of this study was to evaluate the effects of autologous PRF membrane on rabbit conjunctival wound healing.

2. Methods

This was a prospective experimental animal study.

2.1. Experimental Animals. A total of 24 adult female New Zealand white rabbits aged between 12 and 30 weeks, weighing between 3000 and 3500 g at baseline, were used in this study. All animals were transferred from the Center of Refik Saydam Hıfzıssıhha, Ankara, Turkey, to Gazi University Animal Experiments Laboratory, Ankara, Turkey, 10 days prior to the study. The animals were individually maintained in a standard cage condition of a purpose-designed room for experimental animals and exposed daily to 12-hour-light/12-hour-night cycle with free access to a standard laboratory diet. All experimental methods and animal care procedures adhered to the Statement for the Use of Animals in Ophthalmic and Vision Research and were approved and monitored by the Institutional Animal Care and Use Committee at Legacy Health.

2.2. Anesthesia. During the surgical procedure, animals were anesthetized using an injection of 50 mg/kg ketamine (Brema-Ketamin 10%; Bremer Pharma, Germany) and 5 mg/kg xylazine (Alfazyne 2%; Alfasan International BV, Netherlands). After the surgery, all animals were injected with 3 mg/kg ketoprofen (Rifen 1%; Richter Pharma AG, Austria) for analgesia.

2.3. Experimental Design. Unilateral (right eye) conjunctival damage in all rabbits was modeled by excision of the temporal side of the interpalpebral bulbar conjunctiva using an operating microscope. After the injection of 0.5 mL balanced salt solution (BSS) into the subconjunctival space (Figure 1(a)), approximately 5 × 5 mm square shaped conjunctiva and Tenon tissues were excised with Westcott scissors from a distance of 3 mm from the limbus (Figure 1(b)).

All rabbits were equally divided into 2 groups: the PRF membrane group ($n = 12$), in which the defect was secured with PRF membrane prepared from the rabbits' own whole blood samples (Figure 1(c)), and the control group ($n = 12$), in which no further procedure was done after the excision.

2.4. Preparation and Application of PRF Membrane. To prepare the autologous PRF membrane, 5 mL fresh blood sample was drawn from the femoral vein of the rabbit and collected into a glass-coated tube without an anticoagulant under general anesthesia. Samples were immediately centrifuged at 2700 rpm (approximately 400 ×g) for 12 minutes using a table centrifuge system (Hettich EBA-20; Hettich Holding GmbH & Co. oHG, Germany). The fibrin clots were concentrated between the red blood cell corpuscles at the bottom of the centrifuge tubes and the acellular plasma, called platelet-poor plasma (PPP), at the top of the tubes (Figure 2(a)). PPP was then collected by pipetting the supernatant of the centrifuged blood sample. After the removal of PPP, fibrin clots were mechanically separated from the red blood cells with forceps (Figure 2(b)) and gently compressed using a custom-made PRF membrane box (PRF box; Medisoft Medikal, Turkey) to drain the remaining fluid (Figure 2(c)). Subsequently, PRF membrane was placed on the bare sclera and secured to the surrounding conjunctiva with 7/0 absorbable suture material (DLZ-6.4-200 FSSB, Germany) (Figure 3(a)). In order to immobilize the PRF membrane, 3 or 4 bites were placed with 7/0 vicryl interruptedly, 2 of them at the superior and the inferior limbal regions (Figure 3(b)). Postoperatively, moxifloxacin 0.5% (Vigamox; Alcon Lab, Texas) was instilled 4 times daily up to 10 days. Throughout the follow-up period, complications such as secondary infection, scleral necrosis, symblepharon, or any retraction formation in the fornices or eyelids were not observed.

2.5. Process of Enucleation and Tissue Collection. Three rabbits per group were sacrificed under general anesthesia by intravenous injection of 2 cc xylazine (Alfazyne 2%; Alfasan International BV, Netherlands) and the right eyes were enucleated on days 1, 3, 7, and 28 after surgery for histopathological evaluation.

2.6. The Preparation of Histology Slides and Grading of the Staining Pattern. The enucleated eyes of the rabbits in each group were fixed in 10% buffered formalin to prevent tissue autolysis and putrefaction for 24 hours at room temperature and embedded in paraffin. Four-micrometer-thick radial sections (3 or 4 slices) were taken from the paraffin embedding which contains the region between primary and defective tissue zones with a microtome, and sections were stained

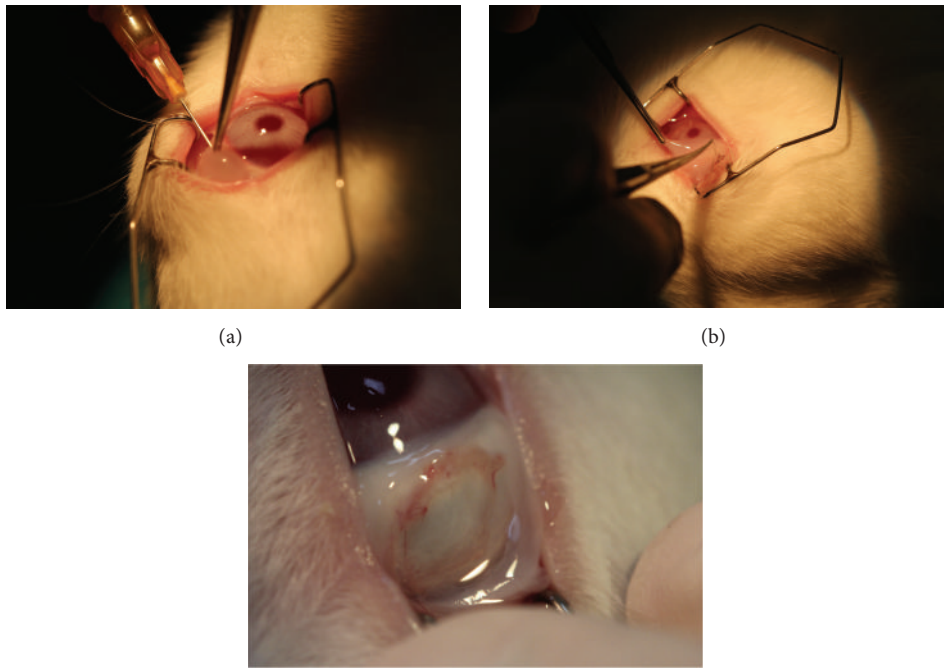

(a) (b)

(c)

Figure 1: (a) Injection of BSS® into the subconjunctival space for dissection. (b) The excision of conjunctiva and Tenon's capsule with Westcott scissors. (c) A 5 × 5 mm square shaped tissue defect in the rabbit eye.

with hematoxylin and eosin (H&E). Inflammation, vascular proliferation, and fibrosis were evaluated considering the prevalence and severity of inflammatory cells, new vessels, and fibroblasts in tissue specimens in microscopic evaluation of 40x high power field (HPF) [26]. Grade 0 indicated that there was no inflammation, vascular proliferation, or fibrosis. Grade 1 demonstrated mild inflammation (<50 inflammatory cells in 40x HPF), mild vascular proliferation (<5 vessels in 40x HPF), and mild fibrosis. Finally, Grade 2 represented moderate to severe inflammation (>50 inflammatory cells in 40x HPF), moderate to severe vascular proliferation (>5 vessels in 40x HPF), and moderate to severe fibrosis.

The conjunctival sections were then mounted on poly-L-lysine coated slides and their controls were immunostained using Leica Bond Max (Leica; Wetzlar, Germany) automated immunostainer for VEGF, TGF-β, PDGF, and alpha-smooth muscle antigen (α-SMA) after antigen retrieval. The control tissues included small intestine for VEGF, breast carcinoma for TGF-β, and prostate adenocarcinoma for PDGF. Antibody detection was performed using a biotinylated secondary antibody and 3,3′-diaminobenzidine, and slides were observed with Olympus Imager BX51, DP25 (Olympus Optical, Tokyo, Japan) microscope. PDGF receptor (1 : 100 dilution; Abcam, Cambridge, MA), VEGF receptor (1 : 100 dilution; Abcam, Cambridge, MA), and TGF-β receptor (1 : 100 dilution; Novocastra Laboratories, Ltd., Newcastle upon Tyne, UK) were obtained from Ser-Med (Ankara, Turkey).

In order to analyse the antibody expressions, immunohistochemical staining patterns were scored with the staining intensity and morphology, a combination of qualitative and quantitative information, by the same examiner [26]. Grades 0, 1, and 2 indicated no staining, minimal staining, and severe staining, respectively. To avoid inaccuracy of the comparison of the staining intensity, all the photographs were taken with the same microscope with the same settings.

3. Results

3.1. Biomicroscopic Evaluation. Biomicroscopic evaluation revealed reepithelialization of the bare sclera on the 1st week in the remaining 6 rabbits of the PRF membrane group (Figure 4(a)). Smooth transition was observed between the reepithelialized region and the primary conjunctival tissue without any ridge formation that might have caused irritation in the postoperative period. Throughout the follow-up period, complications such as secondary infection, scleral necrosis, symblepharon, or any retraction formation of the fornices or eyelids were not observed (Figure 4(b)). However, bare sclera was proceeded throughout the study period in the control group with mild to moderate hemorrhage and secretion formation indicated poor healing (Figure 4(c)).

3.2. H&E Staining. All tissue specimens stained with H&E were examined to evaluate 3 important aspects of wound healing: inflammation, vascular proliferation, and fibrosis. Rabbits in the PRF membrane group showed major differences for inflammation when their condition was compared to rabbits in the control group. There was a severe inflammatory reaction on the 1st day in PRF membrane specimens. In the following days, for day 3 and day 7, the intensity of the inflammatory reaction began to be alleviated and ended on

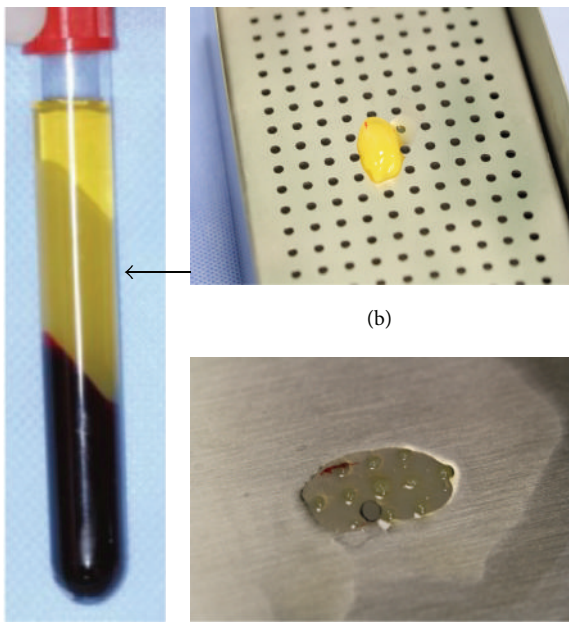

(a) (b) (c)

Figure 2: (a) After centrifugation, a fibrin clot (arrow) was placed between the acellular plasma layer at the top and the red corpuscles at the bottom of the tube. (b) Removal of the PRF clot from the tube using forceps. (c) PRF membrane obtained by compressing the PRF clot with PRF membrane box.

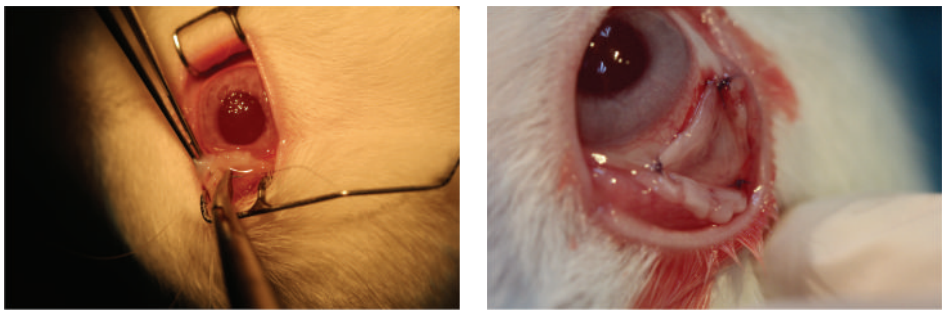

(a) (b)

Figure 3: (a) PRF membrane was placed on the bare sclera and secured with 7-0 absorbable suture. (b) The immobilization of the PRF membrane over the defective zone.

the 28th day. However, moderate inflammatory reaction was observed in the control group, in contrast to severe reaction in the PRF membrane group on the 1st day. Additionally, on day 3 and day 7, inflammation became more pronounced and continued even in the 28th-day specimens in the control group. As Figure 5 shows, there was a significant difference between groups in terms of inflammatory reactions.

Furthermore, there was a significant difference between the groups when the specimens were examined for vascular proliferation. There was minimal vascular proliferation in 3rd- and 7th-day specimens in the PRF membrane group. On the other hand, in the control group, moderate vascular proliferation was observed on the 1st week. The difference between groups became more apparent in the specimens by the 28th day. No vascular proliferation remained in the PRF membrane group, whereas signs of vascular proliferation persisted in the control group.

Additionally, significant differences have been found in certain areas between groups when the specimens were evaluated for fibrosis formation. In the PRF membrane group, mild fibrosis was observed in the 7th-day specimens. By contrast, in the control group, preliminary signs of pronounced fibrosis appeared first in the 7th-day specimens, resulting in significant fibrosis by the 28th day.

The results of the H&E staining are shown in Table 1.

3.3. Immunohistochemistry

3.3.1. α-SMA. Figure 6(a), showing α-SMA staining intensity, illustrates the main differences between groups. In the PRF

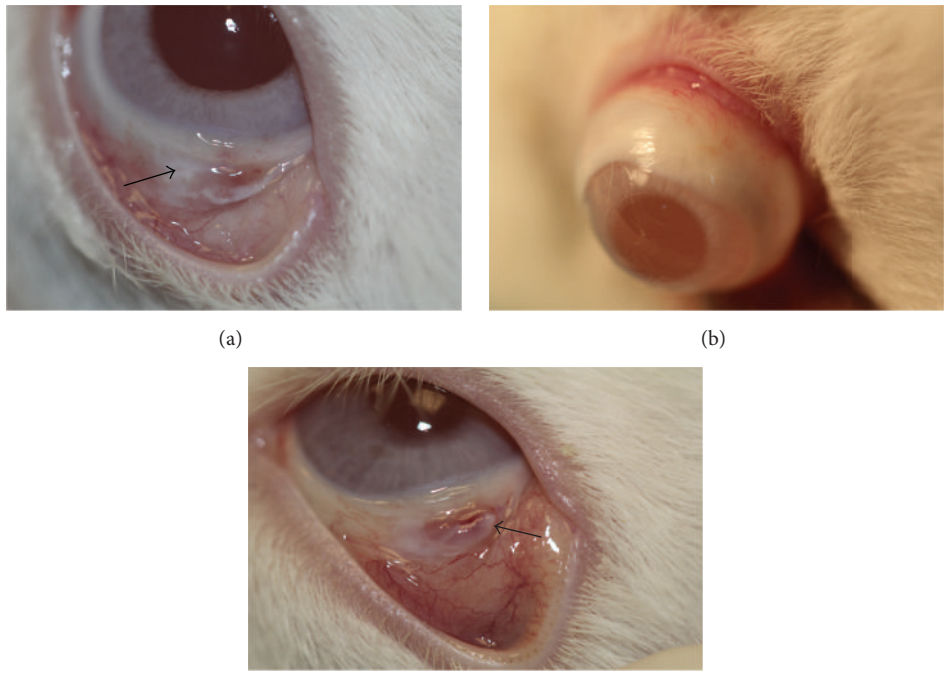

(a) (b) (c)

Figure 4: (a) Almost all of the defective zone reepithelialized on day 7 in the PRF membrane group. PRF membrane was integrated with the surrounding conjunctiva (arrow). (b) Conjunctival healing was completed on day 28 in the PRF membrane group without any complications. (c) The conjunctival defect (arrow) was persistent with mild hemorrhage on day 28 in the control group.

Table 1: The comparison of hematoxylin and eosin staining.

Day	PRF membrane group			Control group		
	Inflammation	Vascular proliferation	Fibrosis	Inflammation	Vascular proliferation	Fibrosis
1	++	+	−	+	+	−
3	++	++	−	++	++	−
7	++	+	+	++	++	+
28	−	+	−	++	+	++

−: Grade 0, no inflammation, vascular proliferation, or fibrosis.
+: Grade 1, mild inflammation (<50 inflammatory cells) (×40), mild vascular proliferation (<5 vessels) (×40), and mild fibrosis.
++: Grade 2, moderate to severe inflammation (>50 inflammatory cells) (×40), moderate to severe vascular proliferation (>5 vessels) (×40), and moderate to severe fibrosis.
PRF: platelet-rich fibrin.

membrane group, α-SMA staining was seen only in 2 cases on day 3. On the other hand, in the control group, the α-SMA staining started on day 3 and increased by the 7th day. The difference between PRF membrane and control groups became more striking on day 28. By that time, a marked α-SMA expression was observed in the control group, contrasting with a negative staining in all specimens in the PRF membrane group.

3.3.2. PDGF. PDGF expressions were significantly different between groups. As Figure 6(b) shows, both on the 3rd and on the 7th days, PDGF expression was more pronounced in the PRF membrane group. On day 28, the PDGF expression could not be detected in the PRF membrane group, while in the control group there was Grade 1 staining in all specimens (Figures 7(a) and 7(b)).

3.3.3. TGF-β. Again, the expression of TGF-β began earlier, and its expression was more marked in the PRF membrane group. Interestingly, in the 28th-day specimens, there was no TGF-β staining in the PRF membrane group, which was in contrast to the Grade 1 staining seen in the control group (Figures 7(c) and 7(d)). The difference between groups with regard to TGF-β expression was similar to the difference in PDGF expression. This similarity was shown clearly in Figure 8(a).

3.3.4. VEGF. The VEGF expression in the PRF membrane group was different from the control group in a number of important ways. In the PRF membrane group, even early specimens from the 1st day depicted moderate VEGF expression, and this expression became maximal on day 3 and stayed in the same level on day 7 (Figure 8(b)). Compared with the

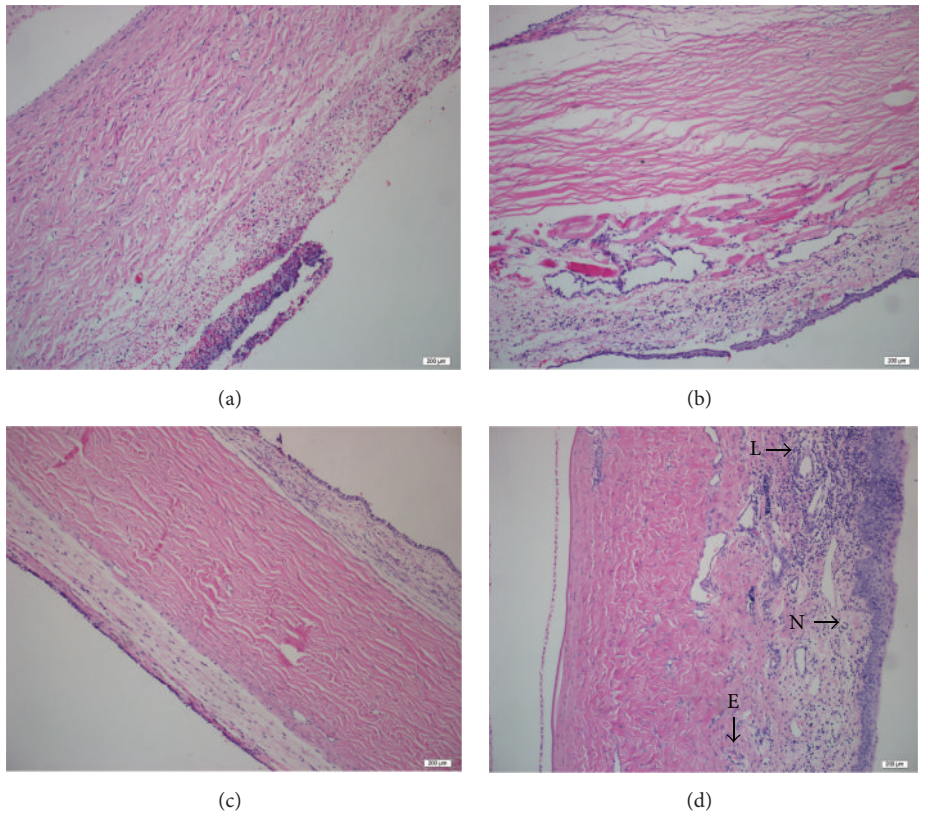

Figure 5: Comparison of the staining intensity of H&E. (a) Severe inflammatory reaction on the 1st day in PRF membrane specimens (×200). (b) Mild inflammation seen on the 1st day in the control group (×200). (c) Conjunctival tissue formation with normal histomorphology seen on day 28 in the PRF membrane group (×200). (d) Mixed cellular inflammation contains neutrophil leucocytes (N), lymphocytes (L), and eosinophils (E) seen on day 28 in the control group (×200).

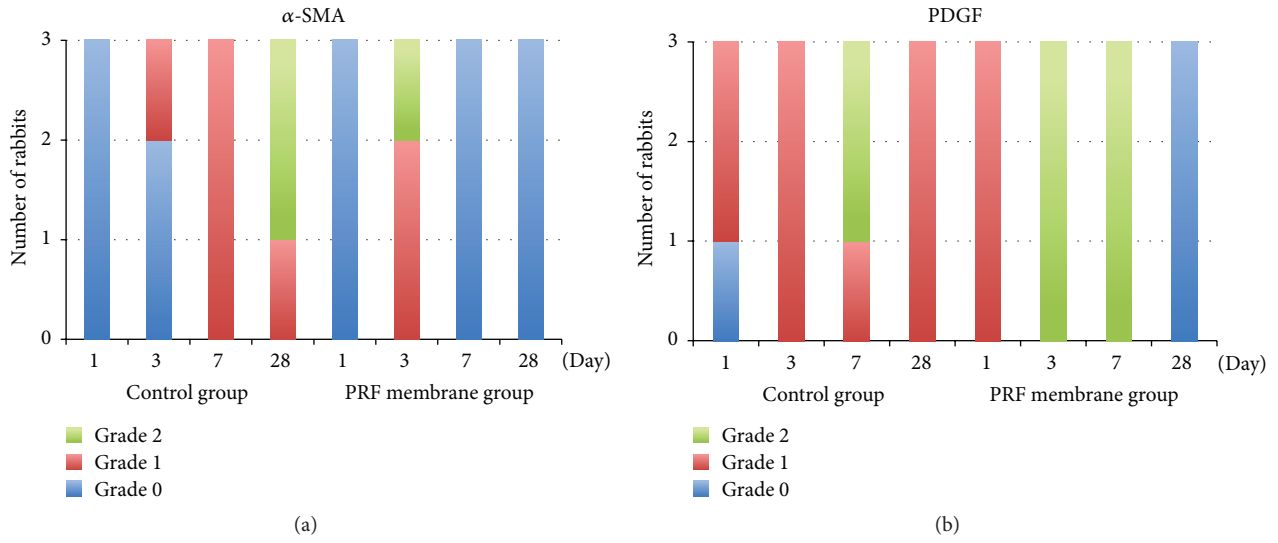

Figure 6: Comparison of the staining intensity of α-SMA and PDGF. (a) Histogram of the α-SMA staining. (b) Histogram of the PDGF staining.

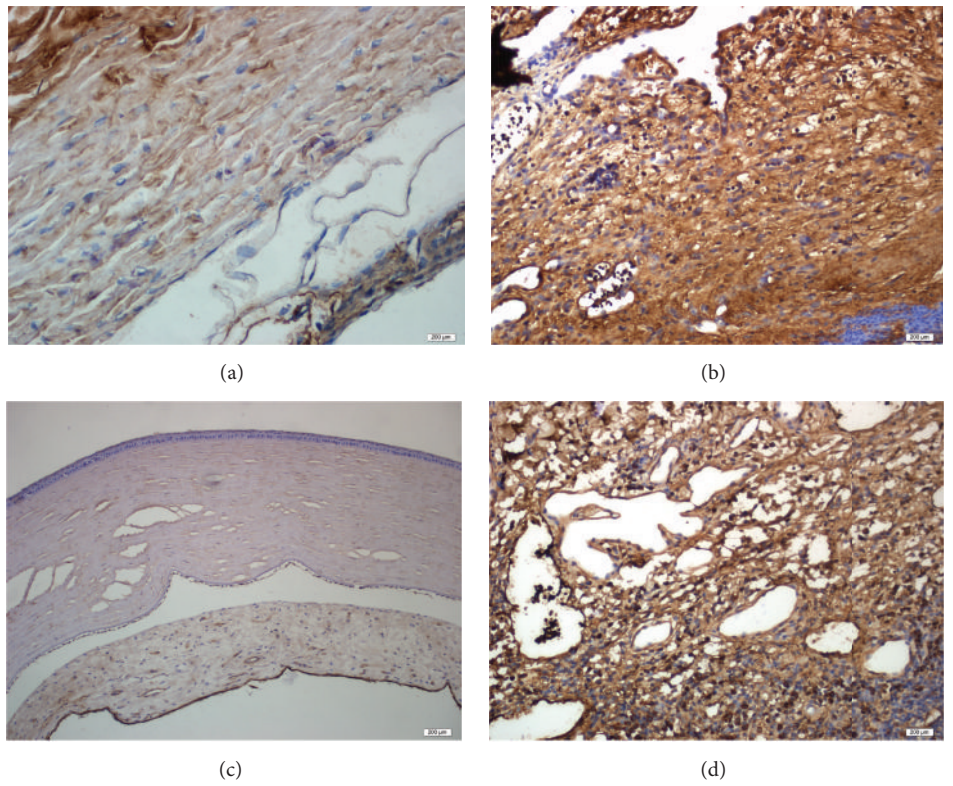

Figure 7: Immunohistochemical analysis of PDGF and TGF-β. (a) Grade 0 staining of PDGF was observed on day 28 in the PRF membrane group. (b) Grade 1 staining of PDGF was observed on day 28 in the control group. (c) Grade 0 staining of TGF-β was observed on day 28 in the PRF membrane group. (d) Grade 1 staining of TGF-β was observed on day 28 in the control group.

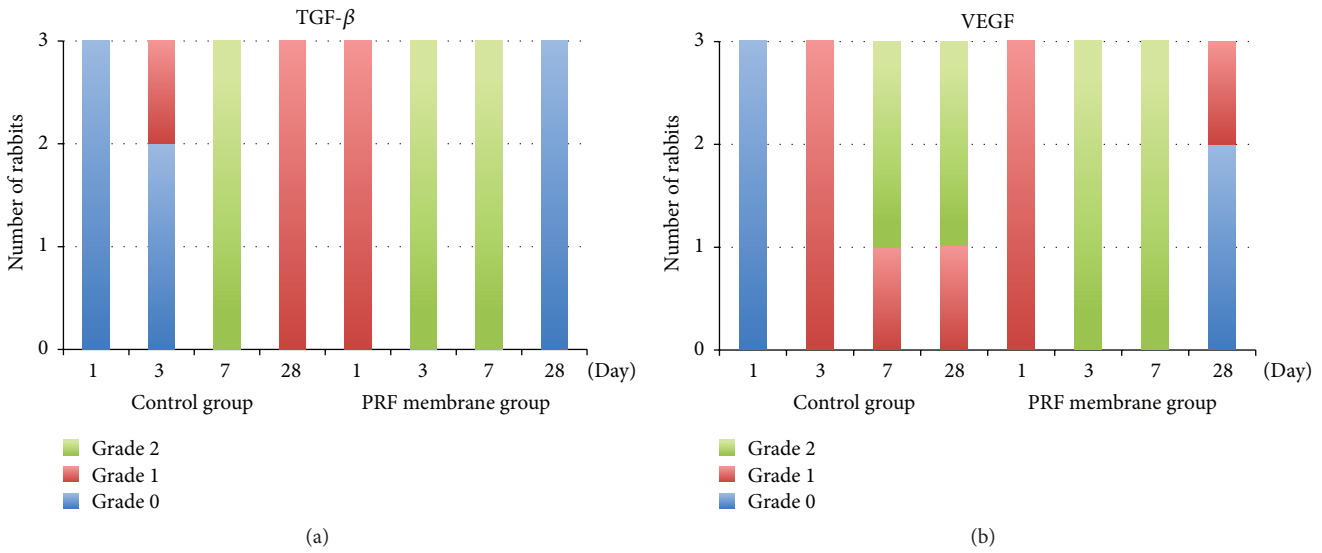

Figure 8: Comparison of the staining intensity of TGF-β and VEGF. (a) Histogram of the TGF-β staining. (b) Histogram of the VEGF staining.

Table 2: The comparison of the immunohistochemical staining.

Day	PRF membrane group			Control group		
	VEGF	PGDF	TGF-β	VEGF	PGDF	TGF-β
1	+	+	+	−	+	−
3	++	++	++	+	++	+
7	++	++	++	++	++	++
28	−	−	−	++	+	+

−: Grade 0, no staining.
+: Grade 1, minimal staining.
++: Grade 2, moderate to severe staining.
PRF: platelet-rich fibrin; VEGF: vascular endothelial growth factor; PDGF: platelet-derived growth factor; TGF-β: transforming growth factor-beta.

PRF membrane group, VEGF expression started later (on day 3) in the control group. Most importantly, examination of the 28th-day specimens showed significant differences between groups. The VEGF staining was continued in the control group, whereas, in the PRF membrane group, only 1 specimen was stained as Grade 1.

The results of the immunohistochemistry staining are summarized in Table 2.

4. Discussion

Conjunctival wound healing is a complex process in which a variety of cytokines, growth factors, and proteases interact to regulate the key phases of the healing.

In general, conjunctival wound healing is similar to wound healing in normal tissue, which is a complex and a dynamic three-phase process. These phases are the inflammatory phase, the proliferative phase, and the remodeling phase [27–29].

The inflammatory phase of wound healing is characterized by the infiltration of neutrophils and monocytes into the wound area. At this stage, plasma proteins and extracellular matrix fragments are released into the wound area due to injury of the connective tissue and blood vessels. Furthermore, platelet aggregation and hemostasis cascade have been activated at the wound site. The hemostatic plugs mainly consist of fibrinogen. The fibrin molecule is the final product, which is derived from fibrinogen, and provides support like a scaffold material over the wound area. Furthermore, growth factors, proteases, and metabolites of arachidonic acids are released as a result of the activated platelets and coagulation cascade [28]. The main factors released from the platelets are PDGF, VEGF, TGF-α, and TGF-β [5, 6]. Releasing growth factors leads to cell migration and proliferation in the healing site. After this stage, the proliferation of macrophages and fibroblast cells occurs in the proliferation phase. In addition, intensive synthesis of collagen, fibronectin, and proteoglycan helps the formation of angiogenesis and granulation tissue. During the remodeling phase, the degradation of extracellular matrix occurs, tensile strength of the tissue increases, and the vascularity and cellularity decrease. This period can last up to 2 weeks to several months.

The PDGF and particularly TGF-β are the key components of the fibrotic response in wound healing. TGF-β stimulates the migration of fibroblasts that synthesize the extracellular matrix. As a result, TGF-β is involved in the mechanism of most diseases arising from excessive fibrosis, like glaucoma and proliferative diabetic retinopathy [30, 31]. The PDGF is a major mitogen for connective tissue cells and it plays an important role in wound healing [32, 33]. It acts on several cell types involved in the wound healing phases. It stimulates fibroblasts, smooth muscle cells, neutrophils, and macrophages [34]. The PDGF also stimulates the production of extracellular matrix molecules like fibronectin, collagen, proteoglycan, and hyaluronic acid [35–38]. At the early stage of the wound healing, PDGF is released by platelets and secreted by activated macrophages, thrombin-stimulated endothelial cells, smooth muscle cells of damaged arteries, and activated fibroblasts [39–42]. As a result of releasing PDGF, reepithelialization, angiogenesis, and extracellular matrix deposition have occurred at the healing site [35]. In the remodeling phase, PDGF stimulates the production and secretion of collagenase by fibroblasts [43]. Therefore, the overactivity of PDGF is related to scarring and fibrosis [33, 44].

Platelet-rich plasma (PRP) and its products have been used in dentistry and maxillofacial surgery for tissue regeneration for many years. PRF, described by Choukroun et al. [5], is a second-generation platelet concentrate, consisting of many growth factors and cytokines which play a key role in hemostasis and wound healing. These growth factors are known to promote cell proliferation, differentiation, migration, and matrix synthesis by binding to specific cell surface receptors [5, 29]. Furthermore, PRF clots trap stem cells, which are circulating in the peripheral blood and contribute to wound healing. The PRF membrane, the resistant fibrin membrane, can be easily obtained by pressing the PRF clot which is localized in the middle part of the centrifuge tube between the PPP and red blood cell layer with a simple press machine.

In this prospective study, we clearly demonstrated that the influence of PRF membrane on conjunctival wound healing is supportive due to its biological and physical properties. In the earlier phase of wound healing, the PRF membrane appeared to promote the release of growth factors in higher amounts than the normal wound healing cycle. However, the expression of growth factors started to diminish by the postoperative 7th day while the PRF membrane was disappearing. Furthermore, PRF membrane provided mechanical support to the migrating conjunctival cells as a scaffold.

Consequently, we did not observe any scar formation or inflammation in H&E staining in the PRF membrane group on day 28. Hence, it could be conceivably hypothesized that PRF membrane modified the TGF-β expression, suppressed its overexpression, and prevented scar formation. In addition, biomicroscopic evaluation revealed that smooth new conjunctival tissue without any roughness was formed over the defective zone in PRF membrane group. However, in the control group, mild immunohistochemical staining intensity was observed on day 3 and day 7, in contrast with the severe intensity on day 28. As a result, the wound healing process had been sustained, resulting in continuing fibrosis and inflammation even on the 28th day. This suggested that the scaffold function of the PRF membrane and excessive and early release of the growth factors from the PRF membrane might have a positive effect on conjunctival healing.

PRF membrane offers many advantages compared to other methods that have been used for conjunctivoplasty. First, the architecture of the PRF membrane facilitates the cellular proliferation, differentiation, and especially migration and provides an important temporary mechanical support to the growing cells. Alongside the conjunctival epithelial cells, the endothelial cells that are necessary for neoangiogenesis, vascularization, and survival of the graft could easily proliferate and migrate on/into this membrane for the regeneration of the defective zone. Second, the platelet cytokines are released gradually as the fibrin matrix gets resorbed, thus creating a convenient process of healing. Lastly, the presence of leukocytes and cytokines in the fibrin network can play a significant role in the self-regulation of the inflammatory and infectious phenomenon within the grafted material [14, 45]. All these features make PRF membrane a feeder layer for conjunctival epithelial cells which is actually used for *in vitro* cell cultivation in cell and tissue engineering applications. Additionally, the gradual release of the growth factors mimics the controlled release mechanism of the biosignals that researchers try to create for tissue engineering applications.

Besides these theoretical advantages, the ease of obtainment and implementation of the PRF membrane makes it suitable when compared to other methods that have been used for clinical applications. Conjunctival autograft, the conventional method for conjunctivoplasty, is the most popular option for the treatment of conjunctival tissue defects caused by the excision of pterygium, tumor, or symblepharon or conjunctival cicatrization caused by SJS or TEN. But it cannot be performed in cases with large defects or cases that need future surgery for glaucoma. Furthermore, conjunctival autograft might cause limbal stem cell deficiency that is important for the ocular surface health. The other option for the reconstruction of the ocular surface is amniotic membrane transplantation (AMT), which is considered one of the major new developments in ocular surface surgery. Similar to PRF membrane, the amniotic membrane promotes epithelialization by acting as a temporary basement membrane and releases growth factors such as epidermal growth factor and keratocyte growth factor that are important for the healing. Further, it has anti-inflammatory and antiscarring effects by the inhibition of TGF-β signaling in the chronic term. However, the preparation of amniotic membrane is complicated and rather expensive. In addition, strong tissue banking expertise is crucial to prevent inadvertent complications. The contagion risk of some serious pathogens always exists and cannot be excluded even in the presence of very strict procedures and measures. Furthermore, amniotic membrane is a natural but an allogenic matrix, and immunologic response to allografts is the major concern. However, PRF membrane is autologous and is prepared from the patient's own blood samples and poses no immunological rejection risk to the grafted tissue. In addition, PRF membrane is cost-effective and carries no risk of allergic reactions. The preparation of PRF membrane is simple and practical. It can be carried out with few instruments. This process does not require complicated and expensive equipment. Moreover, blood samples could easily be taken, and the PRF membrane could easily be prepared in a short amount of time after centrifuging the blood samples.

To the best of our knowledge, this is the first animal study investigating the role of PRF membrane in conjunctival wound healing. Although the results are encouraging, the small number of rabbits and the short follow-up time for the evaluation of the effectiveness of the PRF membrane are the main limitations of our study. Furthermore, some of the parameters, such as imaging wound area and intensity of scar formation, need to be optimized.

In conclusion, PRF membrane appears to be a novel treatment alternative to other treatment modalities which are currently employed for conjunctivoplasty. Intrinsic trophic substances and the micro- and macroarchitecture of the PRF membrane make it an ideal substrate for reconstruction of the ocular surface. These results may encourage us to use PRF membrane for debilitating ocular surface disorders with a pronounced inflammatory reaction resulting in severe vision loss.

Disclosure

The authors alone are responsible for the content and writing of the paper. This research was presented in part at the 2014 Annual Meeting of the Association for Research in Vision and Ophthalmology (ARVO), Orlando, FL, May 4–8, 2014.

Competing Interests

The authors report no competing interests regarding the publication of this paper.

Acknowledgments

This work was supported by the Scientific and Technological Research Council of Turkey (TUBITAK) Short Term R&D Funding Program Grant no. 112S550.

References

[1] S. E. Ti, S. P. Chee, K. B. G. Dear, and D. T. H. Tan, "Analysis of variation in success rates in conjunctival autografting for primary and recurrent pterygium," *British Journal of Ophthalmology*, vol. 84, no. 4, pp. 385–389, 2000.

[2] J. Liu, H. Sheha, Y. Fu, M. Giegengack, and S. C. G. Tseng, "Oral mucosal graft with amniotic membrane transplantation for

total limbal stem cell deficiency," *American Journal of Ophthalmology*, vol. 152, no. 5, pp. 739.e1–747.e1, 2011.

[3] J. H. Kim, Y. S. Chun, S. H. Lee et al., "Ocular surface reconstruction with autologous nasal mucosa in cicatricial ocular surface disease," *American Journal of Ophthalmology*, vol. 149, no. 1, pp. 45–53.e2, 2010.

[4] C. Mai and E. Bertelmann, "Oral mucosal grafts: old technique in new light," *Ophthalmic Research*, vol. 50, no. 2, pp. 91–98, 2013.

[5] D. M. Dohan, J. Choukroun, A. Diss et al., "Platelet-Rich Fibrin (PRF): a second-generation platelet concentrate. Part I: technological concepts and evolution," *Oral Surgery, Oral Medicine, Oral Pathology, Oral Radiology, and Endodontology*, vol. 101, no. 3, pp. e37–e44, 2006.

[6] D. M. Dohan, J. Choukroun, A. Diss et al., "Platelet-rich fibrin (PRF): a second-generation platelet concentrate. Part II: platelet-related biologic features," *Oral Surgery, Oral Medicine, Oral Pathology, Oral Radiology and Endodontology*, vol. 101, no. 3, pp. e45–e50, 2006.

[7] D. M. Dohan, J. Choukroun, A. Diss et al., "Platelet-rich fibrin (PRF): a second-generation platelet concentrate. Part III: leucocyte activation: a new feature for platelet concentrates?" *Oral Surgery, Oral Medicine, Oral Pathology, Oral Radiology and Endodontology*, vol. 101, no. 3, pp. e51–e55, 2006.

[8] D. M. Dohan Ehrenfest, G. M. de Peppo, P. Doglioli, and G. Sammartino, "Slow release of growth factors and thrombospondin-1 in Choukroun's platelet-rich fibrin (PRF): a gold standard to achieve for all surgical platelet concentrates technologies," *Growth Factors*, vol. 27, no. 1, pp. 63–69, 2009.

[9] L. He, Y. Lin, X. Hu, Y. Zhang, and H. Wu, "A comparative study of platelet-rich fibrin (PRF) and platelet-rich plasma (PRP) on the effect of proliferation and differentiation of rat osteoblasts in vitro," *Oral Surgery, Oral Medicine, Oral Pathology, Oral Radiology and Endodontology*, vol. 108, no. 5, pp. 707–713, 2009.

[10] D. M. Dohan Ehrenfest, P. Doglioli, G. M. de Peppo, M. Del Corso, and J.-B. Charrier, "Choukroun's Platelet-Rich Fibrin (PRF) stimulates in vitro proliferation and differentiation of human oral bone mesenchymal stem cell in a dose-dependent way," *Archives of Oral Biology*, vol. 55, no. 3, pp. 185–194, 2010.

[11] J. Choukroun, A. Diss, A. Simonpieri et al., "Platelet-rich fibrin (PRF): a second-generation platelet concentrate. Part V: histologic evaluations of PRF effects on bone allograft maturation in sinus lift," *Oral Surgery, Oral Medicine, Oral Pathology, Oral Radiology and Endodontology*, vol. 101, no. 3, pp. 299–303, 2006.

[12] A. P. Soadoun and B. Touati, "Soft tissue recession around implants: is it still unavoidable?—Part II," *Practical Procedures & Aesthetic Dentistry*, vol. 19, no. 2, pp. 81–88, 2007.

[13] A. Diss, D. M. Dohan, J. Mouhyi, and P. Mahler, "Osteotome sinus floor elevation using Choukroun's platelet-rich fibrin as grafting material: a 1-year prospective pilot study with microthreaded implants," *Oral Surgery, Oral Medicine, Oral Pathology, Oral Radiology and Endodontology*, vol. 105, no. 5, pp. 572–579, 2008.

[14] A. Simonpieri, M. Del Corso, G. Sammartino, and D. M. Dohan Ehrenfest, "The relevance of Choukroun's platelet-rich fibrin and metronidazole during complex maxillary rehabilitations using bone allograft. Part I: a new grafting protocol," *Implant Dentistry*, vol. 18, no. 2, pp. 102–111, 2009.

[15] A. Simonpieri, M. Del Corso, G. Sammartino, and D. M. Dohan Ehrenfest, "The relevance of Choukroun's platelet-rich fibrin and metronidazole during complex maxillary rehabilitations using bone allograft. Part II: implant surgery, prosthodontics, and survival," *Implant Dentistry*, vol. 18, no. 3, pp. 220–229, 2009.

[16] E. Anitua, M. Sánchez, A. T. Nurden, P. Nurden, G. Orive, and I. Andía, "New insights into and novel applications for platelet-rich fibrin therapies," *Trends in Biotechnology*, vol. 24, no. 5, pp. 227–234, 2006.

[17] Y.-C. Chang and J.-H. Zhao, "Effects of platelet-rich fibrin on human periodontal ligament fibroblasts and application for periodontal infrabony defects," *Australian Dental Journal*, vol. 56, no. 4, pp. 365–371, 2011.

[18] E. Öncü and E. Alaaddinoğlu, "The effect of platelet-rich fibrin on implant stability," *The International Journal of Oral & Maxillofacial Implants*, vol. 30, no. 3, pp. 578–582, 2015.

[19] S. H. Jang, J. K. Ha, D. W. Lee, and J. G. Kim, "Fibrin clot delivery system for meniscal repair," *Knee Surgery and Related Research*, vol. 23, no. 3, p. 180, 2011.

[20] S. M. O'Connell, T. Impeduglia, K. Hessler, X.-J. Wang, R. J. Carroll, and H. Dardik, "Autologous platelet-rich fibrin matrix as cell therapy in the healing of chronic lower-extremity ulcers," *Wound Repair and Regeneration*, vol. 16, no. 6, pp. 749–756, 2008.

[21] J. I. Choukroun, F. Braccini, A. Diss, G. Giordano, P. Doglioli, and D. M. Dohan, "Influence of Platelet Rich Fibrin (PRF) on proliferation of human preadipocytes and tympanic keratinocytes: a new opportunity in facial lipostructure (Coleman's technique) and tympanoplasty?" *Revue de Laryngologie Otologie Rhinologie*, vol. 128, no. 1-2, pp. 27–32, 2007.

[22] F. Braccini and D. M. Dohan, "The relevance of Choukroun's platelet rich fibrin (PRF) during facial aesthetic lipostructure (Coleman's technique): preliminary results," *Revue de Laryngologie Otologie Rhinologie*, vol. 128, no. 4, pp. 255–260, 2007.

[23] CharrierJ-B, J.-P. Monteil, S. Albert, S. Collon, S. Bobin, and D. M. Dohan Ehrenfest, "Relevance of Choukroun's Platelet-Rich Fibrin (PRF) and SMAS flap in primary reconstruction after superficial or subtotal parotidectomy in patients with focal pleiomorphic adenoma: a new technique," *Revue de Laryngologie Otologie Rhinologie*, vol. 129, no. 4-5, pp. 313–318, 2009.

[24] A. P. Sclafani, "Applications of platelet-rich fibrin matrix in facial plastic surgery," *Facial Plastic Surgery*, vol. 25, no. 4, pp. 270–276, 2009.

[25] M. E. Can, G. Dereli Can, N. Cagil, H. B. Cakmak, and N. Sungu, "Urgent therapeutic grafting of platelet-rich fibrin membrane in descemetocele," *Cornea*, vol. 35, no. 9, pp. 1245–1249, 2016.

[26] O. Yoldas, T. Karaca, B. C. Bilgin et al., "Tamoxifen citrate: a glimmer of hope for silicosis," *Journal of Surgical Research*, vol. 193, no. 1, pp. 429–434, 2015.

[27] A. J. Singer and R. A. F. Clark, "Cutaneous wound healing," *The New England Journal of Medicine*, vol. 341, no. 10, pp. 738–746, 1999.

[28] M. F. Cordeiro, L. Chang, K. S. Lim et al., "Modulating conjunctival wound healing," *Eye*, vol. 14, no. 3, pp. 536–547, 2000.

[29] H.-J. Lee, B.-H. Choi, J.-H. Jung et al., "Maxillary sinus floor augmentation using autogenous bone grafts and platelet-enriched fibrin glue with simultaneous implant placement," *Oral Surgery, Oral Medicine, Oral Pathology, Oral Radiology and Endodontology*, vol. 103, no. 3, pp. 329–333, 2007.

[30] C. L. Von Zee, K. A. Langert, and E. B. Stubbs Jr., "Transforming growth factor-β2 induces synthesis and secretion of endothelin-1 in human trabecular meshwork cells," *Investigative Ophthalmology and Visual Science*, vol. 53, no. 9, pp. 5279–5286, 2012.

[31] H. Hatanaka, N. Koizumi, N. Okumura et al., "Epithelial-mesenchymal transition-like phenotypic changes of retinal

pigment epithelium induced by TGF-β are prevented by PPAR-γ agonists," *Investigative Ophthalmology & Visual Science*, vol. 53, no. 11, pp. 6955–6963, 2012.

[32] R. H. Alvarez, H. M. Kantarjian, and J. E. Cortes, "Biology of platelet-derived growth factor and its involvement in disease," *Mayo Clinic Proceedings*, vol. 81, no. 9, pp. 1241–1257, 2006.

[33] J. Donovan, X. Shiwen, J. Norman, and D. Abraham, "Platelet-derived growth factor alpha and beta receptors have overlapping functional activities towards fibroblasts," *Fibrogenesis and Tissue Repair*, vol. 6, article 10, 2013.

[34] C.-H. Heldin and B. Westermark, "Mechanism of action and in vivo role of platelet-derived growth factor," *Physiological Reviews*, vol. 79, no. 4, pp. 1283–1316, 1999.

[35] P. Heldin, T. C. Laurent, and C.-H. Heldin, "Effect of growth factors on hyaluronan synthesis in cultured human fibroblasts," *Biochemical Journal*, vol. 258, no. 3, pp. 919–922, 1989.

[36] E. Schönherr, H. T. Järveläinen, L. J. Sandell, and T. N. Wight, "Effects of platelet-derived growth factor and transforming growth factor-beta 1 on the synthesis of a large versican-like chondroitin sulfate proteoglycan by arterial smooth muscle cells," *The Journal of Biological Chemistry*, vol. 266, no. 26, pp. 17640–17647, 1991.

[37] E. Canalis, "Effect of platelet-derived growth factor on DNA and protein synthesis in cultured rat calvaria," *Metabolism*, vol. 30, no. 10, pp. 970–975, 1981.

[38] S. P. Blatti, D. N. Foster, G. Ranganathan, H. L. Moses, and M. J. Getz, "Induction of fibronectin gene transcription and mRNA is a primary response to growth-factor stimulation of AKR-2B cells," *Proceedings of the National Academy of Sciences of the United States of America*, vol. 85, no. 4, pp. 1119–1123, 1988.

[39] K. Shimokado, E. W. Raines, D. K. Madtes, T. B. Barrett, E. P. Benditt, and R. Ross, "A significant part of macrophage-derived growth factor consists of at least two forms of PDGF," *Cell*, vol. 43, no. 1, pp. 277–286, 1985.

[40] L. N. Walker, D. F. Bowen-Pope, R. Ross, and M. A. Reidy, "Production of platelet-derived growth factor-like molecules by cultured arterial smooth muscle cells accompanies proliferation after arterial injury," *Proceedings of the National Academy of Sciences of the United States of America*, vol. 83, no. 19, pp. 7311–7315, 1986.

[41] Y. Paulsson, A. Hammacher, C.-H. Heldin, and B. Westermark, "Possible positive autocrine feedback in the prereplicative phase of human fibroblasts," *Nature*, vol. 328, no. 6132, pp. 715–717, 1987.

[42] J. M. Harlan, P. J. Thompson, R. R. Ross, and D. F. Bowen-Pope, "Alpha-thrombin induces release of platelet-derived growth factor-like molecule(s) by cultured human endothelial cells," *Journal of Cell Biology*, vol. 103, no. 3, pp. 1129–1133, 1986.

[43] E. A. Bauer, T. W. Cooper, J. S. Huang, J. Altman, and T. F. Deuel, "Stimulation of in vitro human skin collagenase expression by platelet-derived growth factor," *Proceedings of the National Academy of Sciences of the United States of America*, vol. 82, no. 12, pp. 4132–4136, 1985.

[44] M. Haisa, H. Okochi, and G. R. Grotendorst, "Elevated levels of PDGF α receptors in keloid fibroblasts contribute to an enhanced response to PDGF," *Journal of Investigative Dermatology*, vol. 103, no. 4, pp. 560–563, 1994.

[45] D. M. Dohan Ehrenfest, M. Del Corso, A. Diss, J. Mouhyi, and J.-B. Charrier, "Three-dimensional architecture and cell composition of a Choukroun's platelet-rich fibrin clot and membrane," *Journal of Periodontology*, vol. 81, no. 4, pp. 546–555, 2010.